INFORMATION TO USERS

This manuscript has been reproduced from the microfilm master. UMI films the text directly from the original or copy submitted. Thus, some thesis and dissertation copies are in typewriter face, while others may be from any type of computer printer.

The quality of this reproduction is dependent upon the quality of the copy submitted. Broken or indistinct print, colored or poor quality illustrations and photographs, print bleedthrough, substandard margins, and improper alignment can adversely affect reproduction.

In the unlikely event that the author did not send UMI a complete manuscript and there are missing pages, these will be noted. Also, if unauthorized copyright material had to be removed, a note will indicate the deletion.

Oversize materials (e.g., maps, drawings, charts) are reproduced by sectioning the original, beginning at the upper left-hand corner and continuing from left to right in equal sections with small overlaps. Each original is also photographed in one exposure and is included in reduced form at the back of the book.

Photographs included in the original manuscript have been reproduced xerographically in this copy. Higher quality 6" x 9" black and white photographic prints are available for any photographs or illustrations appearing in this copy for an additional charge. Contact UMI directly to order.

UMI

University Microfilms International
A Bell & Howell Information Company
300 North Zeeb Road, Ann Arbor, MI 48106-1346 USA
313 761-4700 800 521-0600

Order Number 9224869

Investigation of turbulent structures in a supersonic free shear layer

Zhang, Jianjun, Ph.D.

City University of New York, 1992

U·M·I

300 N. Zeeb Rd.
Ann Arbor, MI 48106

A

INVESTIGATION OF TURBULENT STRUCTURES IN A SUPERSONIC FREE SHEAR LAYER

by

Jianjun Zhang

A dissertation submitted to the Graduate Faculty in Physics in partial fulfillment of the requirements for the degree of Doctor of Philosophy, The City University of New York.

1992

This manuscript has been read and accepted for the Graduate Faculty in Physics in satisfaction of the dissertation requirement for the degree of Doctor of Philosophy.

March 10, 1992
Date

Joseph A. Johnson III
Chair of Examining Committee

March 12, 1992
Date

Joseph B. Krieger
Executive Officer

Martin Cramer
Supervisory Committee

The City University of New York

Abstract

INVESTIGATION OF TURBULENT STRUCTURES IN A SUPERSONIC FREE SHEAR LAYER

by

Jianjun Zhang

Advisor: Professor Joseph A. Johnson III

The compressible, supersonic free shear layer is investigated experimentally in a Ludwieg tube-wind-tunnel. A new measurement technique based on laser induced fluorescence (LIF) is developed, by which simultaneous, multi-point local density and density fluctuation can be obtained in the supersonic free shear layer. From the density measurements, the streamwise and transverse velocity components are calculated. Density, velocity and turbulent intensity profiles and their evolution along the streamwise direction are measured. Large scale structures at inner layer are observed by both shadowgraph photograph and multi-point density measurements. The mean structure spacing, the spatial rate of changing and mean persistent time of the structures are determined. The spreading of the turbulent region of the shear layer is measured by means of velocity profiles obtained along streamwise locations. An analytical investigation of the shocklet provides a generalizable physical model for shocklet processes, which agrees with our experimental results. It is concluded that eddy shocklet is a transient shock wave generated

from the interaction between the convecting eddy and environmental field which reduces the scale of turbulent structure, especially the spreading rate of the shear layer, and generates a vortical field extending into the main flow from the outer region of the shear layer. A connection of eddy shocklets with the streaky structures ejected from the lower layer is suggested with the strong compression between the structures, with slow convecting velocity, and the supersonic flow field generating the pressure field which forms the transient shock wave. The dynamical process of shocklet formation and propagation are observed to be the apparent basic agent for turbulent energy transfer between the inner and outer regions of the layer and also the eddy motion and environmental flow field, hence they contribute significantly to the entire turbulent process in shear layer.

Acknowledgements

I would like to express my gratitude to my advisor, Joseph A. Johnson III, for his guidance and friendship over the past six years. Thanks also for the support from professor Chi Yuan and to the other members of my examining committee, professor Rishi Raj, Joel I. Gersten and Martin Kramer.

I would like to thank Dr. Lynette Johnson for helping me in word processing of computer. The work performed by the mechanical shop is much appreciated and special thanks to Mr. Carlos M. Orta.

Finally, I wish to sincerely thank my wife Zuohua who helps me in my research and who has been very loving throughout my time in the school.

Table of Contents

LIST of FIGURES

Nomenclature

English Symbols

u_o	scale of mean velocity variation
q_o	scale of the turbulent velocity
l_o	length scale of the flow
Rs	flow constant
β	entrainment parameter
Ms	Mach number of the shock wave
γ	specific heat ratio
ω'	the vorticity generated behind a shock wave
S*	shear rate parameter
K*	energy partition parameter
L*	eddy elongation parameter
Tc	temperature for condensation
θv	characteristic temperature for exciting the vibrational motion of the atoms
τ_c	large correlation times
τ_s	small correlation times
Vc	convective velocity of the eddy

n	spectral frequency of the shocklets or spectral index of the Fourier transformation
f	production frequency of the shocklets
p_f	the flow pressure before the outlet region of the nozzle
p_b	the back pressure at the outlet region of the nozzle
θ	the angle between the wave number of the shocklet and the streamwise direction
α	the angle between the boundary of the shear flow and the axis of the shear layer
σ	the angle between the boundary of the shear layer and the axis of the shear layer
P_4	initial filling high pressure
P_1	initial filling low pressure
p_o	reference pressure

I Introduction

Much of recent research in the area of turbulent fluid flow has concentrated on the identification and understanding of relatively ordered or coherent motions within the randomly fluctuating flow field in free shear flow. This intense new interest results from the significance of turbulent shear flow in astrophysics, chemical reactions, supersonic combustion, drag and noise reduction. It is particularly necessary that a complete physical model of turbulence be developed. Through this, we will expect a better understanding of the motion and evolution of the coherent structures (Cantwell 1981).

Many flow visualization experiments and numerical simulations (Brown & Roshko 1974) have shown that when the flow is moving downstream, the shear layer originating from the nozzle's lip develops instability waves which roll up into vortices and the vortices are convected downstream. During their lifetime they interact showing pairing and tearing effects (Hussain 1983). There is already visual evidence that large scale structures exist in supersonic shear layers. This evidence comes from the experiments of Ortwerth and Shine (1977) and Oertel (1979).

However, most of the research in turbulent structures has been done on low Mach number flows where compressibility does not play an important role; it is impossible to form even weak shock wave in this case. In such flows, the turbulent structures show higher coherence; therefore, it is relatively easy to detect and describe the turbulent motion in the flows.

For high Mach number flows, the situation can be quite different. The Reynolds numbers usually are much higher and the turbulent structures show much weaker definitions; the coherent structures also show much less order. This increases the difficulty both for their detection and for an analytic description. Also, for supersonic flows, regions of strong compression can be formed resulting in the formation of shock waves in the flow. The subsequent propagation of such shocks or eddy shocklets will interact with the flow field and other structures (Hussaini 1986, Lele 1989) in supersonic shear flow. The shocklets will affect the structure's size, transfer turbulent energy in the flow field, and produce vorticity behind the shocklets. Another dynamical process, called turbulent bursts, is believed to exist not only in wall boundary shear flow but also in free shear layers (Lee et al.1990). This process is associated with a major part of the Reynolds stress and turbulent energy production.

We, therefore, are motivated to conduct experimental research aimed at identifying the coherent structures, quantitatively describing the spatial and temporal evolution of the structures and establishing the role of each of the structures in the production of turbulence. We will use diagnostic techniques with appropriate spatial and temporal resolution. We will determine the role of turbulent bursts in our system. We will also speculate on a generalizable theoretical model for the supersonic turbulent free shear layer.

1.1 Shock waves and the Generation of Vorticity in Shear Flows

One of the most distinguishing features of compressible fluid motions is the existence of shock waves. For an ideal fluid, in which both viscous and thermal diffusions are negligible, a shock wave is a discontinuity surface of flow field quantities, such as the density, the pressure and the velocity component normal to the shock. The normal velocity relative to a shock wave is supersonic on one side of the shock and subsonic on the other side. The numerical simulation works from Orszag (1990) show that there is a strong relationship between vorticity and shock waves; vorticity is created inside a curved shock wave through the interaction of fluid elements and the intensification of the compression in fluid elements. The generation of vorticity is an important mechanism in transport phenomena such as turbulent mixing and noise generation. In high Mach number fluid flows, the compressibility is effective in the formation of coherent structures (and their interactions) and the subsequent generation of transient shock waves, known as shocklets, which are responsible for the generation of vorticity in both turbulent and non-turbulent flow. The shocklet structures and dynamics play a important role in turbulent shear flows.

1.2 Coherent Structures in Turbulent Shear Layers

Coherent structures, beginning with the work of Bradshaw et al. (1964), Crow and Champagne (1971), and Brown & Roshko (1974) in free shear flows and and with that of Kline et al. (1967), Kim et al. (1971), Kovasznay et al. (1970), and Blackwelder & Kovasznay (1972) in turbulent boundary layers, are now known to be a manifestation of hydrodynamic instabilities. These

instabilities are sensitive to initial and environmental conditions. In general the free shear flows or layers are formed at the outlet of nozzles or solid surfaces. The structures in the boundary layers near the nozzle lips and the steps of the solid surfaces should be related to the coherent structures in the shear flows. Therefore, the understanding of formation and evolution of a structure in boundary layer of incoming flow is necessary in order to understand the formation of the coherent structures in subsequent free shear flows.

Coherent structures of interest in turbulent wall flows are the large scale vortex motions in the outer region and the smaller scale structures in the inner wall region (Laufer 1975). The large scale vortex motions are rotating bodies of fluid which span the height of boundary layer flows and are responsible for the entrainment of the irrotational free stream fluid into the boundary layer. The smaller scale structures in the inner region exist not only in boundary layer but in turbulent internal flows in pipes and channels as well. Within the viscous sublayer, the low velocity fluid tends to accumulate into longitudinal structures known as streaks. The streaks eventually become unstable which result in the vigorous ejection of the low velocity fluid within the streaks away from the wall. The break-up of a streak and subsequent ejections are known as a burst. In the flow visualization studies (Kim, et al. 1971, Corino and Brodkey 1969, and Grass 1971), it was concluded that the burst structures were the major producers of Reynolds stress and turbulent kinetic energy in turbulent wall flows.

Although streaks have been studied by many investigations using different techniques (Oldaker & Tiederman 1977), Tiederman & Bogard (1981), and Gupta et al. (1971), the flow mechanisms responsible for the formation of these streaks are still not well understood. It has been suggested that they are due to counter-rotating vortices which sweep low velocity fluid from the viscous sublayer into a longitudinal streak structure in between them. There have been probe measurements by Bakewell & Lumley (1967) and Blackwelder & Eckelmann (1979) which are consistent with the existence of these vortices. Moreover, results from the large eddy simulation model presented by Moin & Kim (1982) indicate longitudinal streak-like structures in the wall region.

1.3 Spreading Rate of the Shear Layer

As a result of the currently increasing importance of supersonic combustion, research on the compressible turbulent shear layer attracts great interest. Especially there is interest in the spreading rate of the shear layer. The fact that the turbulent shear layer of compressible flow spreads more slowly than incompressible shear layer was shown by Birch and Eggers (1972). Although some inconsistencies exist among the various experimental investigations, there is a definite trend of decreasing spreading rate with increasing free stream Mach number.

To understand the mechanism of this trend, great efforts have been exerted in order to distinguish between density effects and compressibility effects. As a density effect, it was thought that the decrease in spreading rate is due to the associated change in

density ratio across the shear layer. This possibility partially motivated the experiments of Brown and Roshko (1974). Their results showed that density difference has some effect on the spreading rate; but it is an effect very much smaller than what is required to explain the results.

It was therefore concluded that compressibility plays a uniquely important role in the evolution of the supersonic shear layer. In this context, several experiments were conducted (Ortwerth and Shine 1977, Demetriades and Brower 1982 and Chinzei et al. 1986) in the shear layer of mixing flow. In such experiments a parameter, the so called convective Mach number, denotes the compressibility effect, which is defined as the Mach number in a frame of reference convecting with the real phase speed of the disturbance. It was found that the spreading rate of shear layer decreases as the convective Mach number increases.

As a parameter, the convective Mach number gives the description of compressibility kinematically. However it does not explain the physical mechanisms associated with the influence of compressibility on free shear layer transport. Furthermore, the concept of convective Mach number or the definition in common use is not adequate in single flow shear layers such as jet shear flow and shear flow generated by a flow passing a sharp corner.

Another concept which directly comes from the compressibility effect, the so called eddy shocklet, was proposed by Hussaini et al. (1986). The eddy shocklet is a transient shock wave generated from the compression between the eddy motion and supersonic flow field. It can only be produced in supersonic flow in

which compressibility effects are important. From the dynamical properties of shocklets, the connection between a shocklet and the spreading rate of shear layer can be made. The shocklet will affect the turbulence in a shear layer by both a reduction in the turbulence scale and the production of counter fluctuating vorticity.

Therefore, shocklets play an important role in decreasing of spreading rate as the flow speed increase. Since there has been great difficulty in experimental detection, not many actual experimental results on shocklets can be found. A numerical simulation analysis result by Lele (1989) showed a graph of shocklets, but without quantitative description. An experimental result from photographs of shocklets in a free shear layer was reported by Johnson et al. (1988). However, to understand the physical mechanisms of eddy shocklets and to model the dynamical processes, it is necessary to have a diagnostic which provides a quantitative evolution of eddy shocklet effects in turbulence.

1.4 Bursting Process in the Shear Layer

In the flow visualization studies of Kim, et al. (1971), Corrino and Brodkey (1969), and Grass (1971), it was found that, within the viscous sublayer of the wall boundary, the low velocity fluid tends to accumulate into longitudinal structures known as streaks. The streaks eventually become unstable. This results in the ejection of the low velocity fluid away from the wall. The break up of a streak and subsequent ejections are known as a burst. It was also concluded that the burst process was the major producer of

Reynolds stress and turbulent kinetic energy in turbulent wall flow.

A keen interest in the nature of these structures has now been stimulated and has led to numerous experimental investigations. In addition, some conceptual models of the bursting mechanisms have been proposed by Laufer (1975), Offen and Kline (1975) and Praturi and Brodkey (1978). However, the investigations of flows with the burst processes have previously been restricted to low speed, low shear rate and wall bounded shear layers. There is still a serious lack of understanding of the burst process in high shear rate supersonic flow, without the existence of solid wall, and the dynamical effects of such a process on the flow turbulence. Recently, a numerical simulation result by M.J.Lee (1990) shows that in a high shear rate layer without the existence of wall ,the streaky structure still can be formed; he also found that this process is the major production source of turbulence in the shear flow. Therefore, a motivation of present study of burst processes in the supersonic free shear layer is to find out that if there is connection between the burst process and eddy shocklet generation.

1.5 Measurement Technique

Much current activity in high-speed turbulent free shear flow is aimed at: quantitative measures for the scales of the vortex motion and their evolution; the vorticity field associated with their rapid scale distortion; and the mechanism of the shear layer spreading and enhancement. But quantitative analyses of the vortex motion and its effect to the fundamental properties of

turbulence have been limited by the lack of experimental techniques capable of generating simultaneous multi-point data (R.B. Miles et al. 1988) which can give a measure of the quantities directly related to the physical properties of the turbulent motion. Previous measurements on turbulent structures have largely relied on hot wire or hot film probes in low Mach number flows, and on laser Doppler anemometer and Schlieren photography in high Mach number flows. These have many shortcomings in supersonic free shear layers, especially with regard to resolution in space and time and to system response time. Although the LDV system provides useful measurements in many type of supersonic flow, it is nonetheless very difficult for LDV to provide the kind of simultaneous multi-point measurements which would be required for coherent structure measurements in turbulent shear flows. In contrast, laser induced fluorescence (LIF) does not have these problems. We, therefore, developed a new measurement technique using LIF which allows us to take simultaneous multi-point local density and velocity measurements. No particulate additives are required. The use of LIF affords direct assess to intrinsic variations in the flow properties.

II Background

2.1. Boundary-Layer Approximation

The free shear layer is bounded on one side by ambient fluid of nearly the same density which is not turbulent and is in a state of irrotational flow. At any moment, the fluid in turbulent, vortical motion is divided from the fluid in irrotational motion by an intermittent surface. Within the intermittent surface, the turbulence is roughly homogeneous in scale and turbulent intensity. The shear layer spreads into the surrounding fluid and it is inhomogeneous in the stream direction as well as in a transverse direction.

The free shear layer scale in the stream direction is much larger than that in transverse direction, and the rate of change of flow parameters along the stream direction is much smaller than that in transverse direction. Therefore the mean value equations can be simplified by using a boundary layer approximation, similar to that introduced by Prandtl for laminar boundary layer flow at large Reynolds numbers.

Consider the free turbulent flow bounded by non-turbulent flow. While the exact direction of mean flow may vary somewhat from one part of the flow to another, a direction, called the direction of mean flow, is selected as the the coordinate direction x. The gradients of mean value in the x direction are considerably less than in the transverse y direction; the length scale for variation of mean quantities in the x direction is typically an order of magnitude greater than the scale of variation in transverse direction.

The equation of motion of the free shear layer for the y component can be written as

$$U\frac{\partial V}{\partial x}+V\frac{\partial V}{\partial y}+W\frac{\partial V}{\partial z}+\frac{\partial \overline{uv}}{\partial x}+\frac{\partial \overline{v^2}}{\partial y}+\frac{\partial \overline{vw}}{\partial z}=-\frac{\partial P}{\partial y}+\nu\nabla^2 V \qquad (2.1.1)$$

For large Reynolds numbers, the equation can be approximated as

$$\frac{\partial \overline{v^2}}{\partial y}+\frac{\partial \overline{vw}}{\partial z}=-\frac{\partial P}{\partial y} \qquad (2.1.2)$$

where the U, V, W are the mean velocity components of x,y,z respectively, and u, v, w are the velocity fluctuation components of x, y, z respectively. P is the pressure inside the shear layer.

Define the mean flow velocity and pressure just outside the shear flow as U_1, and P_1. For irrotational ambient flow we have

$$\frac{\partial P_1}{\partial x}+U_1\frac{dU_1}{\partial x}=0 \qquad (2.1.3)$$

Making use of (2.1.3) the equation of x component of mean velocity can be expressed as

$$U\frac{\partial U}{\partial x}+V\frac{\partial U}{\partial y}+W\frac{\partial U}{\partial z}+\frac{\partial \overline{uv}}{\partial y}+\frac{\partial \overline{uw}}{\partial z}=U_1\frac{dU_1}{dx}+\nu\left(\frac{\partial^2 U}{\partial y^2}+\frac{\partial^2 U}{\partial z^2}\right) \qquad (2.1.4)$$

If y is in the direction of maximum transverse gradient the approximation can be expressed as

$$U\frac{\partial U}{\partial x}+V\frac{\partial U}{\partial y}+W\frac{\partial U}{\partial z}+\frac{\partial(\overline{u^2}-\overline{v^2})}{\partial x}+\frac{\partial \overline{uv}}{\partial y}+\frac{\partial \overline{uw}}{\partial z}=U_1\frac{dU_1}{dx} \qquad (2.1.5)$$

The requirements of overall conservation of momentum and energy can be expressed as relations between integrals of mean values over planes parallel to xy. The integration of the approximation equation (2.1.5) over the whole section leads to

$$\frac{d}{dx}\iint U(U-U_1)dy\,dz+\frac{dU_1}{dx}\iint(U-U_1)dy\,dz+\frac{d}{dx}\iint(\overline{u^2}-\overline{v^2})\,dy\,dz=0 \tag{2.1.6}$$

2.2 Shear flow parameters

In the free shear layer, the transverse distribution of mean velocity and other mean quantities change with distance downstream. It is often assumed, however, that the distributions retain the same functional forms, merely changing their transverse length scale and the scales of the mean value quantities.

For two dimensional mean flow the variation of the mean value quantities are the form of

$$U=U_1+u_0\,f(y/l_0) \tag{2.2.1}$$

$$\overline{uv}=q_0^2\,g_{12}(y/l_0) \tag{2.2.2}$$

$$\overline{u^2}=q_0^2\,g_1(y/l_0) \tag{2.2.3}$$

where U_1 is the velocity in the free stream, u_0 is the scale of mean velocity variation, q_0 is the scale of the turbulent velocity, and l_0 is length scale of the flow. All the scales are functions of x alone, and the functions are independent of position and are characteristic of

the whole flow. By substituting the distribution functions into the equation (2.1.6) the momentum integral becomes

$$(2a+1)\frac{u_0 U_1 l_0}{x-x_0}(I_1+\frac{u_0}{U_1}I_2)+a\frac{u_0 U_1 l_0}{x-x_0}I_1=0 \qquad (2.2.4)$$

where $I_n=\int_{-\infty}^{+\infty}(f(\eta))^n d\eta \qquad \eta=y/l_0$ (2.2.5)

$$a=-\frac{I_1+(u_0/U_1)I_1}{3I_1+(u_0/U_1)I_2} \qquad (2.2.6)$$

and the conditions for the shear flow are

$$\frac{U_1 l_0}{u_0^2}\frac{du_0}{dx}=\text{ constant} \qquad \frac{U_1}{u_0}\frac{dl_0}{dx}=\text{ constant} \qquad (2.2.7)$$

The equation of momentum integral becomes

$$\frac{d}{dx}\left[U_1 u_0 l_0\int_{-\infty}^{+\infty}f(\eta)\,d\eta\right]+\frac{dU_1}{dx}u_0 l_0\int_{-\infty}^{+\infty}f(\eta)\,d\eta=0 \qquad (2.2.8)$$

showing that

$$I_1 U_1^2 u_0 l_0=\text{ constant }=U_1^2\int_{-\infty}^{+\infty}(U-U_1)dy \qquad (2.2.9)$$

For shear layer $u_0\propto U_1\propto(x-x_0)^a$, the solutions of equation (2.2.7) and (2.2.9) are

$$\frac{u_0}{U_1}\propto(x-x_0)^{-1/2(1+3a)}, \quad l_0\propto(x-x_0)^{1/2(1-3a)} \qquad (2.2.10)$$

For a given velocity distribution $U = U_1 + u_0 f(\eta)$ the stress distribution can be found from

$$u_0 \frac{dU_1}{dx}(f-\eta f') + U_1\left(\frac{du_0}{dx} f - \frac{u_0}{l_0}\frac{dl_0}{dx}\eta f'\right) + u_0 \frac{du_0}{dx}(f)^2$$

$$-\frac{u_0}{l_0}\frac{d(u_0 l_0)}{dx} f' \int f\, d\eta + \frac{q_0^2}{l_0} g'_{12} + (g_1 - g_2)\frac{dq_0^2}{dx} - \frac{q_0^2}{l_0}\frac{dl_0}{dx}\eta(g'_1 - g'_2) = 0$$

For flow symmetric about xy plane, the stress distribution is

$$g_{12} = \frac{(1-a)U_1}{(1-3a)u_0}\frac{dl_0}{dx}(\eta f)$$

for u_0 / U_1 is small and

$$g'_{12} = \frac{(1-a)U_1}{(1-3a)u_0}\frac{dl_0}{dx}(f + \eta f')$$

for u_0 / U_1 is not small

The entrainment parameter is defined as

$$\beta = \frac{U_1 + \frac{1}{2}u_0}{|u_0|}\frac{dl_0}{dx} \qquad (2.2.11)$$

The eddy viscosity parameter is defined as

$$R_s^{-1} = \beta(1-a)/(1-3a) \qquad (2.2.12)$$

if $|u_0| / U_1$ is small, and that

$$R_s^{-1} = (a+1)\beta$$

if $|u_0| / U_1$ is not small.

2.3 Eddy Shocklets

In supersonic flow, the velocity difference between a local flow speed and the structure's convective speed will generate a pressure field. For the strong pressure situation it will form a transient shock wave called a shocklet. This pressure field, which is enhanced by increased Mach number, will always counter the initial structure circulation over a portion of the structure's contour and, for long enough times and weak enough structures (or large enough velocity difference and Mach number), the formation of counter vorticity and consequent structure splitting will occur. The shocklets will greatly affect the turbulence in a shear layer by the effects of both a reduced turbulence scale and production of counter fluctuating vorticity.

The flow conditions will be different across a shock wave, which are called jump conditions. The jump conditions may vary along the shock depending on both the direction and the curvature of the shock. For two dimensional approximation, let the unit normal and tangent vectors be $\mathbf{n}$ and $\mathbf{l}$, the radius of curvature be a and the angle of attack be θ; the density, pressure, the normal and tangential components of velocity ahead of the shock be ρ, p, u_n and u_l, and the corresponding ones behind the shock be ρ', p', u'_n, and u'_l, respectively. Then the jump conditions between these field quantities are

$$\rho' = \frac{(\gamma+1) M_s^2}{(\gamma-1) M_s^2 + 2} \rho$$

$$p' = \frac{2\gamma M_s^2 - (\gamma - 1)}{\gamma + 1}$$

$$u'_n = \frac{(\gamma - 1) M_s^2 + 2}{(\gamma + 1) M_s^2} u_n$$

$$u'_l = u_l$$

where

$$M_s = \sqrt{\frac{\rho |u|^2}{\gamma p} \cos\theta}$$

is the shock Mach number defined by the ratio of the relative velocity normal to the shock and the sound speed ahead of the shock. The spatial derivatives of the jump conditions can be obtained by taking the normal and tangential derivatives respectively.

$$\frac{\partial \rho'}{\partial l} = \frac{4(\gamma + 1) M_s^2 \tan\theta}{a[(\gamma - 1) M_s^2 + 2]^2} \rho$$

$$\frac{\partial p'}{\partial l} = \frac{4\gamma M_s^2 \tan\theta}{a(\gamma + 1)} p$$

$$\frac{\partial u'_n}{\partial l} = \frac{[(\gamma - 1) M_s^2 - 2] \tan\theta}{a(\gamma + 1) M_s^2} u_n$$

$$\frac{\partial u'_l}{\partial l} = -\frac{u_n}{a}$$

$$\frac{\partial \rho'}{\partial n} = \frac{2 M_s^2}{a[(\gamma - 1) M_s^2 + 2} \left[-1 + \frac{(\gamma + 1)[3(\gamma - 1) M_s^4 - (\gamma - 3) M_s^2 + 2(\gamma + 2)]}{(M_s^2 - 1)[(\gamma - 1) M_s^2 + 2]} \tan^2\theta \right] \rho$$

$$\frac{\partial p'}{\partial n}=\frac{2\gamma M_s^2}{a(\gamma+1)}[-\frac{2\gamma M_s^2-(\gamma-1)}{(\gamma+1)M_s^2}+\frac{2(2\gamma-1)M_s^4+(\gamma+5)M_s^2-(\gamma-1)}{(M_s^2-1)[(\gamma-1)M_s^2+2]}\tan^2\theta]p$$

$$\frac{\partial u'_n}{\partial n}=\frac{2}{a(\gamma+1)}[\frac{2\gamma M_s^2-(\gamma-1)}{(\gamma+1)M_s^2}-\frac{3M_s^2+1}{M_s^2-1}\tan^2\theta]u_n$$

$$\frac{\partial u'_l}{\partial l}=\frac{2[(-\gamma+3)M_s^2-(\gamma+5)]\tan\theta}{a(\gamma+1)[(\gamma-1)M_s^2+2]}u_n$$

where

$$a=-\frac{1}{\partial\theta/\partial l}$$

The vorticity generated behind the shock wave can be obtained from the jump conditions and the spatial derivatives of velocity as

$$\omega'=\frac{\partial u'_l}{\partial n}+\frac{u'_l}{a}-\frac{\partial u'_n}{\partial l}$$
$$=\frac{4(M_s^2-1)^2\sin\theta}{a(\gamma+1)M_s^2[(\gamma-1)M_s^2+2]}|u|$$

2.4 Turbulence Production at High Shear Rates

In flow visualization studies for turbulent boundary layers (Kline et al. 1967), it was established that an important characteristic of the near wall region of bounded turbulent flow is the low-velocity streaks in the sublayer and the associated subsequent ejection of the low-velocity fluids to the outer region of the flow. The ejection of low-velocity fluids from the wall region was associated with a major part of the Reynolds stress and turbulent energy production.

Recently numerical simulation results (M.J. Lee et al. 1990) show that the high shear rate alone is sufficient for generation of the streaky structures in shear layer; the wall is not required. These streaky structures are highly elongated in the streamwise direction and narrow in the spanwise direction. The strong shear gives rise to a growth of turbulence length scales with the mean flow; the streaks generated by the high shear rate undergo a series of dynamical processes during which most of turbulence production occurs.

These results have provided a strong impetus for further studies aimed at understanding the dynamics of the generation process of the structures and its association and interaction with the mean flow field. The theory suggests two quantities which indicate the nature of the streaky structures: (i) high concentrations of turbulent kinetic energy in the streamwise component,u; and (ii) elongation of length scales associated with u in the streamwise direction. These two salient features of streaks can be quantified by the dimensionless parameter K* and L*.

$$K^* = \frac{2\overline{u^2}}{\overline{v^2} + \overline{w^2}} \qquad (2.4.1)$$

$$L^* = \frac{L_x}{L_z} \qquad (2.4.2)$$

where K* and L* are energy partition and eddy elongation parameters. The theory suggests, for maximum shear rates S*>35

$$K^* > 5, \qquad L^* > 8$$

In the equation (2.4.1) u, v, and w velocity fluctuations in x, y and z components. L_x and L_z are the length scales of the streaky structures in streamwise and spanwise direction.

III Experiments

3.1 Ludwieg tube-wind-tunnel

The Ludwieg tube-wind-tunnel we used, as shown in fig. 3.1.1, is a conventional shock tube modified by inserting a layer-spilling asymmetric nozzle into the test section. The high pressure section has five parts: a 6-ft-long, 3.6-in x 3.6-in. square test section with five optical ports on each face and corresponding pressure ports; a 3-ft-long transition piece for the change from a 3.6-in. x 3.6-in. cross section to the 6-in.-diam circle; a 5-ft-long, 6-in.-diam cylindrical piece; and two pieces that are each quarter-circle arcs of 2-ft radius with 6-in.-diam cross section. The curved sections conveniently extend the overall length of the high pressure section and thereby increase the duration of the period of steady supersonic flow. The low pressure section has two parts: a 6-in.-diam, 5-ft long cylindrical end piece and a 3-ft-long transition piece that changes from 6-in.-diam circular cross section to a 3.6-in. x 3.6-in. square at the diaphragm. The transition piece has a electric-magnetic-operated plunger for rupturing the diaphragm and providing the trigger signal to the analog to digital converters (ADC).

The high pressure section and low pressure section are separated by a diaphragm. When the diaphragm is ruptured by a magnetic punch, an expansion wave moves upstream into the high pressure section through the nozzle causing the local pressure, density and velocity to change with time, t, and as a function of distance from the location of the diaphragm. At a time determined by the ratio of the nozzle's throat to its exit area, which

is about 4 to 6 ms, the nozzle is choked, the mass flow rate is frozen, and stable, steady supersonic flow is established in the exit region. The overall flow duration time is around 15 ms. When the diaphragm breaks, a shock wave and a contact surface are also produced and travel downstream into the low pressure section. The high pressure section is filled by an admixture of 98% N_2 and 2% NO_2 which provides a target for the incident light and is the source of the fluorescence light.

The free shear layer is generated by the nozzle producing a plane two-dimensional boundary layer which detaches at the sharp corner of the nozzle as shown in Figure 3.1.2. The shear layer is thin compared to the step of the nozzle and it is not affected by the presence of the tube wall. Figure 3.1.3 shows the flow in the measuring region. The flow at the outlet of the nozzle and flow in the free shear layer are characterized by the angles. By changing the nozzles in the Ludwieg tube, Mach numbers in the range 1.6 to 2.5 are obtained. For a given nozzle, we achieve a variation in Reynolds number by changing the starting pressure, P_4, in the high pressure section from 10^6 to 10^8 in free stream unit Reynolds number. Figure 3.1.4 shows the relationship between Reynolds number and the angles which characterize the shear flow.

3.2 Three States of Flow

In the test section of Ludwieg tube, there can be three different typical states of the supersonic flow as follows:

1. There may be a wake and an expansion wave from the outlet of the nozzle. This state means that the back pressure around the outlet of the nozzle is less than the pressure of the flow at the outlet section. In this case, the Mach number of the flow behind the expansion wave will be more than the Mach number of the initial flow at the outlet. The directions of the axis of the wake and the flow behind the expansion wave are different from the direction of the initial flow. They are more or less outward from the axis of the initial flow.

2. There may be a wake and an oblique shock wave from the outlet of the nozzle. This state means that the back pressure is more than the pressure of the flow at the outlet. In this case, the Mach number behind the shock wave will be less than the Mach number of the initial flow. The direction of the axis of the wake and the flow behind the shock wave are inward more or less.

In the above two cases, the Reynolds number behind the expansion wave or the shock wave is also different from the Reynolds number of the initial flow.

3. There may be neither expansion waves nor shock waves from the outlet of the nozzle, just a wake in the form of a free shear layer. This state means that the back pressure around the outlet of the nozzle is the same as the pressure of the flow at the outlet. In this case, the Mach number, Reynolds number and the direction of the initial flow are unchanged and the direction of the axis of the

wake will be same as that of the initial flow. This is the state that we need in our research on the turbulent compressible flow.

Figures 3.2.1 to 3.2.3 show the shadowgraph pictures of shear layer at the three different states. The state of the flow in the test section of Ludwieg tube can be controlled by adjusting, through trial and error, the pressure ratio of the filling pressure P_4 to the initial low pressure P_1. However, the initial low pressure is not the same as the back pressure around the outlet of the nozzle. The reason is that the test section is behind a normal shock wave which is formed in the initial low pressure section of the Ludwieg tube and must move downstream.

3.3 Flat Free Shear Layer Control

As indicated above, the flat free shear layer from the outlet of the nozzle can be produced by controlling the ratio of filling high pressure P_4 to filling low pressure P_1. In such a situation, the environmental pressure is equal to the static pressure of the flow at the outlet section of the nozzle. The pressure sensors which are used to measure the filling high pressure and low pressure must be precise because the flat state of shear layer flow is highly sensitive to the pressure ratio. Therefore, a Baratron system is being used. The accuracy for the high pressure measurement is 0.05 psi (2.6 torr). The accuracy for low pressure measurement is 0.01 torr. The calibration line of the Baratron is shown in Figure 3.3.1. The overall configuration requires frequent calibrations of the Baratron system.

When the low pressure P_1=916.2 ~916.5 torr, high pressure P_4=76.75~77.32 psi, the flat wakes can be obtained even if there is a

weak shock wave or a weak expansion fan at the outlet of the nozzle. Thirteen shadowgraphs with the flat wakes were taken under such a condition. For example, when P_1=916.5 torr, the suitable high pressure value is P_4=77.18 psi (corresponding voltage of Baratron is 1596 mV). For this pressure ratio, 6 shadowgraphs with flat wakes were taken. Two typical shadowgraphs are shown in Figure 3.3.2. In fluorescence measurements, since the high pressure section is filled by an admixture of 2% NO2 and 98% N2 the high pressure and low pressure which can give flat free shear layer become P_4 = 51.84 psi, and P_1 = 110.4 torr respectively.

The location of the nozzle in the Ludwieg tube can strongly influence the results because it can change the distance between the outlet of the nozzle and the diaphragm. The pressure environment around the outlet of the nozzle will be changed.

Humidity in the high pressure gas can influence the results. In the test section when M=2.04, for example, the static temperature T of the flow is much lower that the total temperature to of the flow, T/T_0=0.5458; when the temperature of the laboratory is 298^0 K, then T=163^0 K. At such a temperature, water vapor in the flow will be condensed so that the static pressure of the flow will be decreased. The balance between pressure of the flow and that of the environment can be destroyed. Therefore, we must use high pressure gas which has been dried in order to get stable results.

3.4 Starting Stage of Supersonic Flow

In accordance with the downstream and upstream static pressure measurements of the nozzle, we know that for our M=2

nozzle, the starting stage is 6 ms long (see Figure 3.4.1); after 6 ms, a supersonic flow with M=2 will be established. Simultaneously, the boundary layer which is appropriate for M=2 free stream will be formed after the starting stage.

3.4.1 Free Stream

When the sound signal from a diaphragm arrives at the microphone downstream located near the diaphragm, the head of the expansion waves arrives at some position A upstream relative to the diaphragm. The distance between position A and the Pitot gauge position B is that AB=48.5 cm. The period in which the head of the expansion waves moves from A to B should be:

$$\frac{AB}{a} = \frac{48.5\ \text{cm}}{34.6\ \text{cm/ms}} = 1.40\ \text{ms}$$

It is the same as the times measured by the Pitot gauge.

After the first 1.4 ms, the total pressure measured by Pitot gauge begins to decrease. The reason is as follows: After the first 1.4 ms, the head of the expansion waves and the region of expansion waves which follows (known as the expansion fan) will pass the Pitot gauge upstream. The static pressure at the outlet of the Pitot gauge will be lower than the total pressure in the Pitot gauge. When the expansion waves pass through the nozzle upstream, the gas in the nozzle will begin to move downstream. However, during the starting stage, the nozzle does not work perfectly; the velocity will not be high enough to keep the total pressure ($P_0=P+\frac{1}{2}\rho V^2$) in the nozzle constant. Therefore, at any moment, the total pressure at the outlet of the Pitot gauge is also

lower than that the gas in the Pitot gauge. Thus gas in the Pitot gauge will leave and will be brought downstream. Of course in this situation the pressure in the Pitot gauge will be decreased. That is why the total pressure measured by the Pitot gauge decreases after a time lag with respect to gas at the head of the Pitot gauge.

However, the nozzle's performance will improve as time passes and the velocity of the gas in nozzle will increase downstream. Ultimately, the total pressure will increase and will be higher than that in the Pitot gauge so that a part of the gas in the nozzle will go into the Pitot gauge. That is why the total pressure measured by the Pitot gauge will show an increase as the flow stabilized.

If, in front of the Pitot gauge, no shock waves were produced, the total pressure recovers to its original value. But in fact, after the speed of the flow at the throat of the nozzle increases to the local sonic speed, a shock wave will be produced and move downstream along the divergent section of the nozzle. In the meantime the shock wave will be stronger with its increasingly downstream location in the divergent section of the nozzle until it stands in front of the outlet of the Pitot gauge. The Pitot gauge, in supersonic flow, can only measure the total pressure behind a shock wave. It is lower than that in front of the outlet of the Pitot gauge owing to the loss of the total pressure. That is why the total pressure measured by the Pitot gauge can not be recovered to its original value. However, using the ratio between these two total pressure values, the Mach number at front of the shock wave in the free stream can be calculated easily.

3.4.2 Boundary Layer of the Nozzle's Surface

When the Pitot gauge is in the subsonic region of the boundary layer, there is no shock wave produced in front of the Pitot gauge. But there is the obvious viscosity loss of the total pressure so that, even when there is no shock wave, the total pressure measured still can be much lower than the original value and the value in free stream, especially, after the starting stage. Using the total pressure distribution within the subsonic region of the boundary layer and the static pressure value which is a constant along the direction perpendicular to the surface of the model, the velocity within the subsonic region of the boundary layer can be determined.

When the Pitot gauge is in the supersonic region of the boundary layer, in front of the Pitot gauge, there is a shock wave. Thus there is shock wave loss of the total pressure as mentioned in the last section. In the meantime, there is the viscosity loss of the total pressure as mentioned above. Therefore the total pressure measured by the Pitot gauge still can not be recovered to its original value. In this situation there is the interaction between shock wave and boundary layer around the Pitot gauge so that the static pressure is not a constant any longer along the direction perpendicular to the surface of the model. Therefore it is more complicated and difficult to calculate the velocity distribution accurately. Fortunately, this region has a narrow window of opportunity and not important in our measurements.

3.4.3 Moving Shock Waves and Bow Shock Waves

When the normal shock wave which is formed in divergent section of the nozzle moves downstream, the strength of the shock wave will increase and the total pressure behind the shock wave will decrease. When the normal shock wave arrives at the front of the outlet of the Pitot gauge, it will become a standing and detached bow shock wave. All of this is an unsteady process. The history of the total pressure behind the shock wave can be partially observed when the shock wave moves near to the probe. A "vibration" of the trace appears on the photo of the total pressure history.

When the Pitot tube is in the subsonic region of the boundary layer, even if there is no shock wave in front of the Pitot tube (but in the supersonic region of the flow), a shock wave must sweep over the location of the gauge. This shock wave can still influence the pressure value in the subsonic region owing to the existence of a possible interaction between the shock wave and the boundary layer. Therefore, some changes of the trace still can be seen when the shock wave sweeps that location.

When the probe is in the boundary layer, during the starting stage, the total pressure goes down again after the shock wave sweeps. The reason is that the boundary layer is being formed during that period; the total pressure within the boundary layer should go down in the meantime owing to the viscosity loss of the total pressure. Correspondingly, during that period, a part of the gas in the Pitot gauge should go out again.

3.5 Optical System

The optical system used to collect the fluorescence signals from the test region is shown in Fig. 3.5.1. A laser light beam from

an argon ion laser at 488.0 nm wave length is split into three beams with the same diameter and the same intensity; they are separated by 1.5 mm. The cross section of the set of beams is a triangular form. The beams are sent through the free shear layer along the Y direction. The fluorescence light signals emitted from arranged measuring points are collected by sets of optical systems, then passed on to the photomultiplier tubes. A filter which can only allow the light with wave length longer than 5900 angstrom to pass is placed before the photomultiplier tubes to remove scattered laser light. The measuring points are arranged such that three dimensional velocity components can be obtained. The separation between the measuring points along each beam is 1.5 mm. By changing measuring locations along the X and Y directions, the turbulent behavior for different regimes inside the shear layer can be obtained. The spatial resolution of the measurement mainly depends on the separation between the measuring points, and this has been limited because of the vibration of incident laser beams causing by the vibration of the optical table.

3.6 Density Calibration

In general, the NO_2 spectrum extends from 800 nm to near 400 nm and this entire 400 nm region contains a very high density of lines. Within the range 570 nm to 670 nm the spectrum is mainly the vibronic bands (Richard E. Smally, 1975). In our measurement, the NO_2 molecules, which are mixed with N_2, provide a target for the incident light and are pumped to vibrational excitation states by an Argon ion laser with a 488 nm light beam. The intensity of the fluorescence emitted by NO_2

molecules depends on the density of the NO_2 molecules in the flow and the intensity of incident laser beam. The intensity signals collected by the photomultiplier tubes represent the local density of NO_2 molecules which is mixed with N_2 as the flow gas. Therefore, the density or density fluctuation of NO_2 represent the flow density or density fluctuation.

For a certain percentage of NO_2 filling in the flow gas and the power of incident laser beam, the intensity of fluorescence is a function of density. This is shown in Figure 3.6.1. The function of $I=I(\rho)$ can be obtained from the data fit shown in Figures 3.6.2 and 3.6.3. The results of data fitting show that the function is an exponential, i.e., the intensity of emitted fluorescence decays exponentially as the density of NO_2 increases. The fact that the intensity of fluorescence decreases when the density of NO_2 increases can be explained by the interactions between the NO_2 molecules. The NO_2 molecule is excited to a higher energy level by incident laser light; if it interacts with another NO_2 molecule before falling back to a lower energy level and radiating fluorescence light, it can transfer energy to another molecule. Therefore, the higher concentration of NO_2 molecules, the larger the number of interactions of NO_2 molecules, and the greater the likelihood that energy will transfer to unexcited molecules and result in a decreasing fluorescence. The relation between density and intensity is called the calibration relation. For a different percentage of NO_2, the calibration is shifted but the functional relation between intensity of fluorescence and the density is unchanged.

Figure 3.6.4 shows that the intensity of fluorescence is also the function of the power of incident laser beam. When the laser output power increases, the emitted fluorescence intensity increases. There is a bending point of laser power, P_0; for $P<P_0$ the relation between the intensity of fluorescence and the laser power is linear; for $P>P_0$ the relation is not longer linear and it shows a saturation behavior. For a different density of NO_2, the intensity of fluorescence is different and the bending point, P_0, is also different. The higher the density of NO_2, the smaller the value of P_0. This feature is showing in Fig. 3.6.3. It is obvious that in our experiments the intensity of incident laser beam should remain within the linear range.

For multi-channel measurements, extra care is taken in the calibrations. For different channels, the intensity at focusing point of the laser beam can hardly be exactly the same, and the sensitivities of the photomultiplier tubes are also slightly different. Therefore, it is necessary that each channel be calibrated independently in order to get the calibration curve for each channel. Examples of the small differences in calibration curves are shown in Fig. 3.6.4.

The measured intensity history signals therefore provide the density histories. The time history fluctuation signals give the turbulent fluctuations in the free shear flow at different spatial locations. By using the calibration curves those intensity histories can be converted into density histories as shown in Fig. 3.6.5. Since the NO_2 gas is mixed the N_2 gas as the flow gas, the local point density fluctuation of NO_2 represents the local density fluctuation

of the flow; therefore, the turbulent density properties of the free shear layer are obtained. This conversion, using calibration curves such as those shown in Fig. 3.6.3, is illustrated in Fig. 3.6.5.

3.7 Velocity Calculation

The mean flow at the exit region of the nozzle can be considered as one dimensional flow. For such moving flow the energy balance equation is

$$q+p_1 v_1 - p_2 v_2 = (e_2 + \frac{1}{2}u_2^2) - (e_1 + \frac{1}{2}u_1^2)$$

where q is the heat quantity transferred to the system.

For supersonic flow generated by our Ludwieg tube the duration time is 15 ms, the sample rate of measuring is 500 ns and the Reynolds number is as high as 10^8; therefore, the process can be considered isentropic process. Since the percentage of NO_2 is low, the gas of flow still can be considered as an ideal gas, then

$$h_2 + \frac{1}{2}u_2^2 = h_1 + \frac{1}{2}u_1^2$$

where h = h (T)

If the experimental temperature T and pressure p satisfy

$$Tc << T << \vartheta_v$$

$$p << p_c$$

the energy equation can be written as

$$C_p T + \frac{1}{2}u^2 = C_p T_0 \qquad (1)$$

Together with the sound speed equation we can rewrite the equation (1)

$$a^2 = (\frac{\partial p}{\partial \rho})_s = \gamma R T$$

$$\frac{1}{2}u^2 + \frac{a^2}{\gamma - 1} = \frac{a_0^2}{\gamma - 1}$$

or

$$\frac{\rho_0}{\rho} = (1 + \frac{\gamma - 1}{2} M^2)^{\frac{1}{\gamma - 1}} \qquad (2)$$

$$M = \frac{u}{c}$$

For isentropic flow the local frozen value ρ_0 equals the initial frozen value. When the the density, ρ, is measured from the experiment, the free stream velocity can be calculated from above equations.

For turbulent shear layers, the 3 - dimensional situation should be considered. If the Reynolds number is high and the measuring time is short (in our case the Reynolds number is in 10^8, and the sample time of measurement is 500 ns), we can consider the flow is inviscid and nonconducting. The energy equation in such flow is

$$\rho f_i u_i + \rho q - \frac{\partial}{\partial x_i}(p u_i) = \frac{\partial}{\partial t}(\rho e + \frac{1}{2}\rho u^2) + \frac{\partial}{\partial x_j}[(\rho e + \frac{1}{2}\rho u^2)u_j] \qquad (3.7.3)$$

where f_i is external force per unit mass.

By using the Eulerian derivative

$$\frac{D}{Dt} \equiv \frac{\partial}{\partial t} + u_k \frac{\partial}{\partial x_k}$$

the energy equation can be written in two parts

$$\rho \frac{D}{Dt}\left(\frac{1}{2}u^2\right) = -u_i \frac{\partial p}{\partial x_i} + \rho f_i u_i \tag{3.7.4}$$

$$\frac{De}{Dt} + p\frac{D}{Dt}\left(\frac{1}{\rho}\right) = q \tag{3.7.5}$$

The total enthalpy is

$$\frac{D}{Dt}\left(h + \frac{1}{2}u^2\right) = q + f_i u_i + \frac{1}{\rho}\frac{\partial p}{\partial t}$$

For ideal gas

$$h + \frac{1}{2}u^2 = C_p T + \frac{1}{2}u^2$$

the first and second terms in the total enthalpy equation can be consider zero. Then

$$\frac{D}{Dt}\left(C_p T + \frac{1}{2}u^2\right) = \frac{1}{\rho}\frac{\partial p}{\partial t} \tag{3.7.6}$$

From the above equations and the isentropy relation

$$\frac{p}{p_0}=(\frac{\rho}{\rho_0})^{\gamma}=(\frac{T}{T_0})^{\frac{\gamma}{\gamma-1}}$$

we get the equation from which the three component of velocities can be calculated.

$$C_p\frac{\partial T}{\partial t}+[C_pT_0(\frac{1}{\rho_0})^{\frac{\gamma-1}{\gamma}}\frac{\gamma-1}{\gamma}(p)^{-\frac{1}{\gamma}}-\frac{1}{\rho}]u_i\frac{\partial p}{\partial x_i}=\frac{1}{\rho}\frac{\partial p}{\partial t} \qquad (3.7.7)$$

From the isentropy relation the pressure, p, and the temperature, T, can be calculated when the density, ρ, is measured. Since the multi-point measurements are set such that three dimensional local density histories are obtained, the time and space derivatives of density, pressure, and temperature can be calculated from measured quantities. Specifically, the x component of Navier-Stokes equation in inviscid and nonconducting flow is

$$\frac{\partial u_1}{\partial t}+u_1\frac{\partial u_1}{\partial x_1}+u_2\frac{\partial u_1}{\partial x_2}+u_3\frac{\partial u_1}{\partial x_3}=-\frac{1}{\rho}\frac{\partial P}{\partial x_1} \qquad (3.7.8)$$

From equation (2), (7), and (8) the three components of velocity can be obtained.

The flow in our free shear layer is predominantly two dimensional. Therefore, for our study, the two dimensional velocity components (streamwise and transverse components) are calculated. Figures 3.7.1 to 3.7.7 show the streamwise velocities at different x locations. In each plot seven channel measurements

were taken along different transverse locations separated from each other by 1.5 mm. Figures 3.7.1 and 3.7.2 show some negative velocities; at positions lower than the low edge of the shear layer and near the nozzle's lip the flow moves in opposite direction to that of the main flow. Figure 3.7.8 shows the transverse velocities at 2.5 cm downstream from the nozzle's lip and at different transverse locations. Figure 3.7.9 shows the spatial development of the transverse profile of mean streamwise velocities. The velocity profile across the shear layer provides a shear flow picture which will be used to understand the turbulent structure of the shear layer.

3.8 The Calculation of Reynolds Number at the Outlet of the Nozzle of Ludwieg Tube during the Measuring Time

The stagnation pressure of the flow at the outlet section of the nozzle during the measuring time is $P_0=P_4$ and the stagnation temperature of the flow at the outlet section of the nozzle during the measuring time $T_0=T_4=T_a$. The density, velocity, and Reynolds number in the free shear layer can be written as

$$\rho = \frac{P_4}{T_a R'}\left(1+\frac{\gamma-1}{2}M^2\right)^{-1/(\gamma-1)}$$

$$v = M\sqrt{\gamma R T_a\left(1+\frac{\gamma-1}{2}M^2\right)^{-1}}$$

where $R = 8.31\ J\ mol^{-1}\ K^{-1}$, $R' = 2.841\ atm\ cm^3\ Kg^{-1}$

$$R_e/D = \frac{\rho v}{\mu}$$

$$= 0.3293 \times 10^7 \{ (P_4 (1 + \frac{\gamma-1}{2} M^2)^{-1/(\gamma-1)}$$

$$M \sqrt{\frac{1}{T_a^3 (1 + \frac{\gamma-1}{2} M^2)^{-1}} [T_a (1 + \frac{\gamma-1}{2} M^2)^{-1} + 110.6]} \} \text{ cm}^{-1}$$

Generally, $R_e/D = R_e/D\ (P_4, T_a, M)$ and $M = M(A^*/A_{outlet})$. Therefore,

$$R_e/D = R_e/D\ (P_4, T_a, A^*/A_{outlet})$$

where

$$\frac{A^*}{A_{outlet}} = \frac{M}{[\frac{2}{\gamma+1}(1+\frac{\gamma-1}{2}M^2)]^{\gamma+1/2(\gamma-1)}}$$

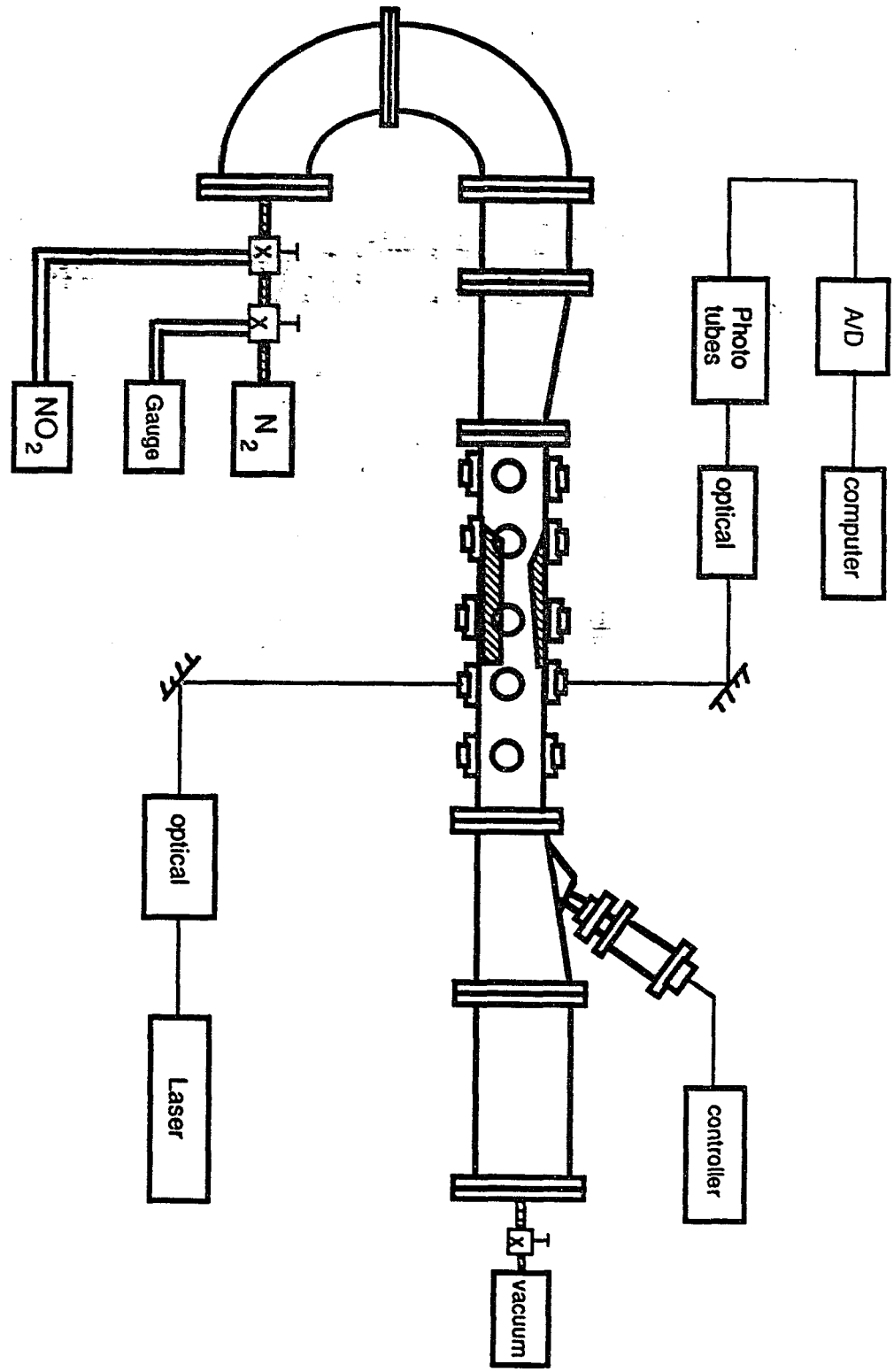

Fig. 3.1.1 Schematic of the Ludwieg tube-wind-tunnel

X (mm)	5	10	15	20	25	30	35
SR	.740	.727	.714	.701	689	.676	.663
D (mm)	2.45	3.10	3.90	4.65	6.35	8.65	9.80

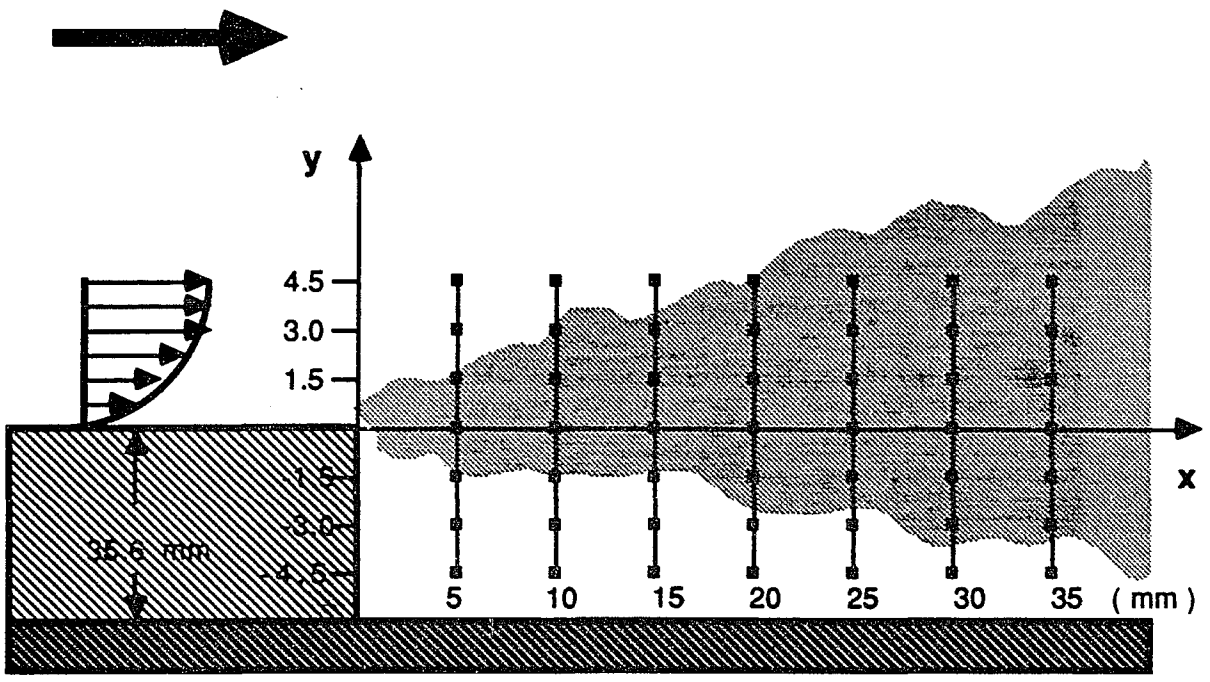

Fig. 3.1.2 Schematic of the free shear layer at the outlet region of nozzle and meassuring alignments.

α --- The angle between the boundary of the shear flow and the axis of shear layer

θ --- The angle between the shocklet and the axis of the shear layer

σ --- The angle between the boundary of the shear layer and the axis of the shear layer

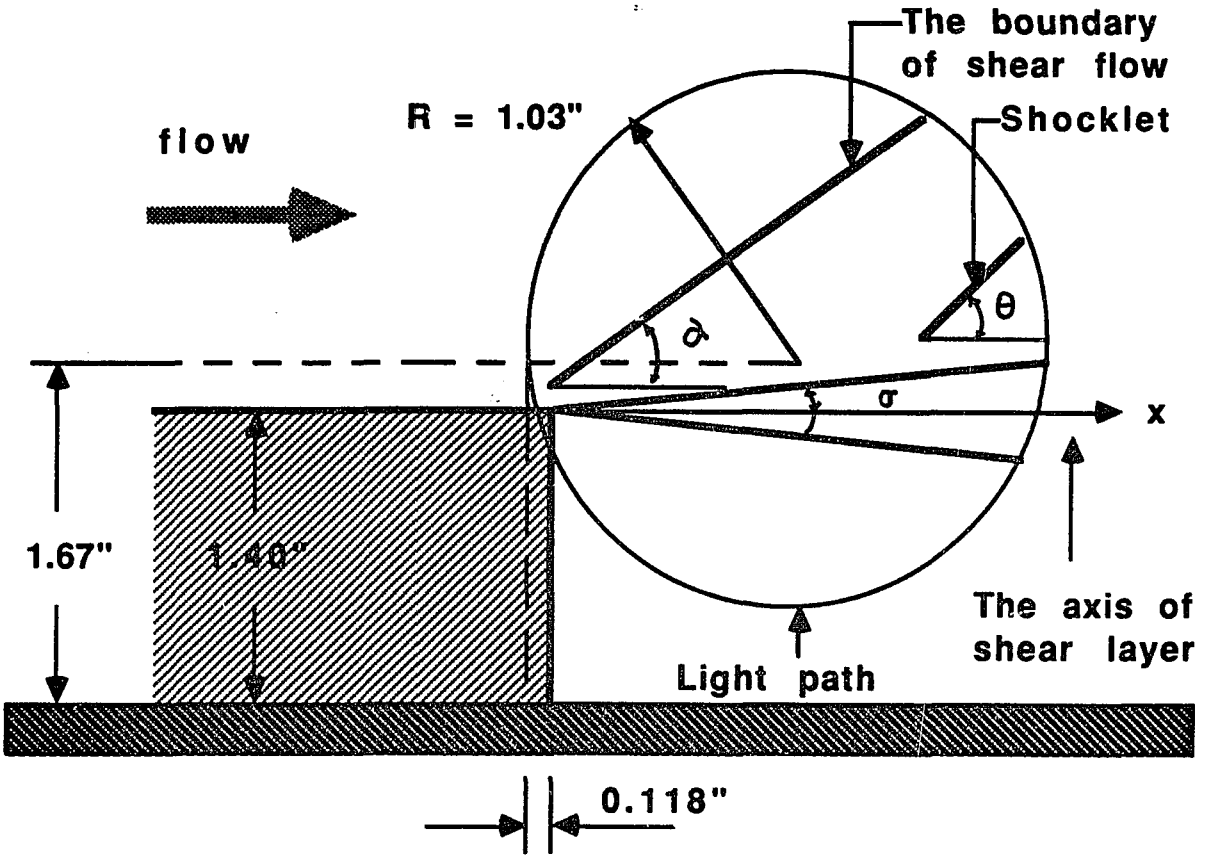

Fig. 3.1.3 Schematic of the measuring region in the shear flow

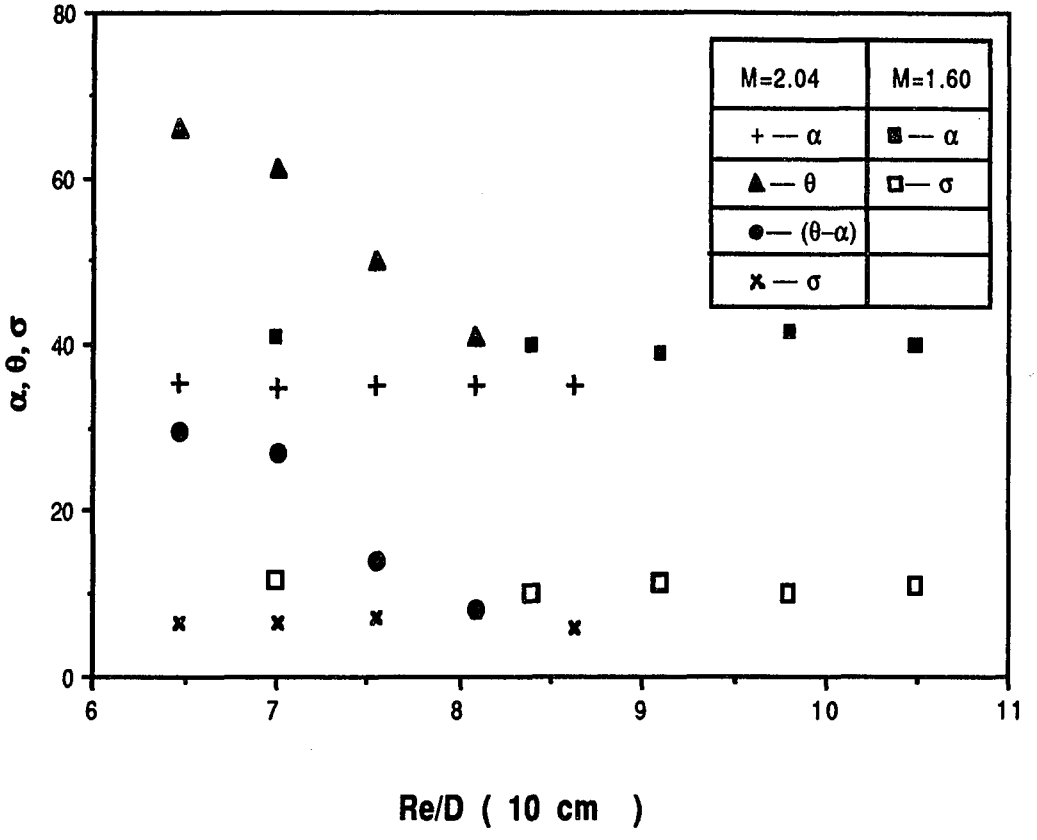

Fig. 3.1.4 The relationship between Reynolds number and slop of the boundary of the shear flow

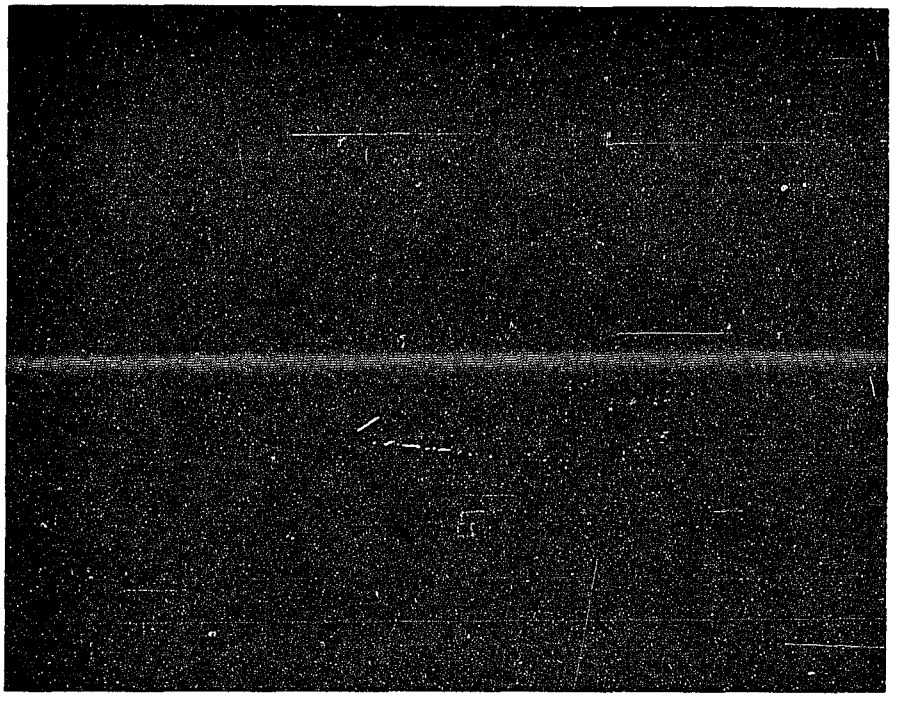

Fig. 3.2.1 Shadowgraph picture of nozzle outlet flow with flow pressure larger than back pressure $P_f > P_b$.

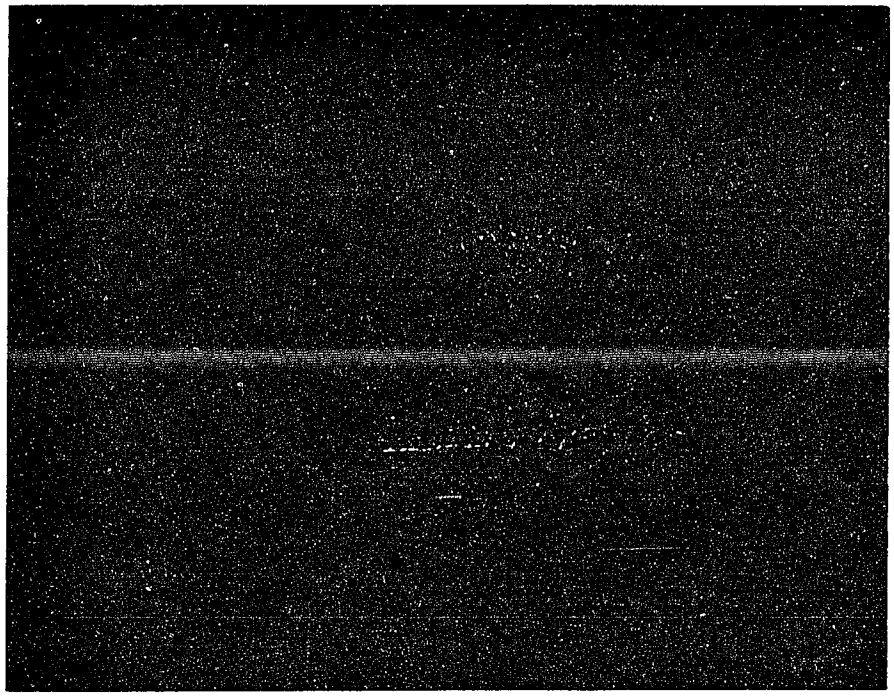

JS4,

Fig. 3.2.2 Shadowgraph picture of nozzle outlet flow with flow pressure equal to back pressure $P_f = P_b$.

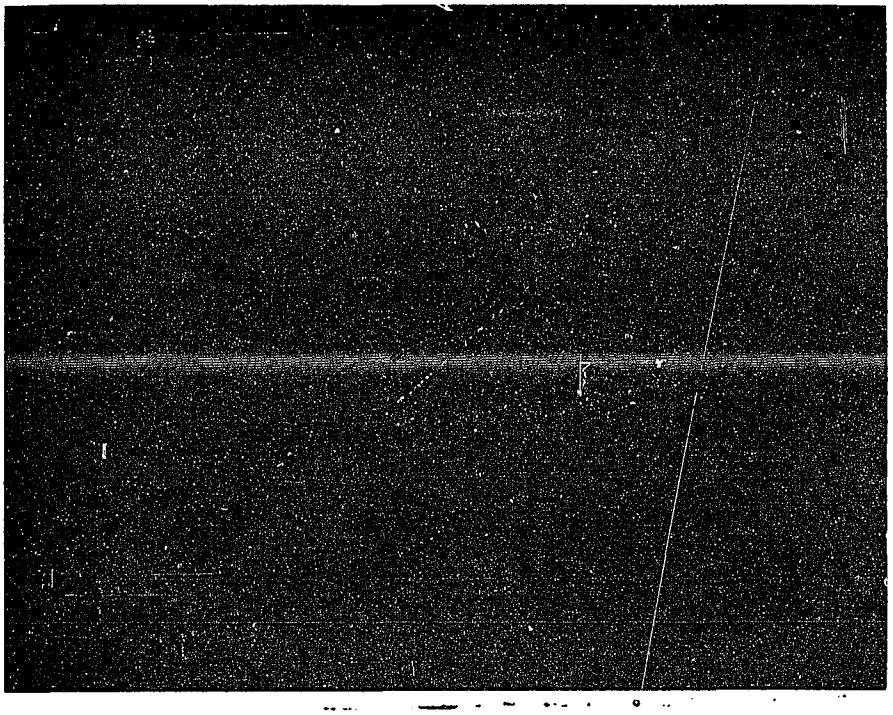

6

Fig. 3.2.3 Shadowgraph picture of nozzle outlet flow with flow pressure less than back pressure $P_f < P_b$.

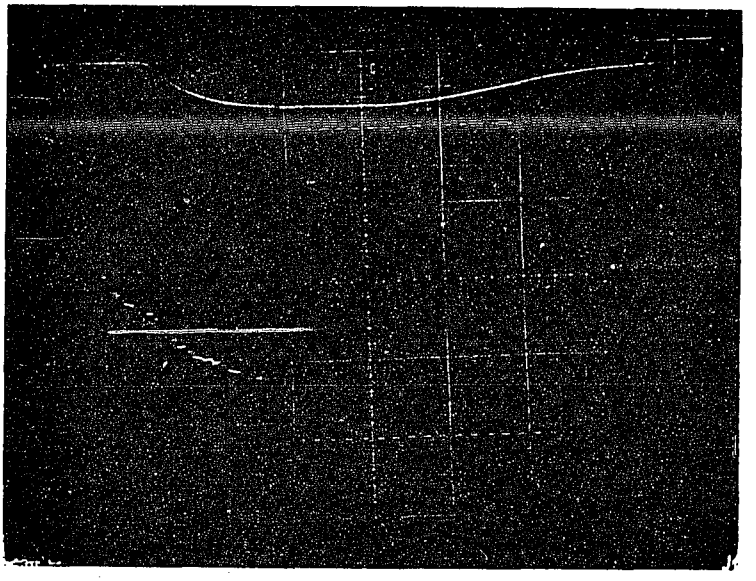

Fig. 3.4.1 A typical history of downstream and upstream static pressure of the nozzle.

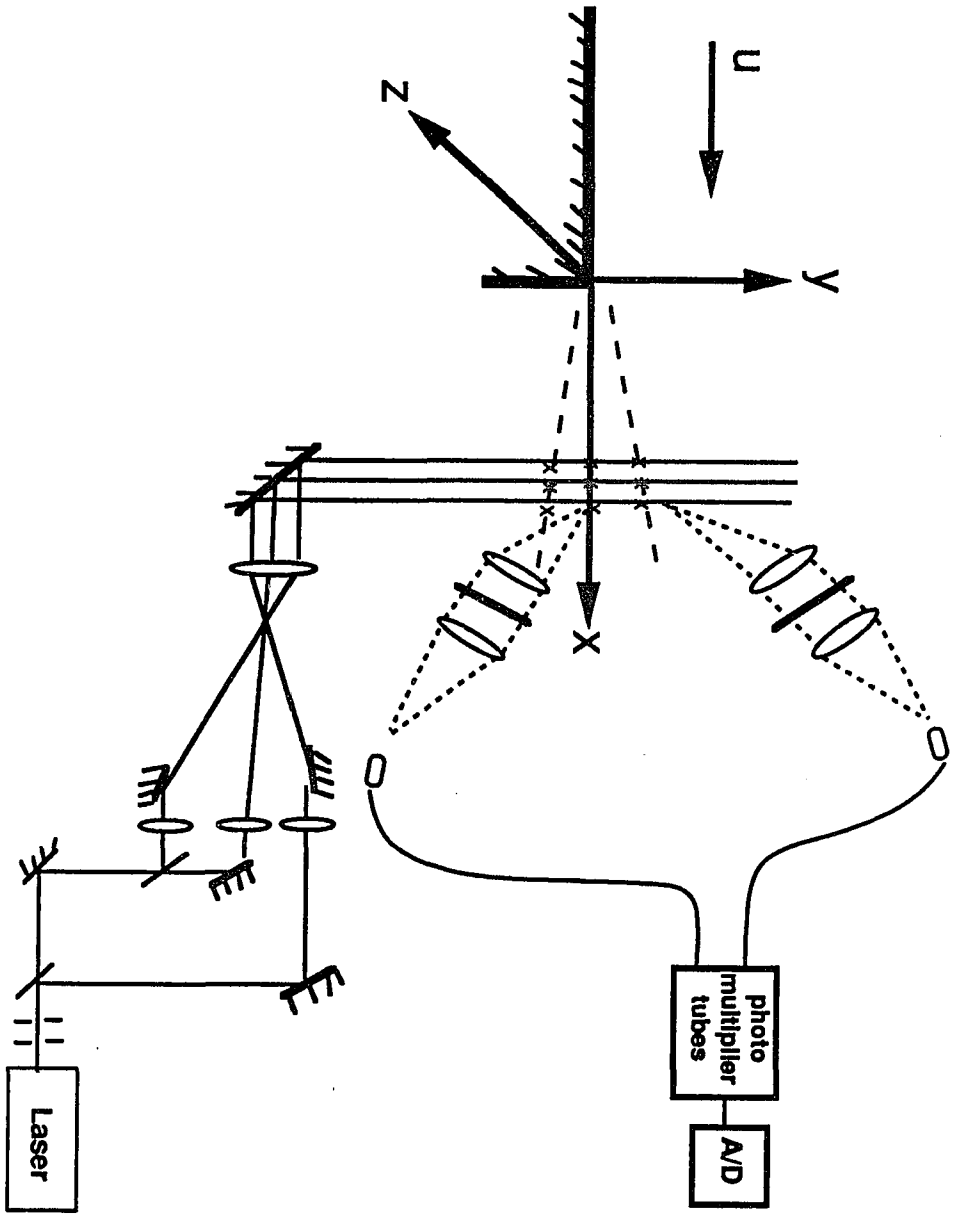

Fig. 3.5.1 Schematic of the optical system for fluorescence measurements

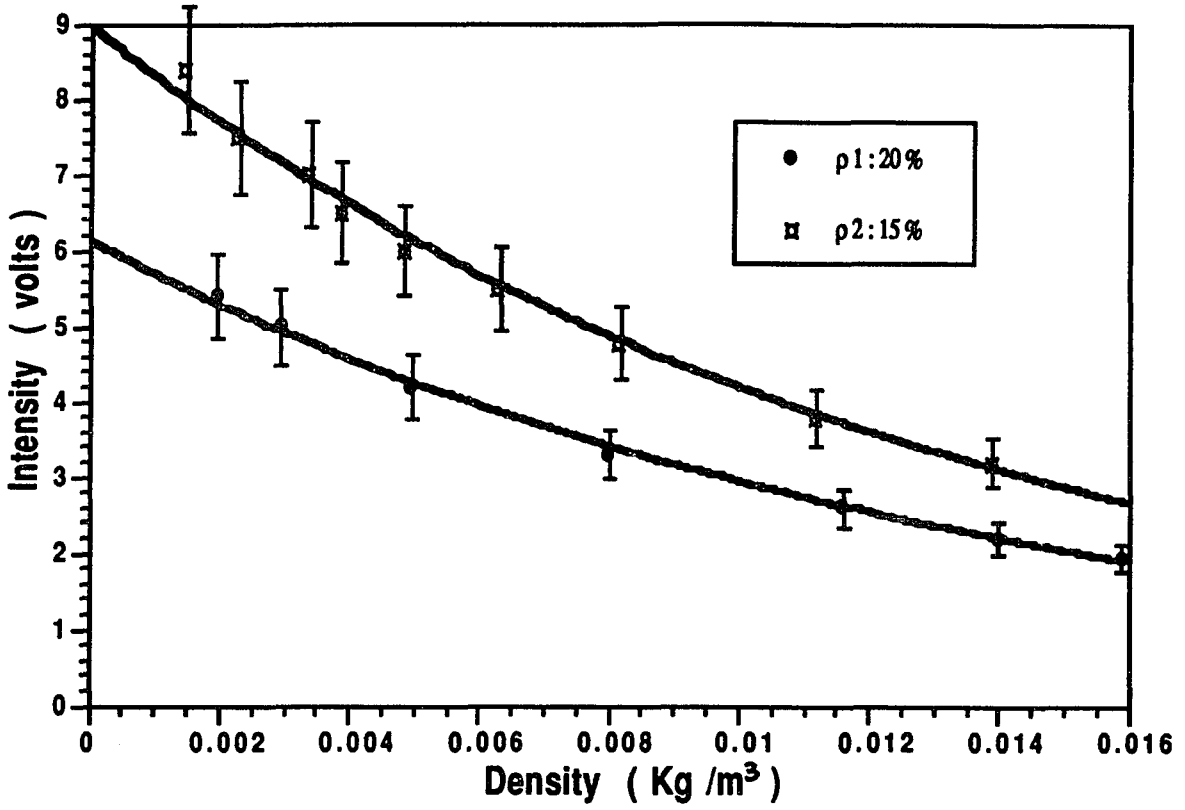

Fig. 3.6.1 Intensity of fluorescece varies with the density of NO_2 and different percentage of NO_2.

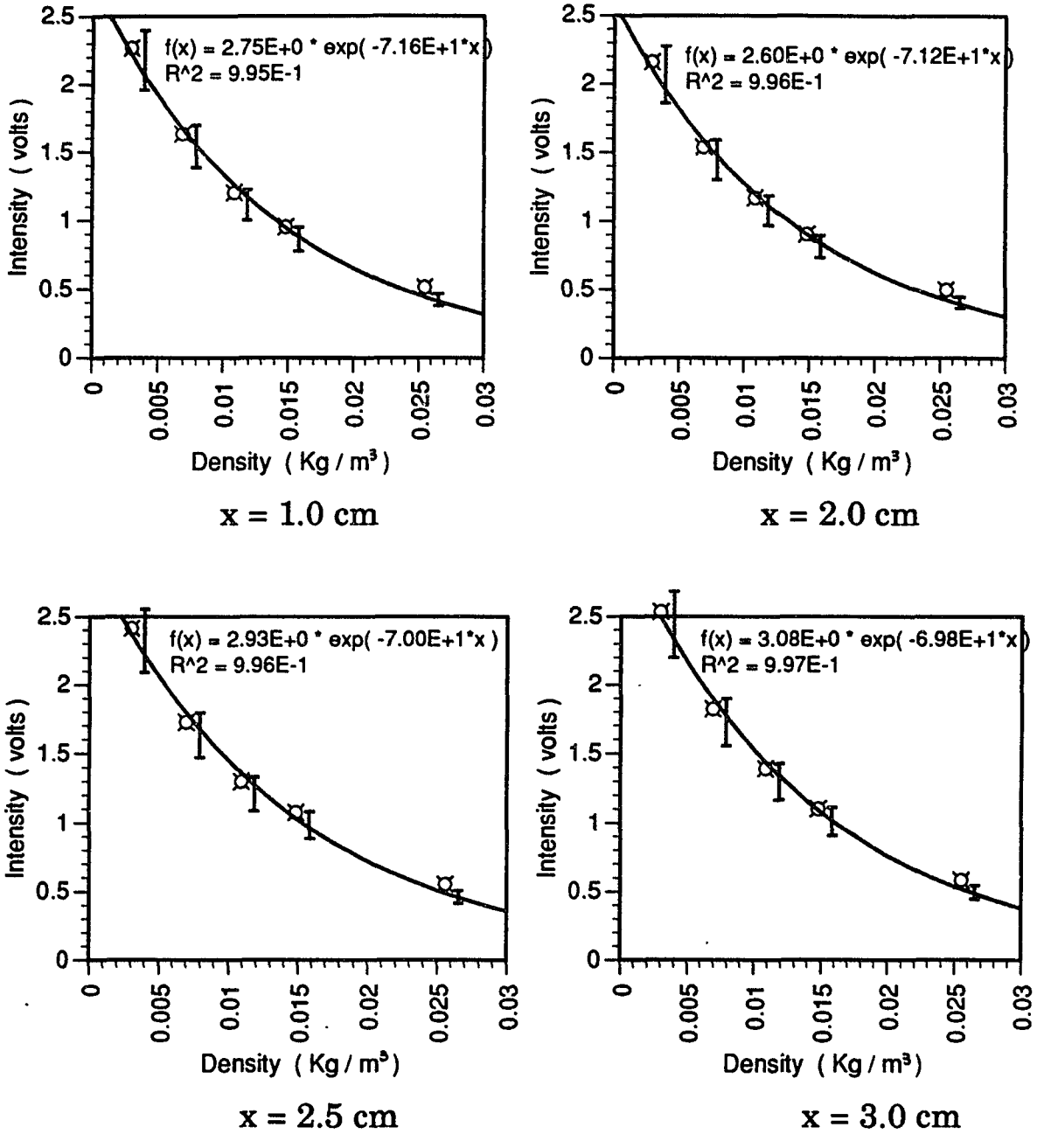

Fig. 3.6.2 The calibration curves for fluorescence signal at y = 1.5 mm and different streamwise locations

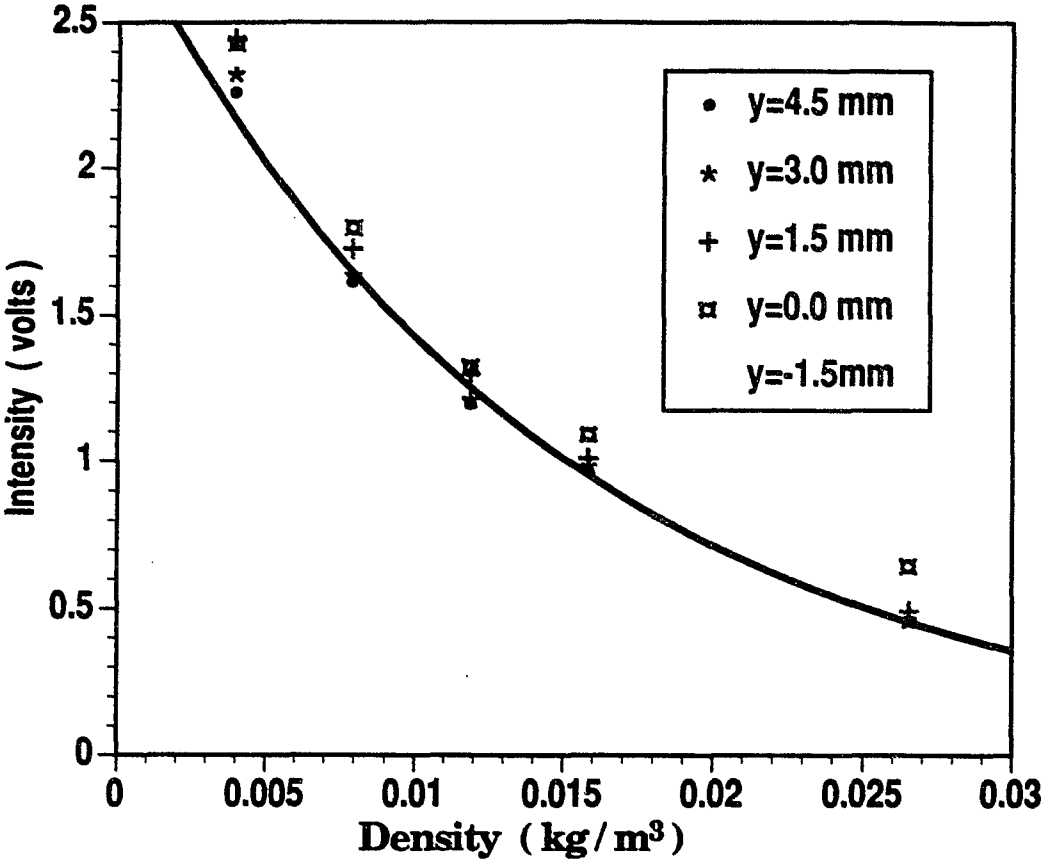

Fig. 3.6.3 The calibration curve for 2% NO2 at different transverse locations and 1.5 cm downstream from the nozzle's lip.

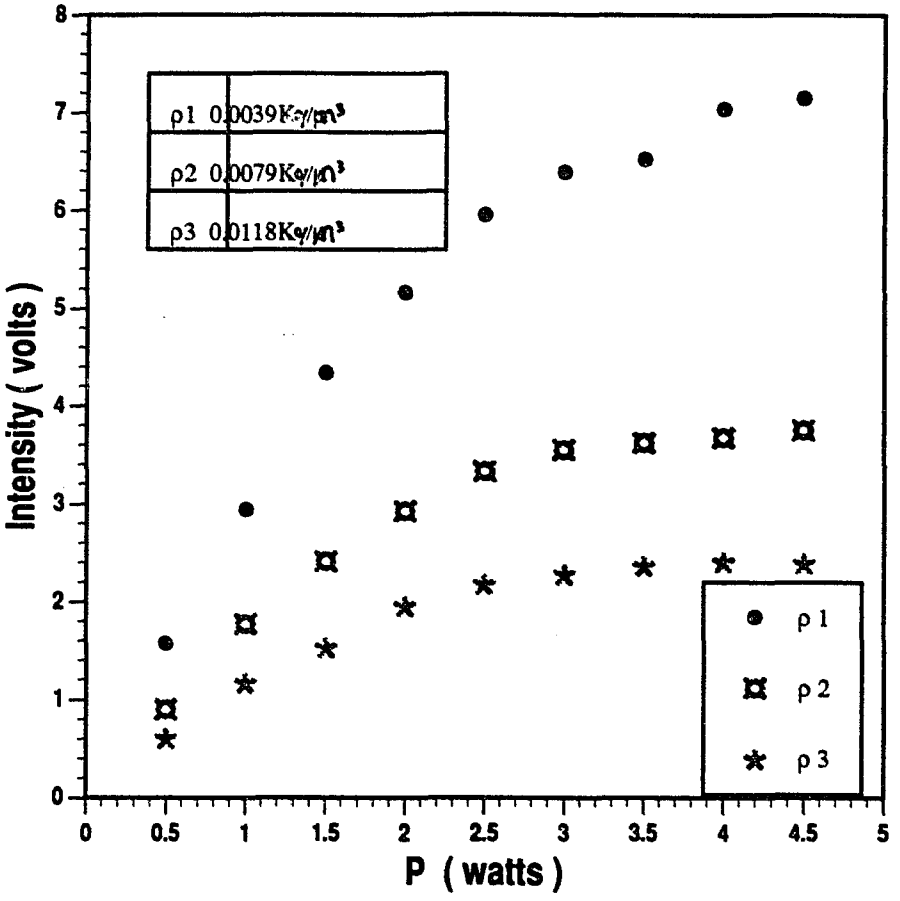

Fig. 3.6.4 The linear calibration of incident laser powerand the output intensity of NO_2 fluorescence.

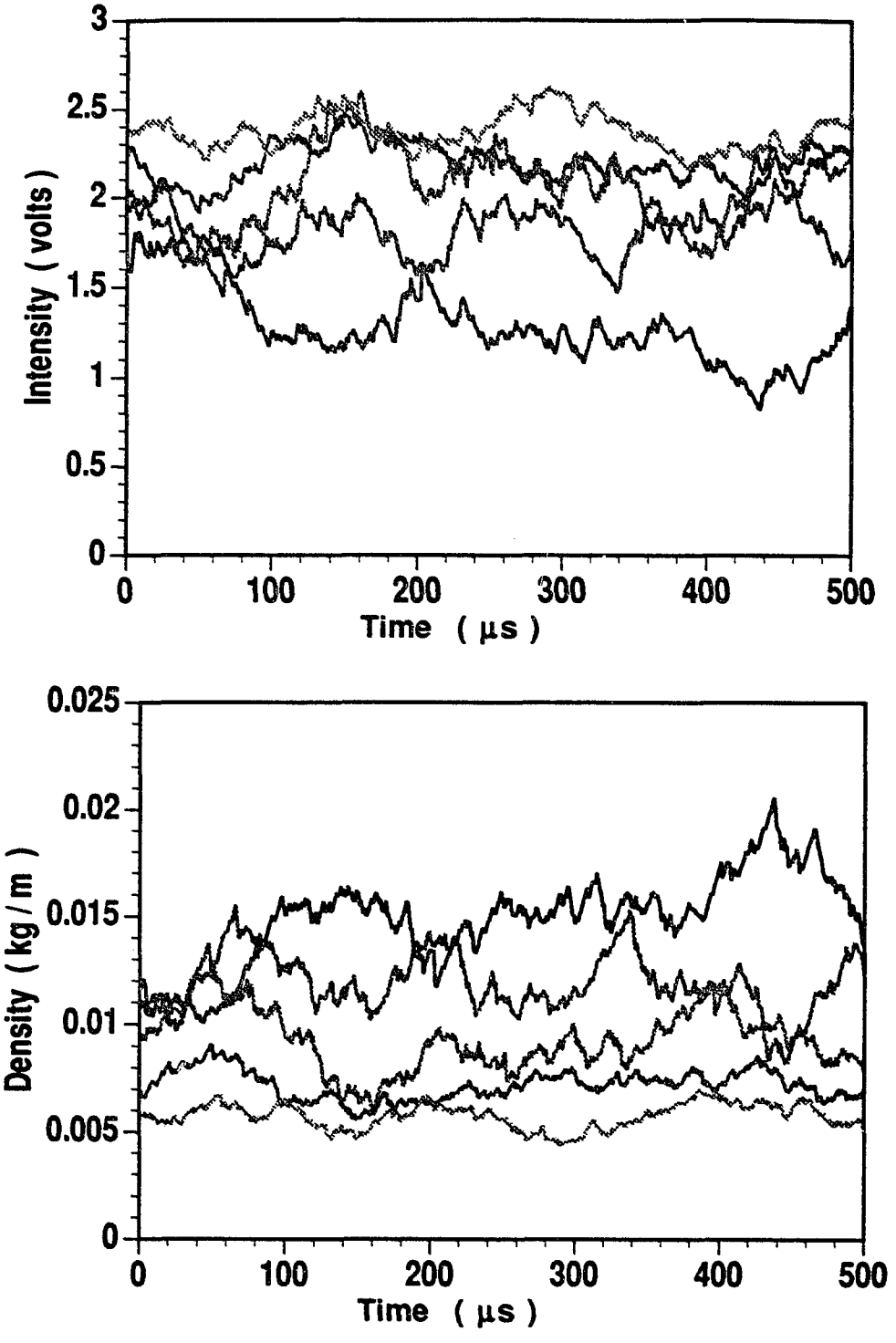

Fig. 3.6.5 The conversion from intensity of fluorescence to density of the fluorescence

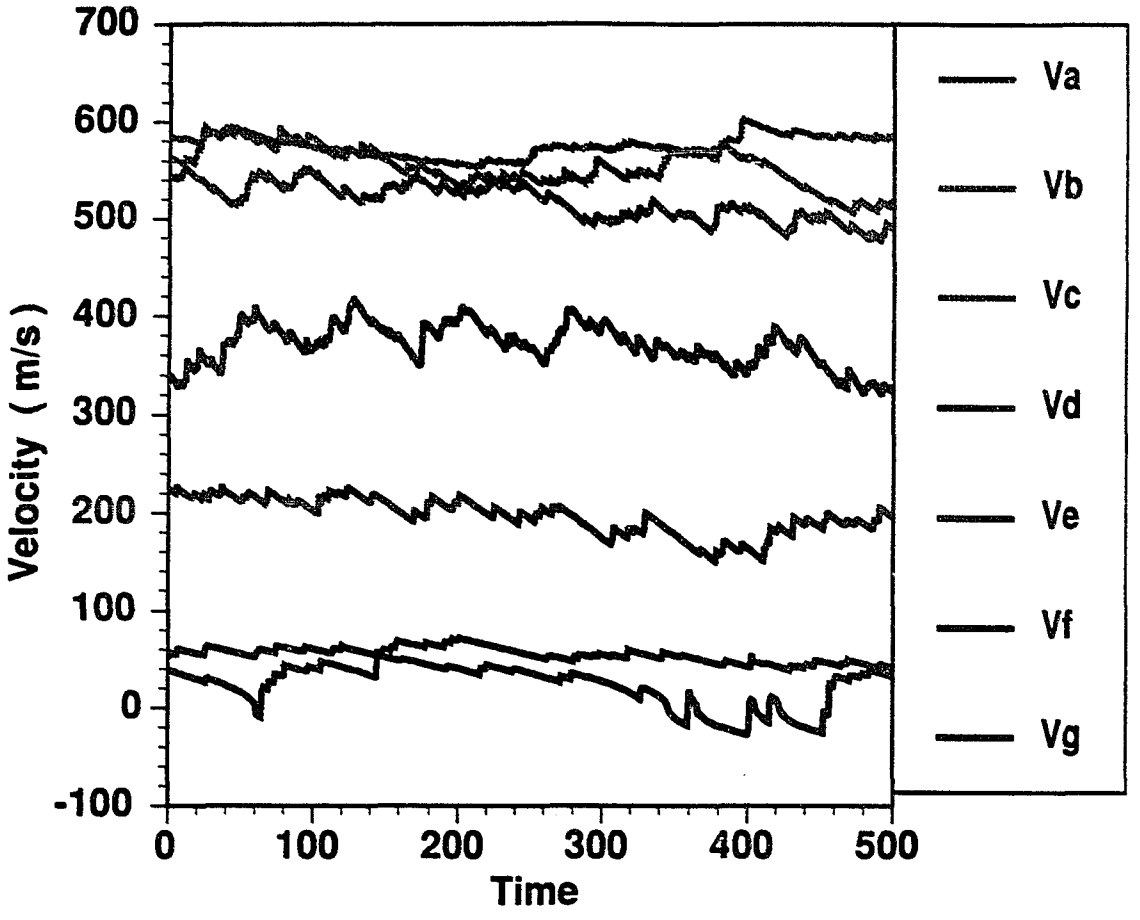

Fig. 3.7.1 Streamwise velocity at x = 0.5 cm downstream from the nozzle's lip. Va, Vb, Vc, Vd, Ve, Vf and Vg correspond to Y = 4.5 mm, 3.0 mm, 1.5 mm, 0.0 mm, -1.5 mm, -3.0 mm, and -4.5 mm.

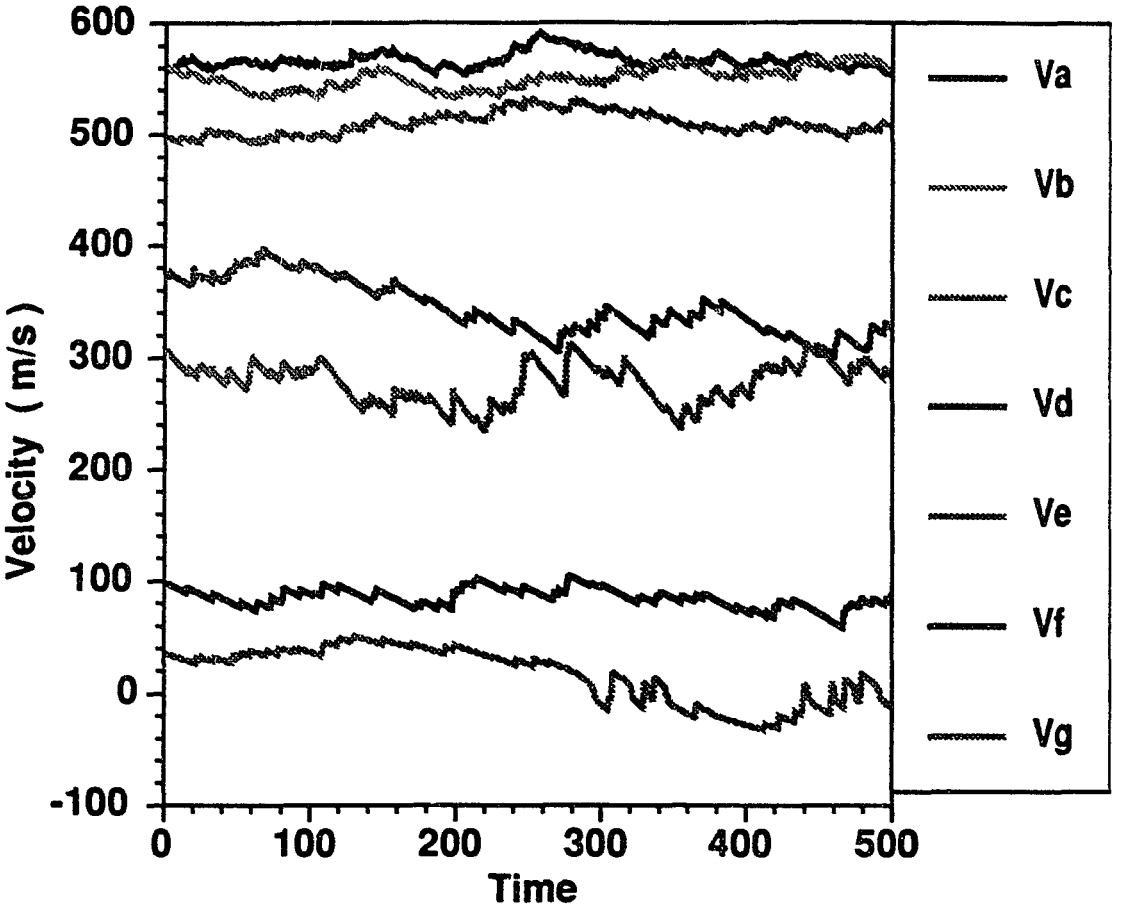

Fig. 3.7.2 Streamwise velocity at x = 1.0 cm downstream from the nozzle's lip. Va, Vb, Vc, Vd, Ve, Vf and Vg correspond to Y = 4.5 mm, 3.0 mm, 1.5 mm, 0.0 mm, -1.5 mm, -3.0 mm, and -4.5 mm.

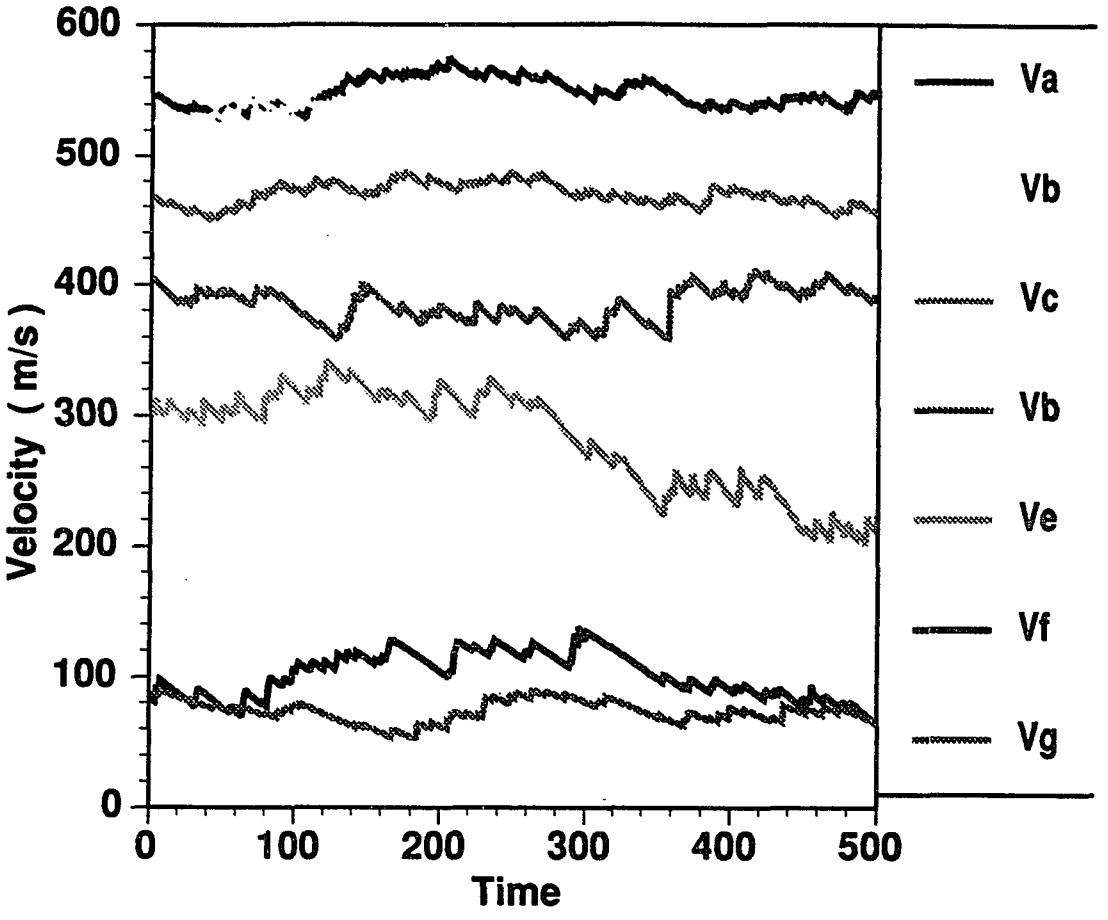

Fig. 3.7.3 Streamwise velocity at x = 1.5 cm downstream from the nozzle's lip. Va, Vb, Vc, Vd, Ve, Vf and Vg correspond to Y = 4.5 mm, 3.0 mm, 1.5 mm, 0.0 mm, -1.5 mm, -3.0 mm, and -4.5 mm.

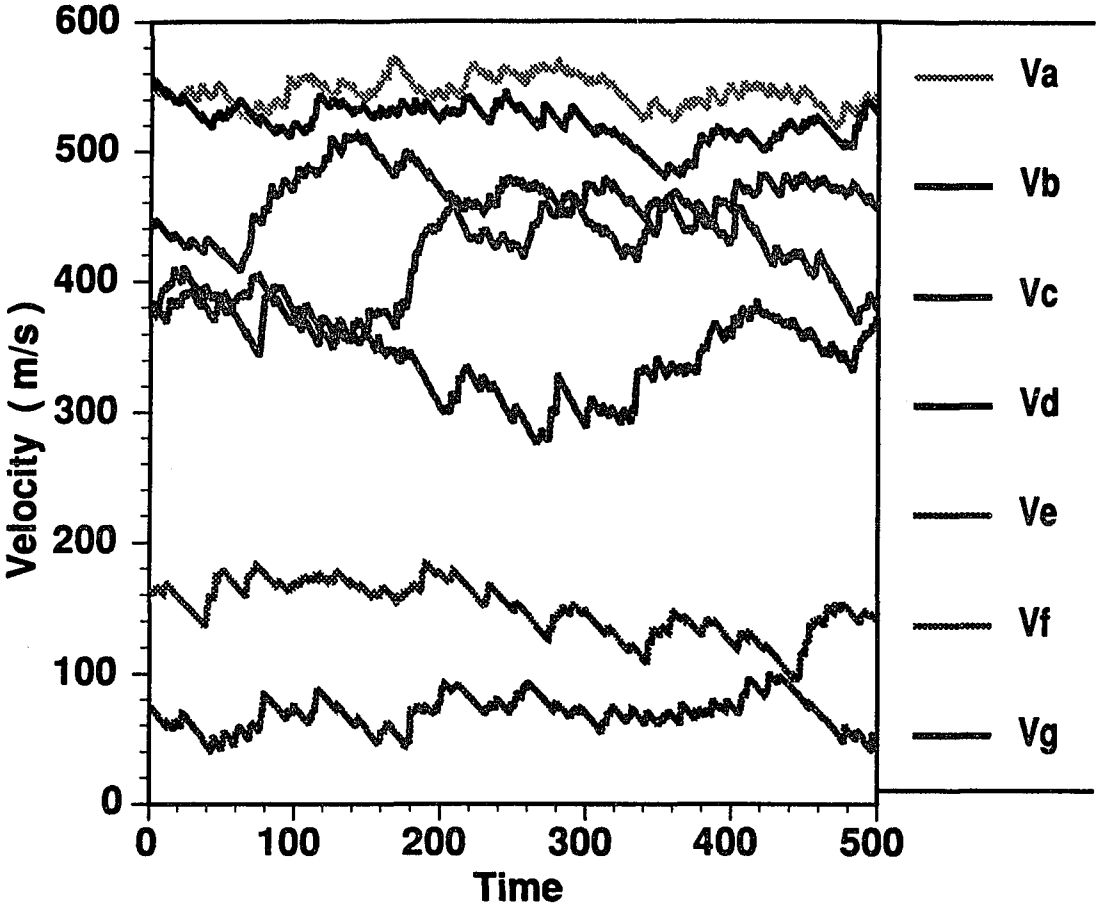

Fig. 3.7.4 Streamwise velocity at x = 2.0 cm downstream from the nozzle's lip. Va, Vb, Vc, Vd, Ve, Vf and Vg correspond to Y = 4.5 mm, 3.0 mm, 1.5 mm, 0.0 mm, -1.5 mm, -3.0 mm, and -4.5 mm.

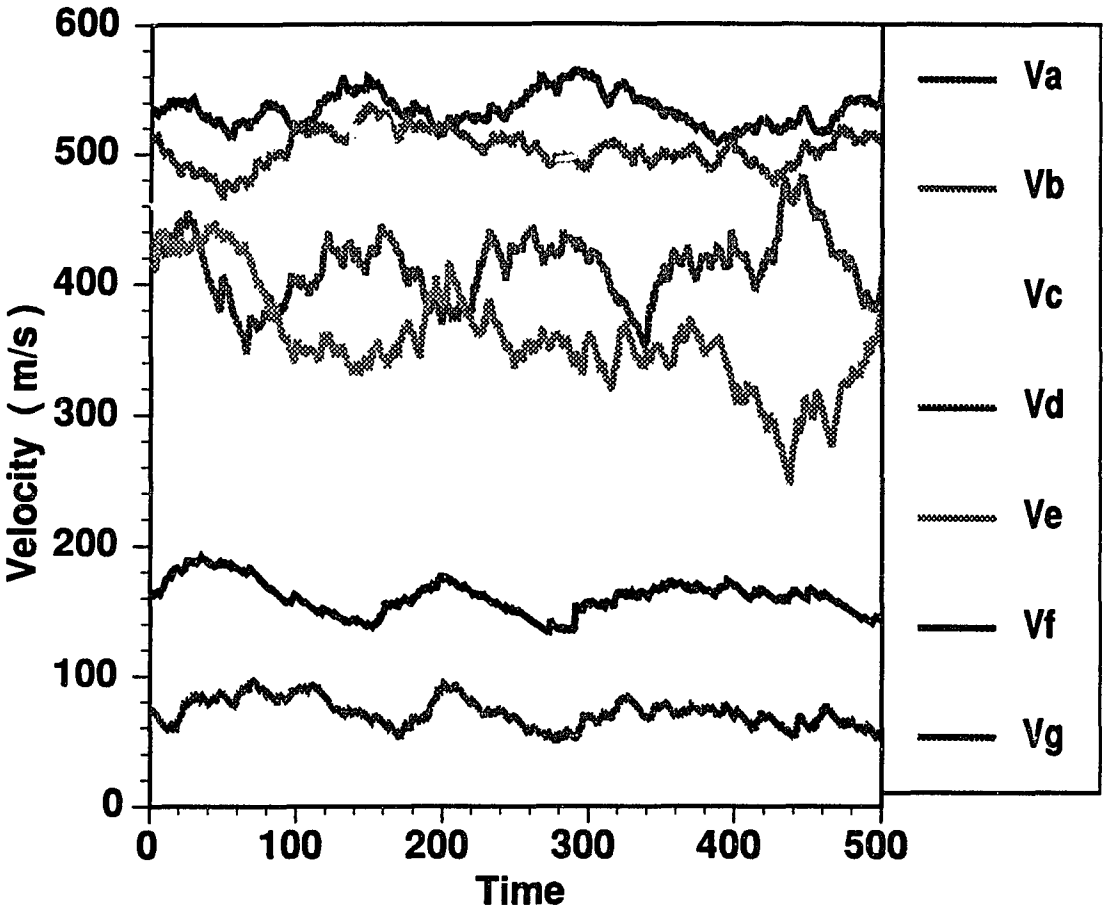

Fig. 3.7.5 Streamwise velocity at x = 2.5 cm downstream from the nozzle's lip. Va, Vb, Vc, Vd, Ve, Vf and Vg correspond to Y = 4.5 mm, 3.0 mm, 1.5 mm, 0.0 mm, -1.5 mm, -3.0 mm, and -4.5 mm.

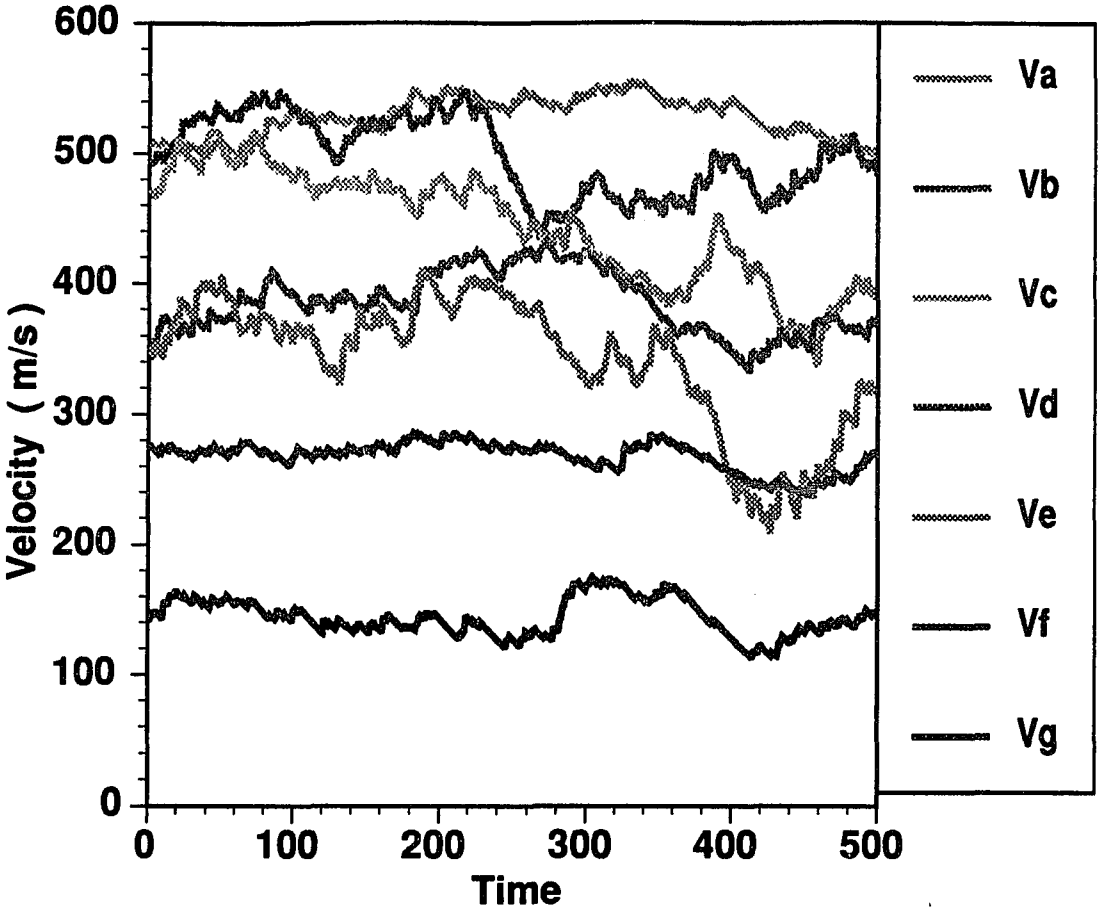

Fig. 3.7.6 Streamwise velocity at x = 3.0 cm downstream from the nozzle's lip. Va, Vb, Vc, Vd, Ve, Vf and Vg correspond to Y = 4.5 mm, 3.0 mm, 1.5 mm, 0.0 mm, -1.5 mm, -3.0 mm, and -4.5 mm.

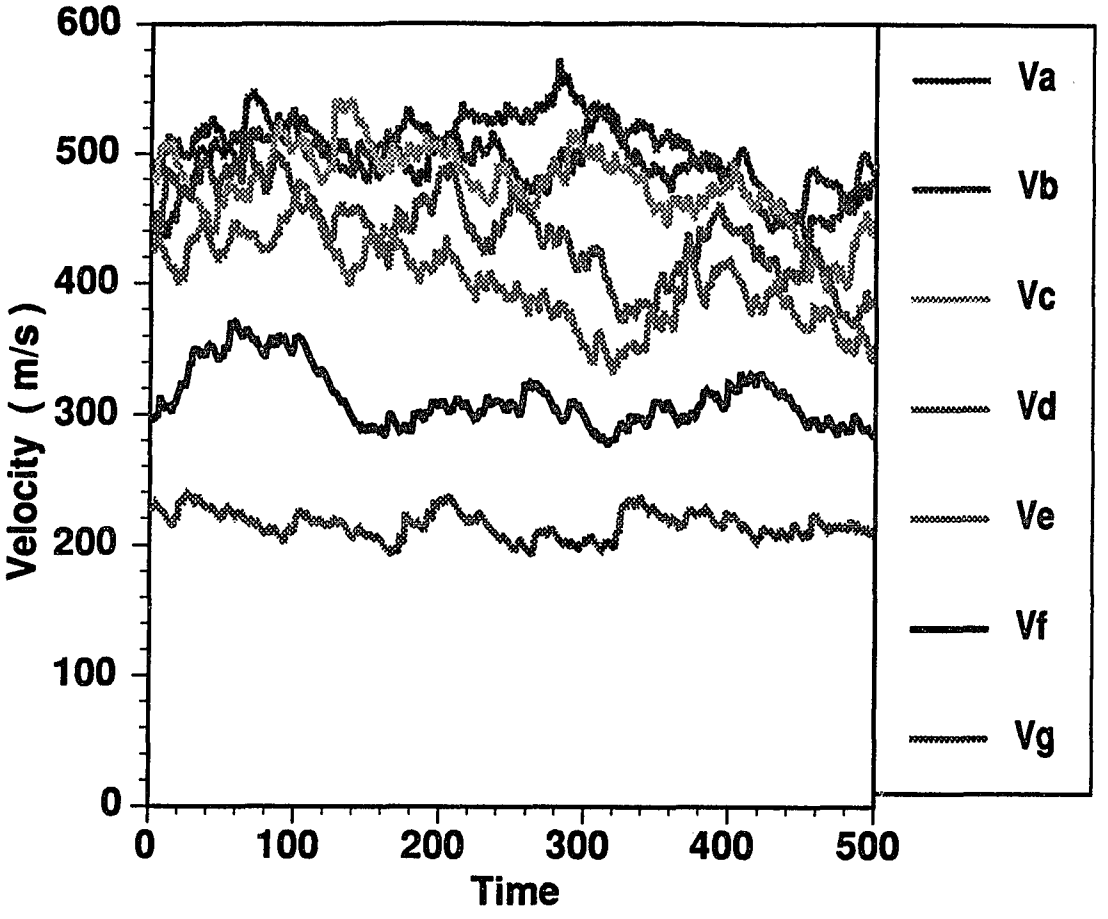

Fig. 3.7.7 Streamwise velocity at x = 3.5 cm downstream from the nozzle's lip. Va, Vb, Vc, Vd, Ve, Vf and Vg correspond to Y = 4.5 mm, 3.0 mm, 1.5 mm, 0.0 mm, -1.5 mm, -3.0 mm, and -4.5 mm.

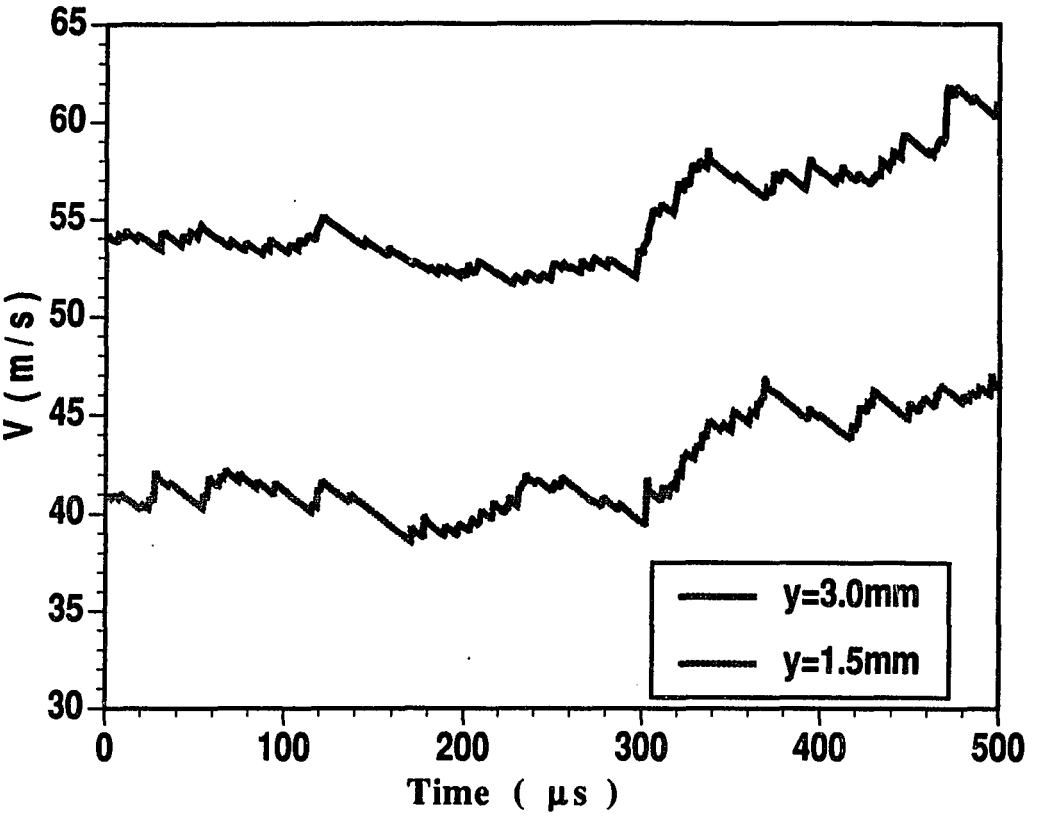

Fig. 3.7.8 The transverse velocity histories at 2.5 cm downstream from the nozzle's lip and different y locations

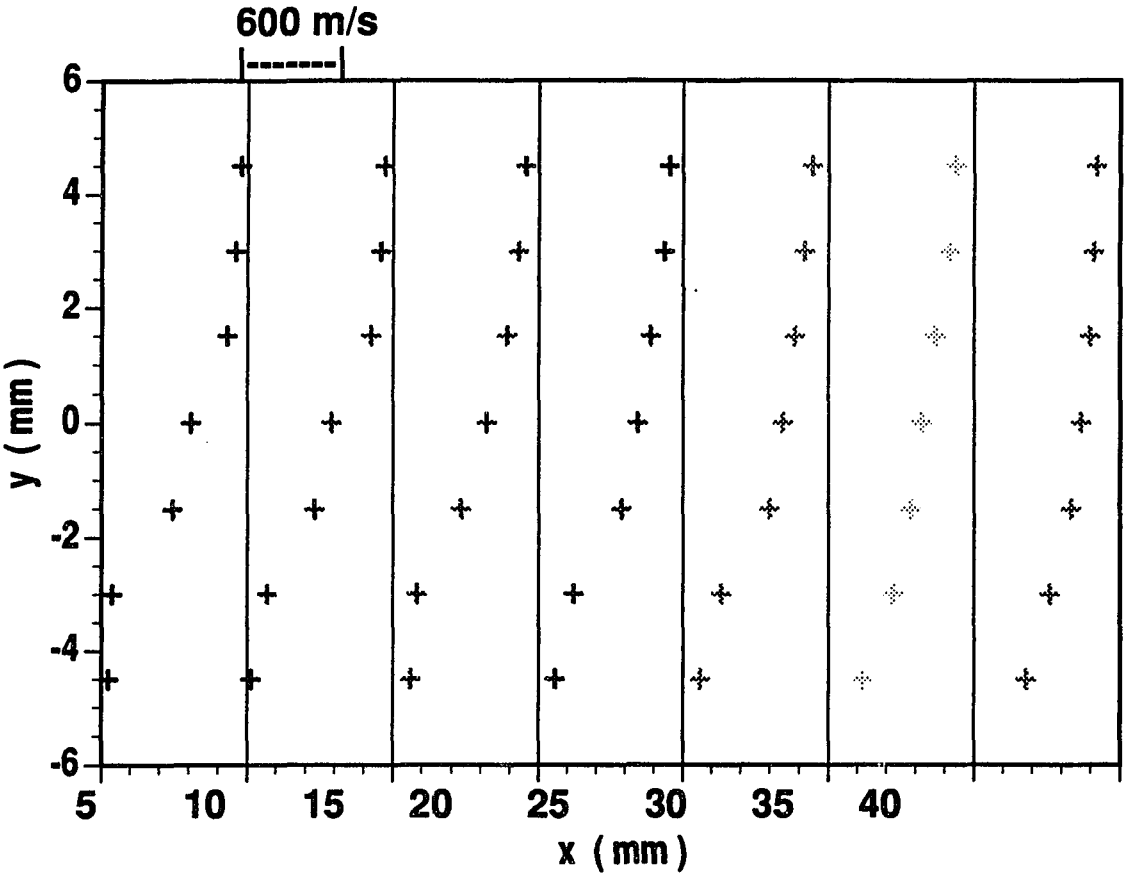

Fig. 3.7.9 Spatial development of transverse profiles of the mean streamwise velocity.

IV Data and Analysis

4.1 Large Scale Structures and Their Evolution

Based on laser induced fluorescence measurements, the local density distributions and density fluctuations are measured along streamwise and transverse directions within the shear layer. The density and density fluctuation measurements can provide a clear picture of flow field and flow structures.

Those structures are spatial and temporal; they are convecting downstream changing in time and space. Since the scale of the structure is inversely proportional to the flow velocity, high spatial resolution and short response time are necessary in measuring the structures in supersonic shear layers. Figure 4.1.1. and 4.1.2. are the density measurements at 2.5 cm and 3.0 cm downstream from the nozzle's lip. Six measuring points are arranged along the y direction; each measuring point is separated by 1.5 mm. Figures 4.1.1 and 4.1.2 show the turbulent structures and their spatial evolution at different location for the same run condition. For lower values of y where the shear layer has a smaller velocity and a smaller shear rate, the structures have large size and have low fluctuation frequency. As y increases the structures are split to smaller sizes and have a higher fluctuation frequency as shown in Figures 4.1.1 and 4.1.2. The scales of the structures are in the range from 0.26 ± 0.08 mm to 8.2 ± 2.7 mm. These scales are calculated based on the time scales of the structure and the local speed of the structures. By counting the sample points covered by a certain structure, the time scale of the structures can be calculated. The minimum magnitude of mean

period is 0.12 ± 0.03 ms at x = 25 mm and y = 1.5 mm. The rate of spatial change is defined as $\partial l / \partial y$, where l is the scale of the structure. The mean maximum rate of spatial change is 18.6 ± 0.16.

Figure 4.1.3 shows the mean density profiles across the shear layer and the spatial development along the streamwise direction. The coordinate is set such that the origin is at the nozzle's lip. The x axis is in the streamwise direction and y is in transverse direction. The y=0 plane is at the surface of the nozzle. Along increasing y the density is decreasing; density is increasing with increasing x.

Figure 4.1.4 shows the turbulent intensity across the shear layer and the spatial development along the streamwise direction. Along the transverse direction, near the nozzle's lip, the turbulent intensity has its maximum value at the center of the shear layer; however, further downstream the turbulent intensity spreads along the y direction and splits. This means that at locations further from the nozzle's lip, the flow turbulence increases and has a more complicated structure. The density and turbulent intensity profiles across the shear layer provide a basic description of the free shear layer.

4.2 Shocklet Profiles

From our experiments using both shadowgraph pictures and fluorescence measurements of local densities and velocities, we confirmed the existence of turbulent shocklets in supersonic free shear layer. The shocklets are thought to be produced in two ways: (a) when the speed of the structure is smaller than the speed of

local flow; (b) when the speed of shocklets is larger than the speed of local flow. But our results show that only the shocklets associated with the speed less than local speed exist(i.e. type (a) above). This means that the deceleration, due to the shear flow, of the vortex motion in the shear layer is apparently not great enough to produce the pressure field which might form the shocklets by the type (b) process.

We found that the shocklet Mach angle associated with the motion of shocklets in the shear layer has a sensitivity to changes in Reynolds number. This strongly suggests that the shocklet is related to the turbulent intensity. The change in angle is related to the change in velocity of the shocklet with respect to the local flow. Specifically, the velocity of a shocklet can be represented as $V_S = M_S\, a$, where a is the local speed of sound in the supersonic free stream, and the Mach number of shocklets, $M_S = (\sin \theta)^{-1}$.

Typical shocklet profiles are showing in Figures 4.2.1 and 4.2.2. In those figures the density measurements are taken at the spatial position 2.0 cm downstream from the nozzle's lip, at locations in y where a high likelihood of shocklet production is found. Since point density measurements were taken, the signals give good spatial resolution. When shocklets appear in the outer layer of the shear flow they seem to show up as a sharp increase in the density. The apparent time of appearance of shocklets are quit random; i.e., from the results it can be seen that for the same run condition and the same measuring location the shocklets show up at different times for different runs. This result agrees with the association of shocklets with eddies convecting in shear flow; eddies

appear in a random manner, and their interactions with flow field are also random.

From the figures it is obvious that shocklets have different thickness. The word thickness means the persistence time of shocklets. This difference in thickness is caused because of the difference in distribution of shocklets. At certain times, the shocklets have higher concentration than other times. This means that several shocklets are generated within a small time range, rather than a single shocklet which lasts a longer time. If the spatial resolution can be increased to higher than 0.1 mm, then we can expect that the thick peaks will split into many thin, sharp peaks.

Thus a shocklet transfers the turbulent energy from eddy motion to flow field; therefore, they will reduce the size of eddies and slow down the eddy motion and produce density and velocity fluctuations. The shocklet also increases the density and pressure when it passes by the measuring point. Since the inhomogeneities and density changes will generate vorticity, these vortical motions will dissipate the turbulent energy and moderate the relative large scale structure motion.

4.3 Distributions of Shocklets in the Shear Layer

Although the generation of shocklets is quite random because of the randomness of eddy convection motion, the measurement results show that the shocklets have a localized spatial and directional distribution which varies with spatial position and angular direction. Figure 4.3.1 shows that the mean frequency of shocklets varies with the angle θ, which is the angle between the

streamline of main flow and the shocklet. This angle is related to the velocity of the shocklet, or, more precisely, the velocity difference between the mean flow velocity and the convective velocity.

The angular distribution of shocklets suggests that within a certain velocity range the shocklets have relatively higher concentration. From our measurements, the shocklets are mainly distributed in the angle between 20 and 70 degrees and the associated velocities are between 276 m/s to 520 m/s. The maximum value is at about 38 degrees, which is about 422 m/s. Figure 4.3.1 also shows that the angular distribution varies at different streamwise locations. Near 28 degrees the distribution is increases sharply and then decreases relatively slowly at the angles larger than 40 degrees.

The distribution of shocklets not only varies in direction but also with changes in spatial location. Figure 4.3.2 shows the mean shocklet frequency distribution at different transverse location. The seven measuring points are set along the transverse direction, and each point is separated by 1.5 mm. The plot includes five set of data with the same run conditions but different x locations. At low locations (small y) in the free shear layers, below the surface of the nozzle, the shocklet has a much lower apparent production frequency; near the upper edge of the shear layer, the production frequency is high. At the range between roughly 1.5 mm to 4 mm the mean production frequency is in the range of 0.8 kHz to 2.4 kHz; for different streamwise locations, the mean production frequency is also quite different.

The trend that the shocklets concentrate near the upper edge of the shear layer suggests that only the small size structures can generate the shocklet. Near the upper edge, the mean shear flow speed is supersonic and the structures originating from the lower layer with large size are broken during the motion from the low layer to the upper region. So the production of shocklets mainly remains in the convection motion of small size structures.

Figure 4.3.3 shows the mean shocklet frequency distribution along the streamwise direction. The mean apparent frequency sharply increases at about 1.5 cm downstream from the nozzle's lip, and slowly decreases as the distance increases. Beyond 2.0 cm from the nozzle's lip, the mean frequency slowly decreases. This is apparently caused by a slowing down of the mean velocity of the shear flow. Therefore, only the eddies with a lower convective velocity can satisfy the condition to generate the shocklet.

In Figure 4.3.3 three sets of data are plotted at three different run conditions, where R_1 is with Reynolds number 7.6×10^6, $R_2 = 2.3 \times 10^6$ and $R_3 = 7.1 \times 10^5$. The Reynolds numbers are based on the free stream flow at the outlet of the nozzle. The mean frequency distribution increases as the Reynolds number increases. At higher Reynolds number flow, more small size structures are produced in the shear layer. The mean periods associated with the Reynolds numbers are 0.133 ms, 0.152 ms and 0.189ms.

4.4 The Spectrum and Correlation of Shocklets

The Fourier transform is one of the ways to identify and to characterize a dynamical regime. The usefulness of the Fourier

spectrum is that it reveals the periodic properties of the evolution of fluctuations in the system. One defines the Fourier transform of a discrete time series x_j to be the operation creating a corresponding discrete series x_k such that:

$$x_k(f_k) = \frac{1}{\sqrt{N}} \sum_{j=1}^{N} x_j \exp(-i \frac{2\pi jk}{N})$$

$$k = 1, ..., N$$

$$i = \sqrt{-1} \text{ pure imaginary}$$

$$f_k = k\,\Delta f = k \frac{1}{t_{max}}, \qquad t_{max} = N\,\Delta t.$$

For convenience we have taken Δt as the unit of time.

The graph representing $|x_k|^2$ as a function of the frequency f is called the power spectrum. The area under each peak in the spectrum is proportional to the strength of that mode. The spectrum of turbulence indicate that in the turbulent state, the power spectra falls off as f^{-n}, where n can be obtained from the slope of the plot of log $|x_k|^2$ versus logf. Fourier spectra are an indicator of the existence turbulent motion. Therefore, it is possible to determine experimentally the spectral index n from the power spectra, and determine if the flow is turbulent.

In principal, there is no difficulty in using the formula to calculate $|x_k|^2$ explicitly. But in practice, the extent of the task becomes substantial as soon as N takes on appreciable values. However, when N is a power of two, an algorithm, called a Fast Fourier Transform (FFT), permits calculation of the spectrum

with a tremendous saving in computer execution time relative to the direct Fourier transform. Therefore, FFT has been applied to compute the Fourier transform.

Correlation methods have been used in the study of fluid turbulence. Correlation methods can be used to obtain information regarding the statistical characteristics of the turbulence.

One use of correlation techniques is to determine whether and to what extent different signals are related. Autocorrelation function measures the correlation between subsequent signals. It remains constant or oscillates for regular motion and decays rapidly (mostly with an exponential tail) if the signals become uncorrelated in the chaotic regime (J. C. Roux, et al. 1981). The correlation $C(\tau)$ between the values of x at two different times is called the autocorrelation. It is defined as

$$C(\tau)=\langle x(t)x(t+\tau)\rangle/\langle x(t)^2\rangle$$

where $\langle x(t)x(t+\tau)\rangle = \lim_{T\to\infty} \frac{1}{T}\int_0^T dt\, x(t)x(t+\tau)$ in a continuous case, and $\langle x(t)x(t+\tau)\rangle = \frac{1}{n}\sum_{j=1}^{n} x_{j+\tau}x_j$ for discrete signals. The Wiener-Khinchin theorem states that the autocorrelation function is merely the Fourier transform of the power spectrum of the quantity of interest:

$$\langle x(t)x(t+\tau)\rangle = \frac{1}{n}\sum_{k=1}^{n} |x_k|^2 \cos\left(\frac{2\pi\tau k}{n}\right)$$

where the Fourier transform has been defined above.

From the autocorrelation profile, two characterizing time parameters are determined. A characterizing correlation time τ_c is calculated from $\tau_c = \int_0^{t_z} C(\tau)d\tau$, where t_z is the value of τ for which $C(\tau)$ first becomes zero.

A small correlation time τ_s is generally considered a measure of the dimensions of the smallest structure or the lifetime of the most rapidly decaying structure. It is defined by the curvature of the autocorrelation coefficient at the origin:

$$d^2C/d\tau^2 \mid_{\tau=0} \equiv -2/\tau_s^2$$

Expanding C in a Taylor series about the origin, we can write, for small τ,

$$C(\tau) \approx 1-\tau^2/\tau_s^2$$

Although spectral and correlation analysis are equivalent in principle, in practice they complement one another. Results obtained from their combined use will generally be more complete than those obtained by either alone.

Figure 4.4.1 shows a typical plot of power spectrum of density fluctuations before and after a shocklet at 2.5 cm downstream from the nozzle's lip and 3.0mm in transverse direction from the nozzle's surface. There seem to be no explicit modes generated after the shocklet passes; but the decay rate of the power spectrum increases. This means that after the shocklet, part of the turbulent

energy is transfered from the turbulent region of the shear layer to the region outside the shear layer through the shocklet process. Smaller scale vorticity motions should thereby be generated in the post-region of shocklet, resulting in the increase of dissipation of turbulent energy. Using $P \propto \omega^{-n}$, the spectral decay rate n in the pre- shocklet region is about 1.64 ± 0.04; the decay rate in the post-shocklet region is about 1.79 ± 0.06.

Figures 4.4.2 and 4.4.3 show the variation of correlation time along streamwise direction and at different transverse locations. The large correlation time plot shows that when x increases the correlation time decrease This means the scale of the turbulent structures is decreasing when x increases. This is the dynamical effect of the eddy shocklet, which reduces the turbulent scale by breaking the structures convecting in the shear layer. The small scale correlation time does not show an explicit trend. This is not a surprise since the small correlation time characterizes the motion scale much smaller than the scale in this shear flow.

4.5 Spreading Rate of the Free Shear Layers

Spreading rate of a free shear layer is defined as $Ds = \tan \alpha$, where the α is the angle between the upper and lower boundary of the free shear layer. The spreading rate of the free shear layer was measured using the calculated velocity profiles. At different transverse locations, mean streamwise velocities were measured. Since the velocities fluctuate strongly, many measurements had to be done in order to get relatively smooth values for a determination of the boundary.

For the upper boundary of the free shear layer the threshold was determined by dividing the entire boundary into three parts. The first part is used from x=0 to x=10 mm, the second one from x=10 mm to x=25 mm, and a third one from x=25 mm to x=35 mm. This procedure is necessary because at different streamwise locations, the thickness of the boundary is quite different. For the boundary close to the nozzle's lip (x < 10) mm the boundary is very sharp; the threshold for this part is 95% ± 0.05 of the free stream velocity. The threshold for the second part is 90% ± 0.10 of the free stream velocity. Because of the entrainment effect in the third part, x> 25 mm, the flow in the shear layer is quite mixed with that outside the shear layer, and the threshold for this part is 75% ± 0.2 of the free stream velocity.

There are three different states of flow at the outlet of the nozzle as shown in Figure 3.2.1 to 3.2.3. From shocklet measurements, the properties of these three states are quite different. For $P_f > P_b$ situation, the shocklet has broadest distribution in x and the highest apparent frequency; when $P_f < P_b$ the distribution and production rate of shocklets is much lower. This is shown in Figure 4.5.1.

For spreading rates, one also sees three different states of flow. This is shown in Figures 4.5.2 to 4.5.4. These are typical plots of the extent of the free shear layer at various streamwise location for $P_f > P_b$, $P_f = P_b$ and $P_f < P_b$. Shocklets seem to break the structures into smaller sizes thereby reducing the spreading rate. For the $P_f < P_b$ case the effect of a shocklet can be neglected because of the low distribution. However, comparing Figures 4.5.1 and 4.5.3, the

spreading rate has much higher value than that in the $P_f > P_b$ case. The spreading rate for those three different type of flows are 0.31 ± 0.11, 0.24 ± 0.09, and 0.11 ± 0.04.

4.6 Dynamical Analysis of Turbulence In Shear Flow

The dimension of an attractor may describe the statistics of fully developed fluid turbulence. The dimension of a chaotic or turbulent system is the first level of knowledge necessary to characterize its properties. The dimension is also a lower bound on the number of essential variables needed to model the dynamics. Fluid systems have infinite-dimensional phase spaces, but the strange-attractor theory postulates that there are finite-dimensional attractors that represent the asymptotic dynamical behavior of the fluid. One can present projections of these attractors onto phase spaces of low dimension that correspond to experimental measurements. From a time-delay approach (Ruelle 1971), a single time series x(t) can be converted into a multiple time series $x(t)=[x_0(t),x_1(t),...,x_{n-1}(t)]$ by selecting a delay τ and defining $x_k(t)=x(t+k\tau)$.

Consider the d-dimensional phase space to be covered by total number, M(l), d-dimensional cubes with side l. The probability P_i of finding a point of the attractor in cube i is $P_i=\lim_{n\to\infty}\frac{N_i}{N}$, where is the number of points in this cube. The Hausdorff dimension is defined as

$$D_f=\lim_{l\to 0}\frac{1}{f-1}\frac{\log\left(\sum_{i=0}^{M(l)}P_i^f\right)}{\log l};\ f=0,1,2,...$$

$$D_2 = \lim_{l \to 0} \frac{\log(\sum_{i=0}^{M(l)} p_i^2)}{\log l} < D_0 = -\lim_{l \to 0} \frac{\log M(l)}{\log l}$$

where D_2 provides the lower bound of Hausdorff dimension. D_2 can be computed by the correlation integral.

$$D_2 = \lim_{l \to 0} \frac{\log C(l)}{\log l}$$

where $C(l)$ is correlation integral function defined by

$$C(l) = \lim_{N \to \infty} \frac{1}{N^2} \sum_{ij} \theta[l - |\vec{x}_i - \vec{x}_j|]$$

where $\theta[l - |\vec{x}_i - \vec{x}_j|]$ is the Heaviside function.

The results of our D_2 dimension determination for the shear layer are plotted in Figures 4.6.1 and 4.6.2. In the first one, two sets of data are plotted. These two sets of data were measured at the streamwise locations 0.5 cm and 3.5 cm downstream from the nozzle lip. These data were also measured simultaneously. The dimension has higher value at x = 3.5 cm than that at 0.5 cm.

This means that the shear layer detaching at the nozzle lip has a more complicated structure than that near the nozzle lip. When the shear layer detaches before it becomes fully developed turbulence, it goes through a transition process forming a

transition region. Although the flow in the transition region should not be laminar under our supersonic conditions, it has a relatively simple structure. At this region, if we neglected the structures coming from the boundary layer of the nozzle wall, the instability is still at an early stage, the structures formed due to the instability waves are quite ordered, i.e. the structures have a relatively higher order of coherence. When these structures convected downstream, they break up due to the entrainment motion and interaction with other structures. Therefore, at the region further from the nozzle's lip, the turbulent structures are less coherent and the dimension of the system is higher.

From the same plot it can be seen that at the upper region system has higher dimension. As it is shown in section 4.1 at the lower layer the flow speed is subsonic, structures have relative larger size and the motion is relatively simple. However, at the upper layer region the flow speed is supersonic; a strong intermittent effect is causing fluctuations in density, pressure and velocity, and the shocklet generated in this region also interacts with those structures. All those processes and effects make the flow extremely complicated.

The results of fractal dimension evolution at different transverse location and along the x direction are plotted in Figure 4.6.2. In this plot four sets of data were used; these were taken with transverse location at y = 4.5 mm, y = 3.0 mm, y= 1.5 mm, and y = 0.0 mm. The run conditions for these measurements were the same. For each measurements seven channels were used at seven measuring points along the streamwise direction. The results

show that at a certain value Xc, which is 1.8 ± 0.4 cm in this free shear layer, downstream from the nozzle lip the fractal dimension increases sharply. This also shows as one moves further from the nozzle's lip; the turbulent structure becomes more complicated. It is believed that the value Xc depends on the flow type, Mach number, and the angle of detachment. These fractal dimension profiles give a basic picture of turbulent structure of the shear layer, and help in the analytical modeling of the shear flow.

4.7 Formation of Streaky Structures

The principal effects of mean shear on turbulence may be represented by a parameter, S*, called shear rate parameter. It is defined as

$$S^* = \frac{Sl}{q}$$

where l is a length scale for 'energy-containing' eddies, $q = \overline{u_i u_i}^{\frac{1}{2}}$ is a turbulent velocity scale and S is assumed to be a function of y only. Based on the velocity measurements shown in Figures 3.7.2, 3.7.4, 3.7.6 and 3.7.8, the shear rate parameter is calculated along the transverse direction at different streamwise locations and shown in Figure 4.7.1. The eddy scale used in that calculation is from the density measurements of large scale structures along the transverse direction. Since large eddies contain the main turbulent energy, as confirmed by procedures used for the detection of the streaky structures, it was shown by others that the streaks were the major producers of Reynolds stress and turbulent kinetic energy in turbulent flow. Therefore, the scale of large

structure in shear flow may be used to calculate the shear rate parameter. The energy partition parameter, K*, in equation (2.4.1) is calculated based on the two dimensional shear flow approximation. The average value of that is 9.2 ± 1.6 at x = 1.0 cm, and 6.7 ± 0.7 at x = 3.0 cm.

Figure 4.7.2 shows the contour plot of streaky structures along the transverse direction and at different streamwise locations. The plot shows that the streaks are narrow in transverse scale. The average ratio of longitudinal scale to transverse scale is 12.5 ± 1.8.

4.8 Detection of Burst and Distribution of Bursts along the Shear Layer

From the flow visualization investigation by Corino and Brodkey (1969) and Kim et al. (9171) it is indicated that the burst or ejection process was responsible for a major proportion of the Reynolds stress production. It naturally follows that detection of the burst or ejection might be based on the occurrence of high negative uv or high Reynolds stress value.

From the boundary layer approximation theory, the free shear layer can be described as two dimensional shear flow (as discussed in Chapter 2). The Reynolds stress term can be derived from equation (2.1.3) which is

$$U\frac{\partial U}{\partial x}+V\frac{\partial U}{\partial y}+W\frac{\partial U}{\partial z}+\frac{\partial \overline{uv}}{\partial y}+\frac{\partial \overline{uw}}{\partial z}=-\frac{1}{\rho}\frac{\partial P}{\partial x}+U_1\frac{dU_1}{dx}+\nu\left(\frac{\partial^2 U}{\partial y^2}+\frac{\partial^2 U}{\partial z^2}\right) \tag{4.8.1}$$

Since the Reynolds number is high the viscous stress term can always be neglected, and giving a two dimensional treatment, equation (4.8.1) becomes

$$U\frac{\partial U}{\partial x}+V\frac{\partial U}{\partial y}+\frac{\partial \overline{uv}}{\partial y}=-\frac{1}{\rho}\frac{\partial P}{\partial x}+U_1\frac{dU_1}{dx} \qquad (4.8.2)$$

When we calculate the velocity in shear flow which is not concerned with a rapid distortion process (like shock wave structure), the shear flow can be consider as incompressible flow. From the continuity equation, the transverse velocity can be obtained by

$$V=-\int_{y_1}^{y_2}\frac{\partial U}{\partial x}\,dy \qquad (4.8.3)$$

where the integration is over the transverse direction across the shear layer, and y_1 and y_2 can set the transverse position values of the edges of the shear layer. For convenience, the coordinates can be set such that y_1 is the origin of the coordinate. Substituting (4.8.3) in to (4.8.2), integrating over y again we get

$$\rho\,\overline{uv}=(h-y)\frac{dP}{dx}-\rho\left[U_m\int_0^{y}\frac{\partial U}{\partial x}\,dy+\int_0^{y}U_1\frac{dU_1}{dx}\,dy\right] \qquad (4.8.4)$$

where h is the width of the shear layer, U_1 is the free stream flow velocity, U_m is the mean streamwise velocity of the shear flow, and

P is the mean pressure in shear layer. When taking the measurements, the free shear layers were forced to be flat. Therefore, the pressure, P, is only function of x. The free stream velocity U_1 is just a function of x. The mean streamwise velocity, U, is a function of x and y; its expression can be obtained from the velocity profile shown in figure 3.7.9. Therefore, the Reynolds stress including its dependence on x and y can be calculated from equation (4.8.4).

Experimentally, the streaky structure and subsequent burst process are fluid structures which have different velocity and density from the environmental fluid field. The LIF measuring system provides high spatial and time resolution, therefore, the burst process can be detected by density measurements. In fact it has been done and shown in Figures 4.1.1 and 4.1.2. In those plots, relative large structures are formed; when they move to upper layer during the convecting they break up to smaller structures.

To distinguish the burst a normalized parameter is defined as

$$H = \frac{|\rho'|^2}{(\rho_0)^2} \qquad (4.8.5)$$

where ρ_0 is the density at initial state. Figures 4.8.1 to 4.8.6 show the burst measurements at different streamwise locations. Near the nozzle lip where the shear flow has higher shear rate, the density measurements show more thin peaks; further from the nozzle's lip the peaks are grouped. This phenomenon means that at high shear rate regions, the streaky structures more frequently

break up, or bursts have higher production frequencies. At other regions further away, the shear rate is lower; the flow is more vortical; bursts, have lower production frequencies, and the structure scales associated with the ejection is larger.

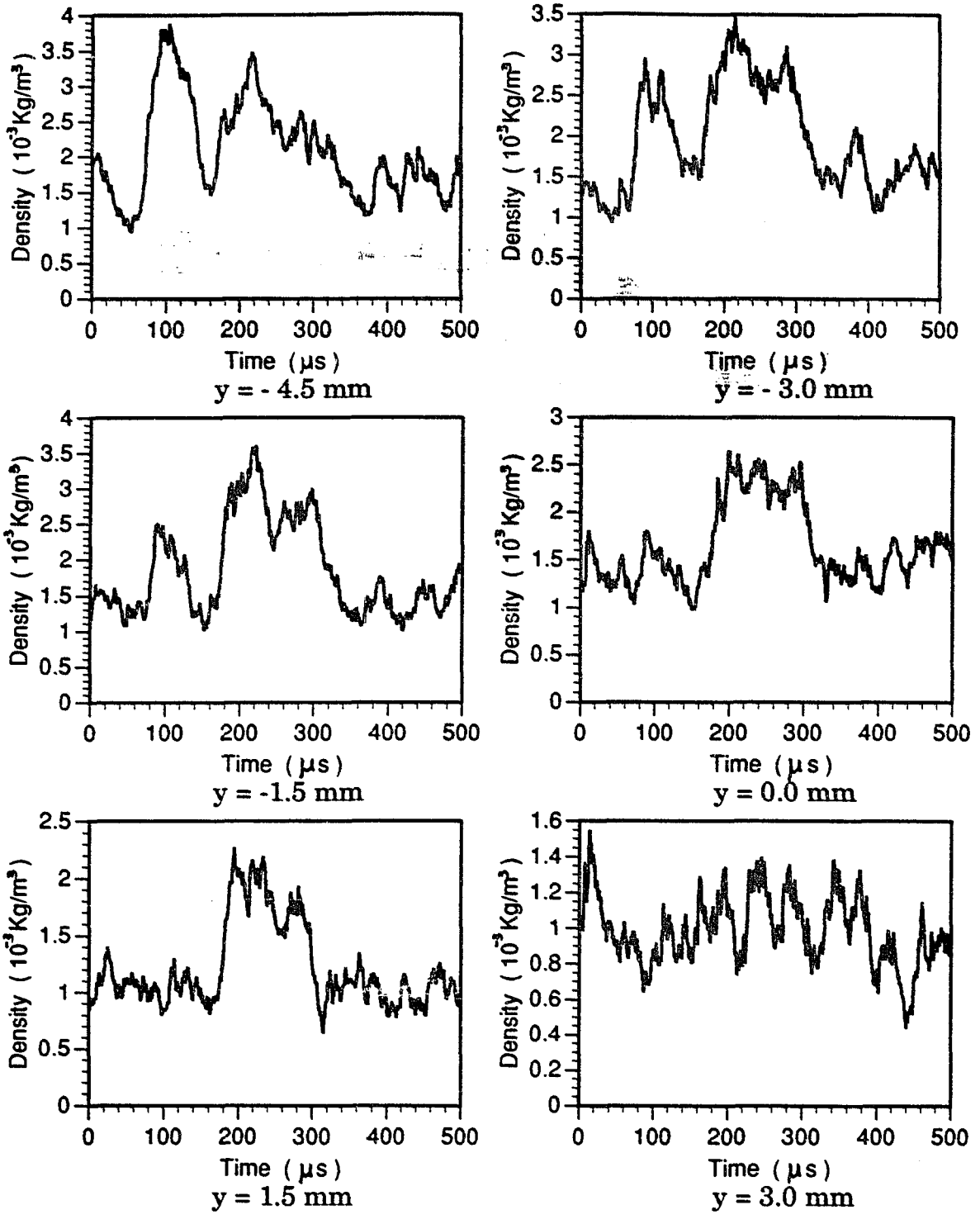

Fig. 4.1.1 Spatial and time evolution of density along y direction and 1.5 cm downstream from the nozzle's lip.

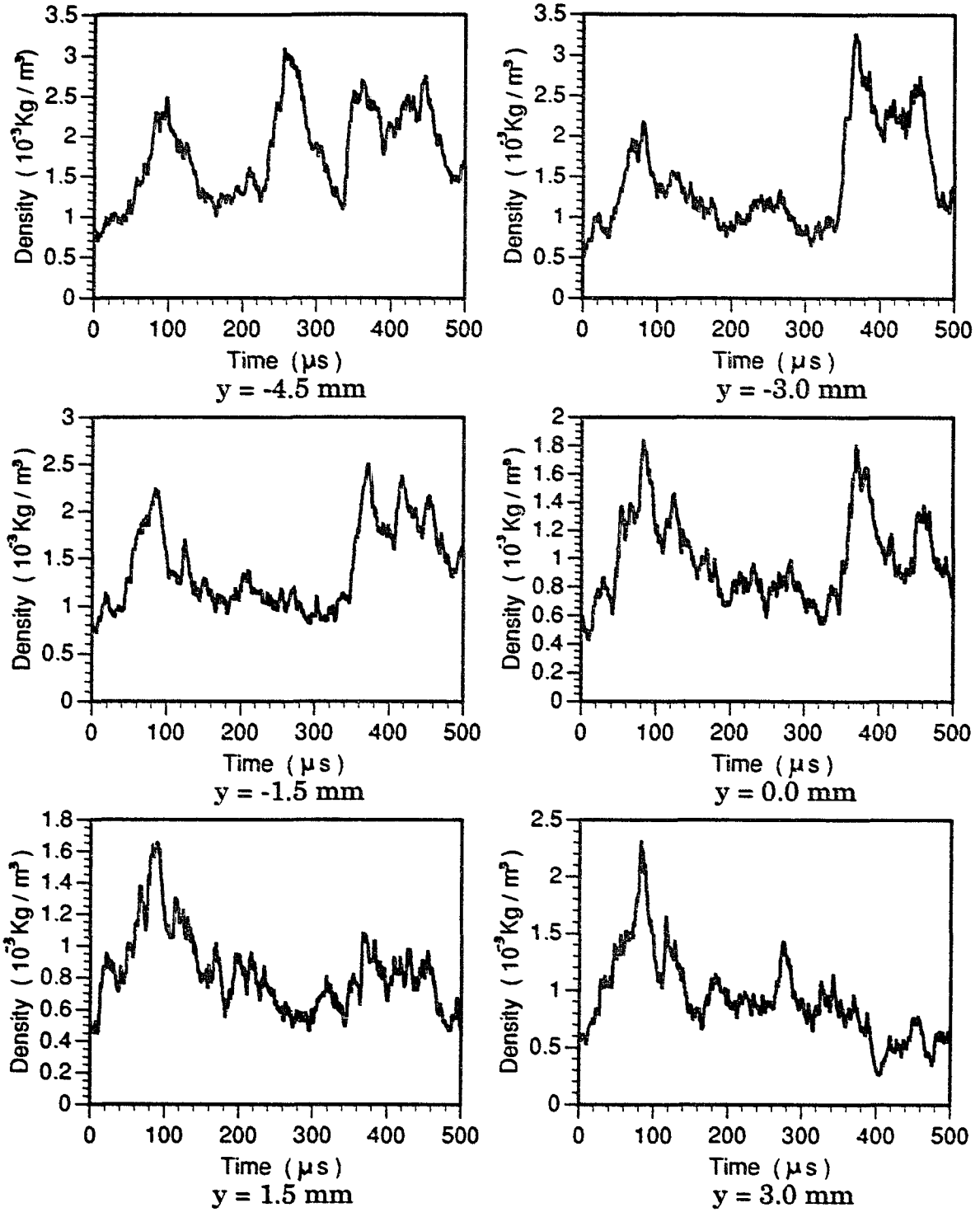

Fig. 4.1.2 Spatial and time evolution of density along y direction and 2.0 cm downstream from the nozzle's lip.

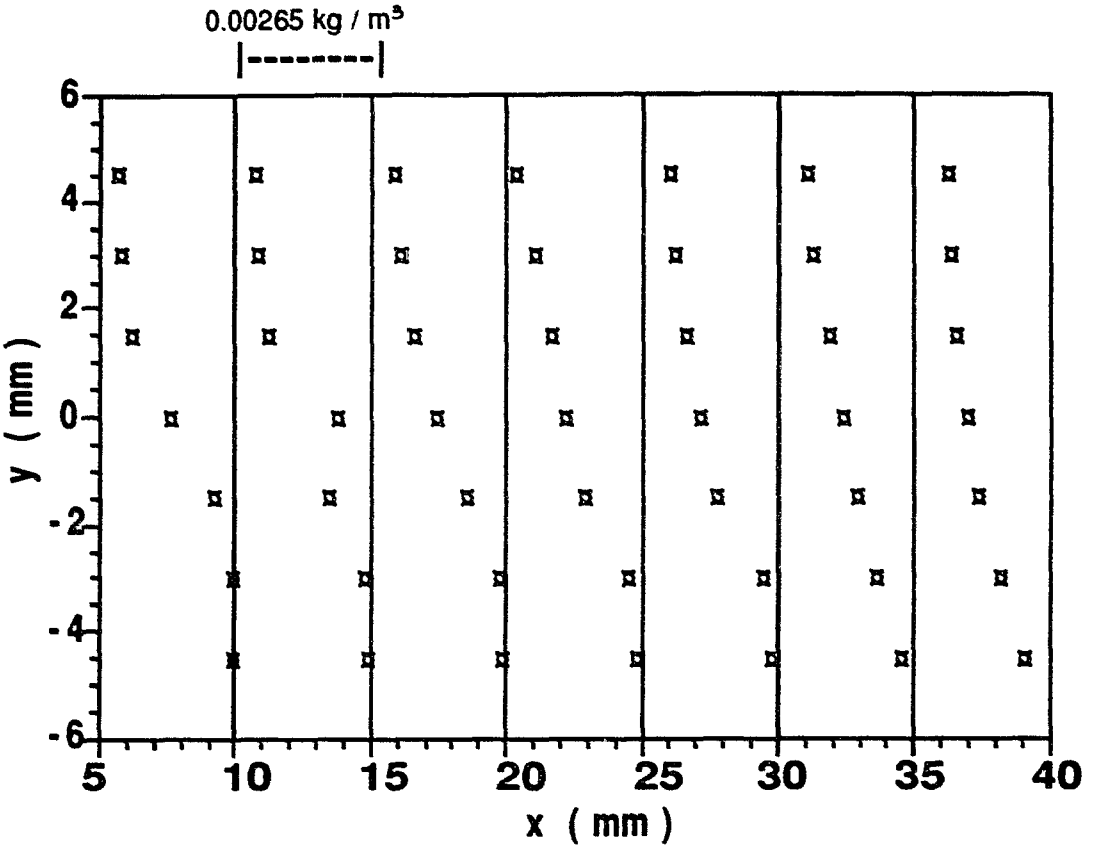

Fig. 4.1.3 Spatial development of mean density profiles along the streamwise direction.

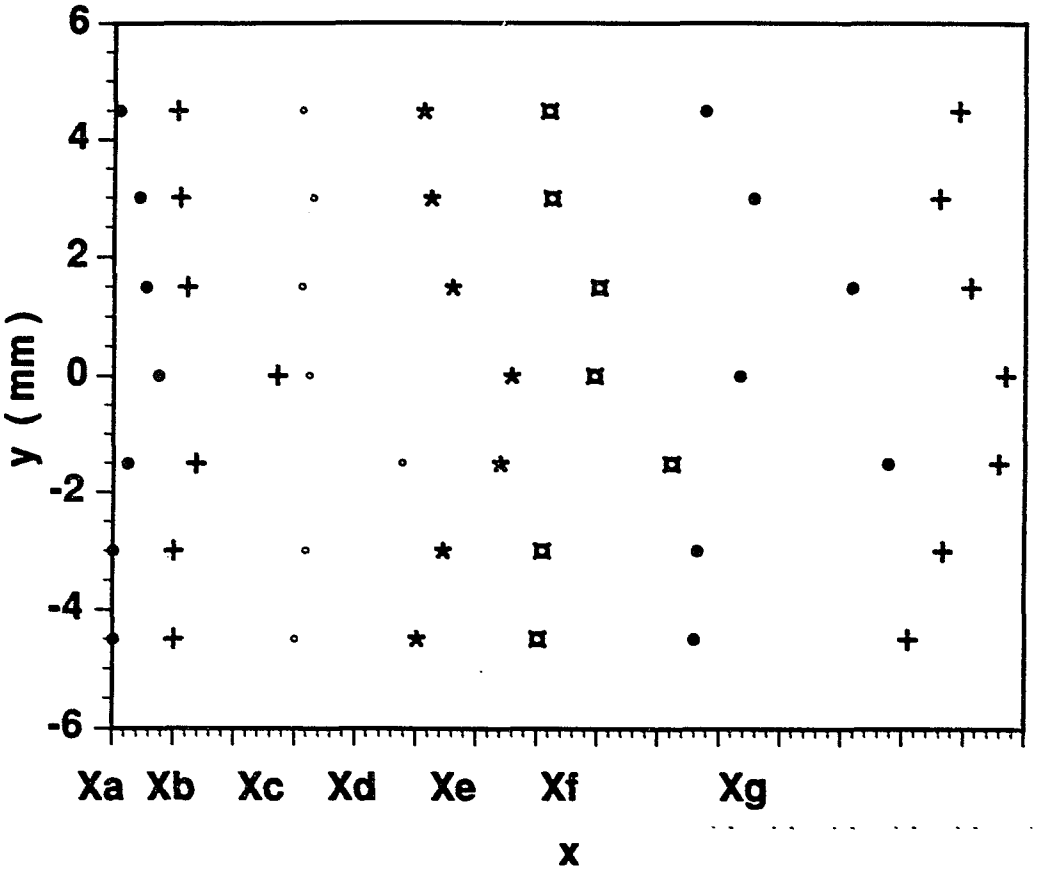

Fig. 4.1.4 Spatial development of transverse profiles of turbulent intensity.

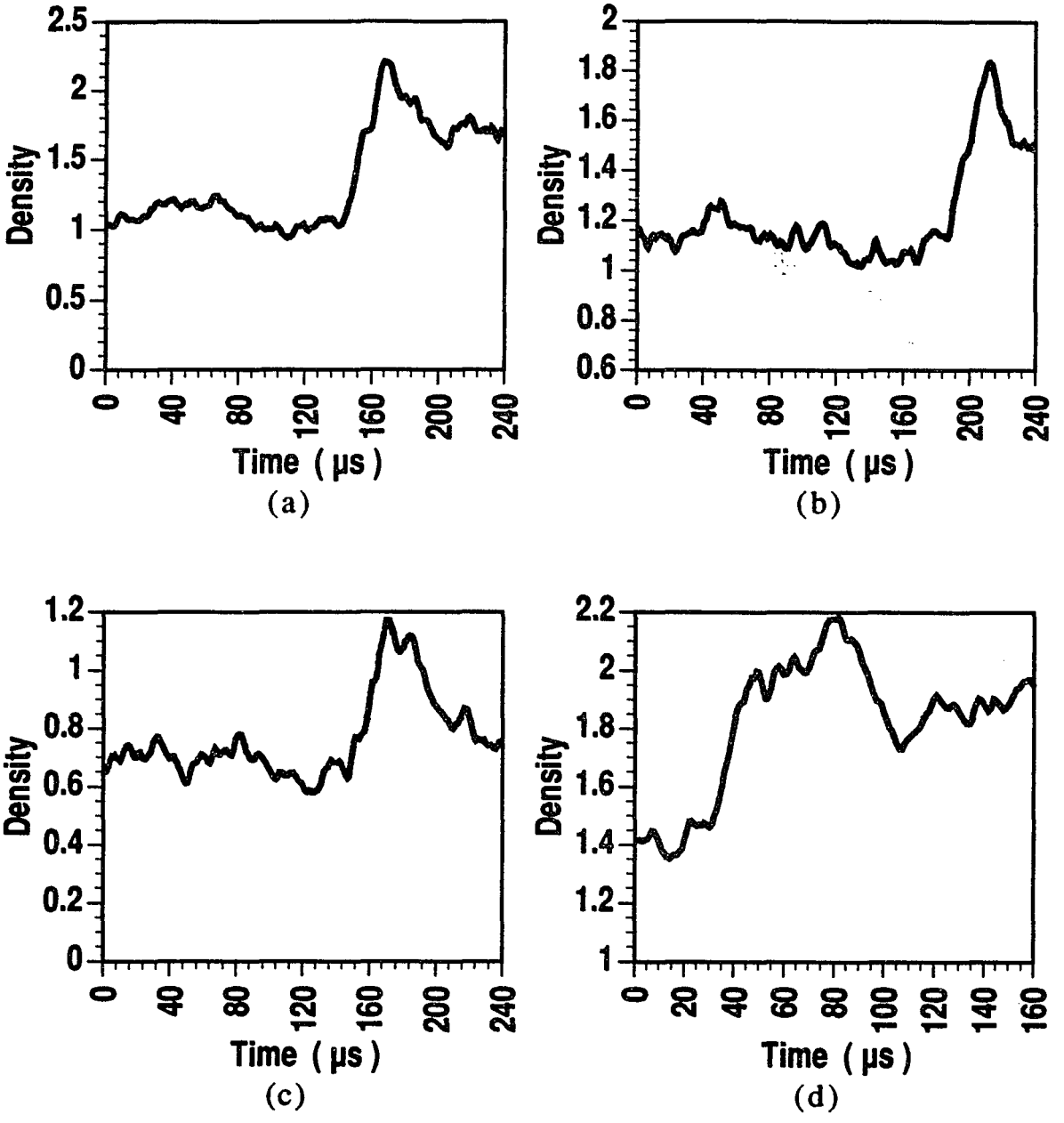

Fig. 4.2.1 The shocklet profiles of different runs at x = 2.0 cm downstream from the nozzle's lip

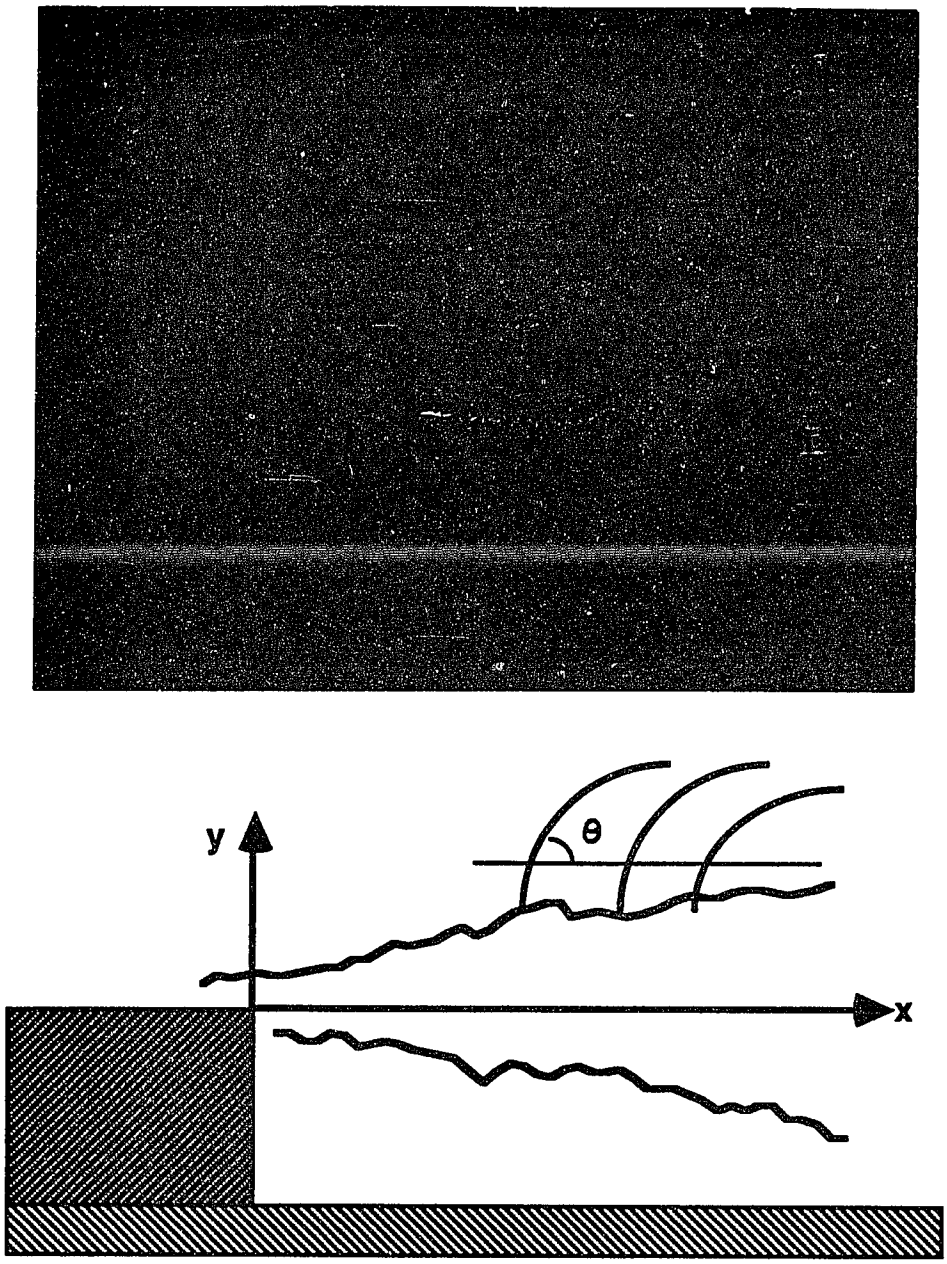

Fig. 4.2.2 A shadowgraph of the shocklet in the free shear flow.

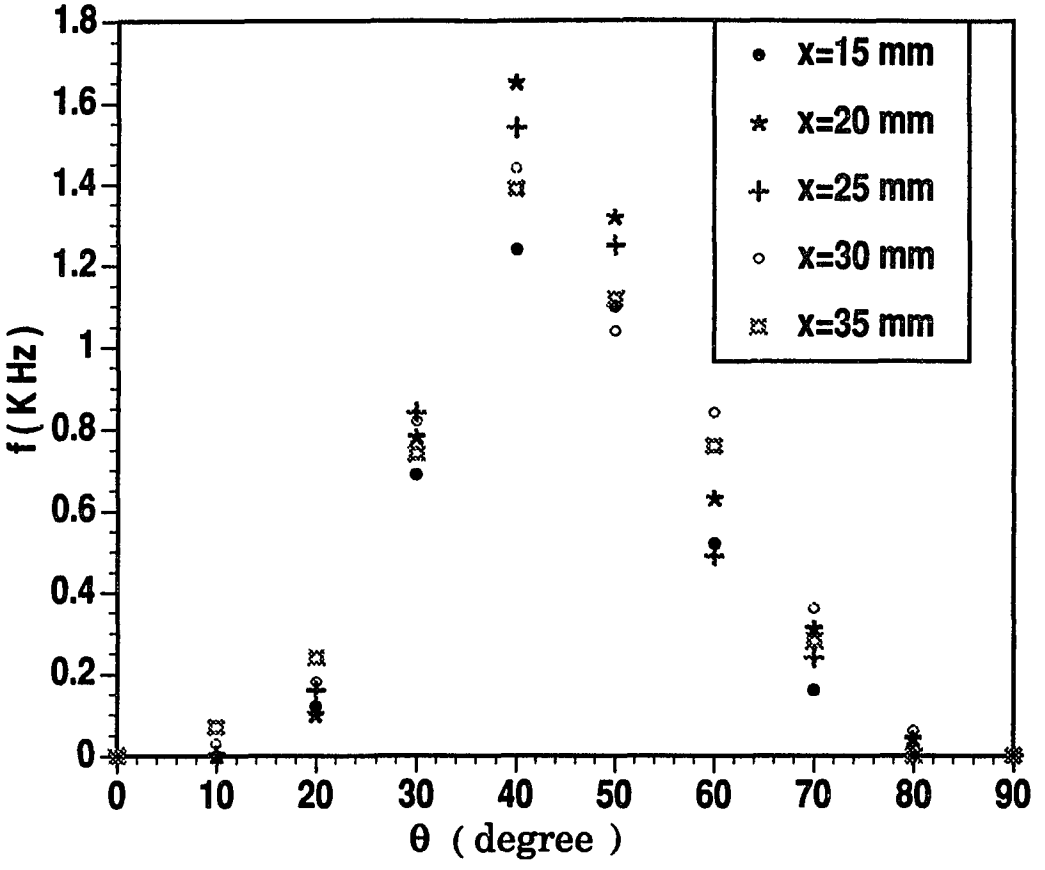

Fig. 4.3.1 The angular distribution of shocklets at different streamwise locations.

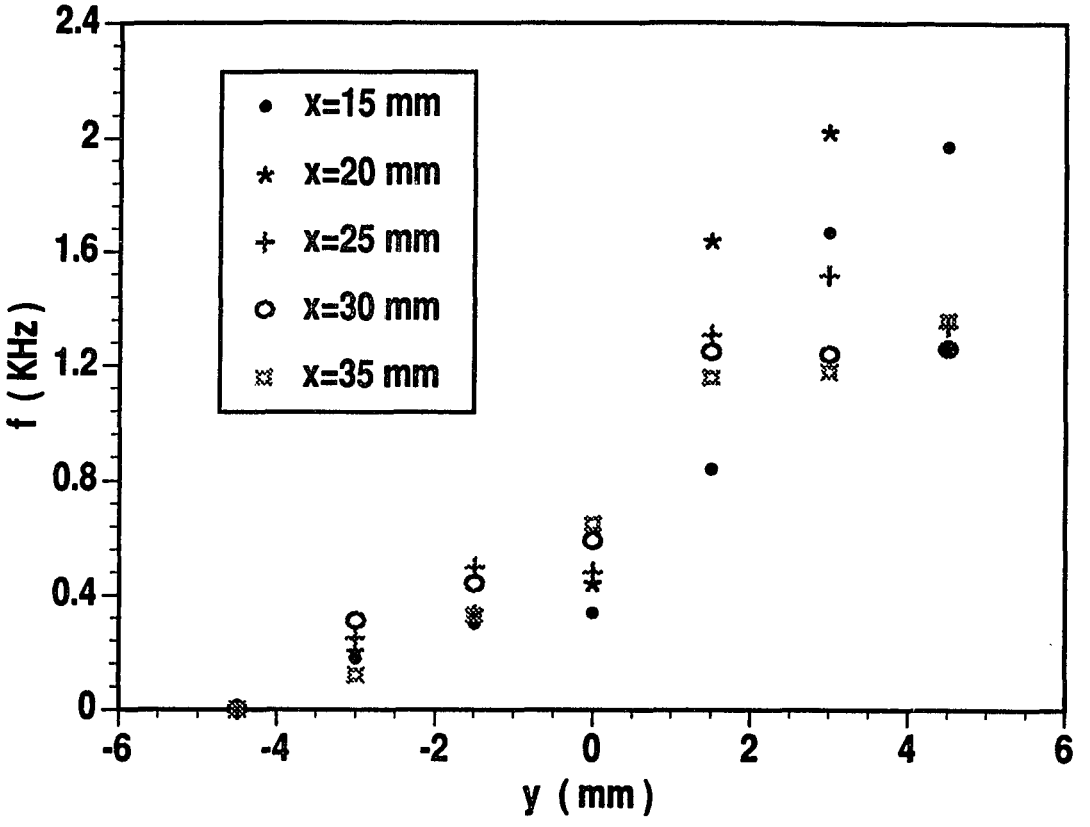

Fig. 4.3.2 The mean frequency distribution of shocklets along the transverse location.

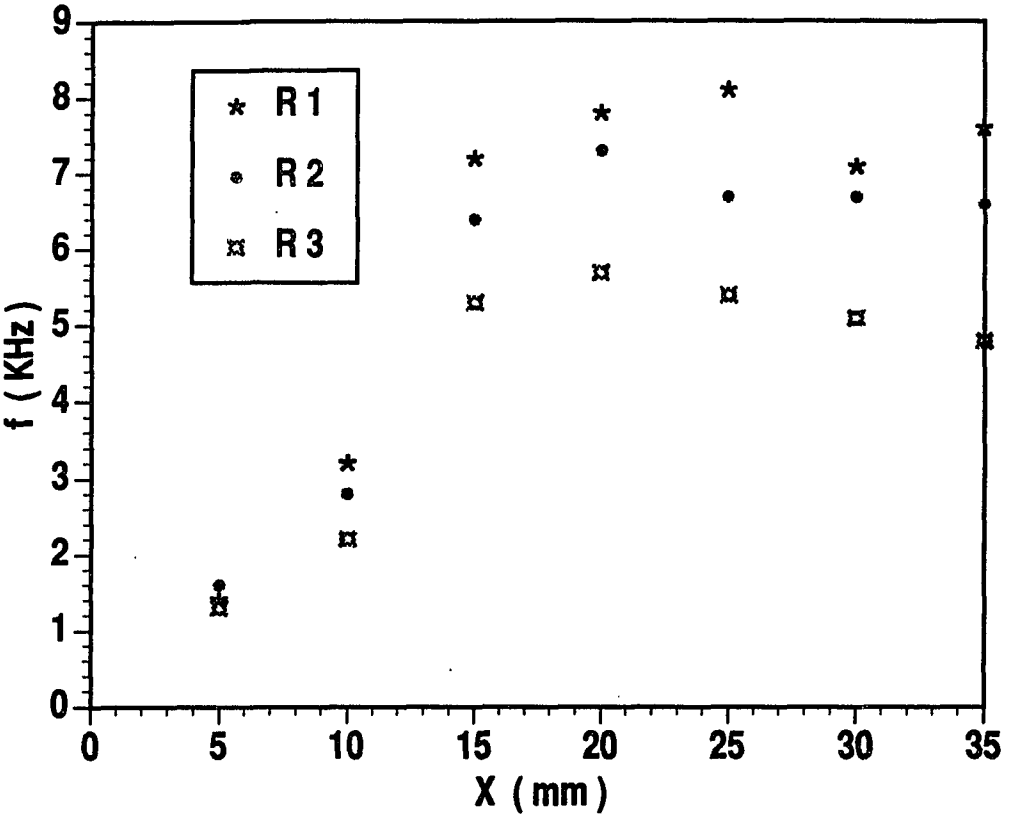

Fig. 4.3.3 The mean frequency distribution of shocklets along the streamwise locations.

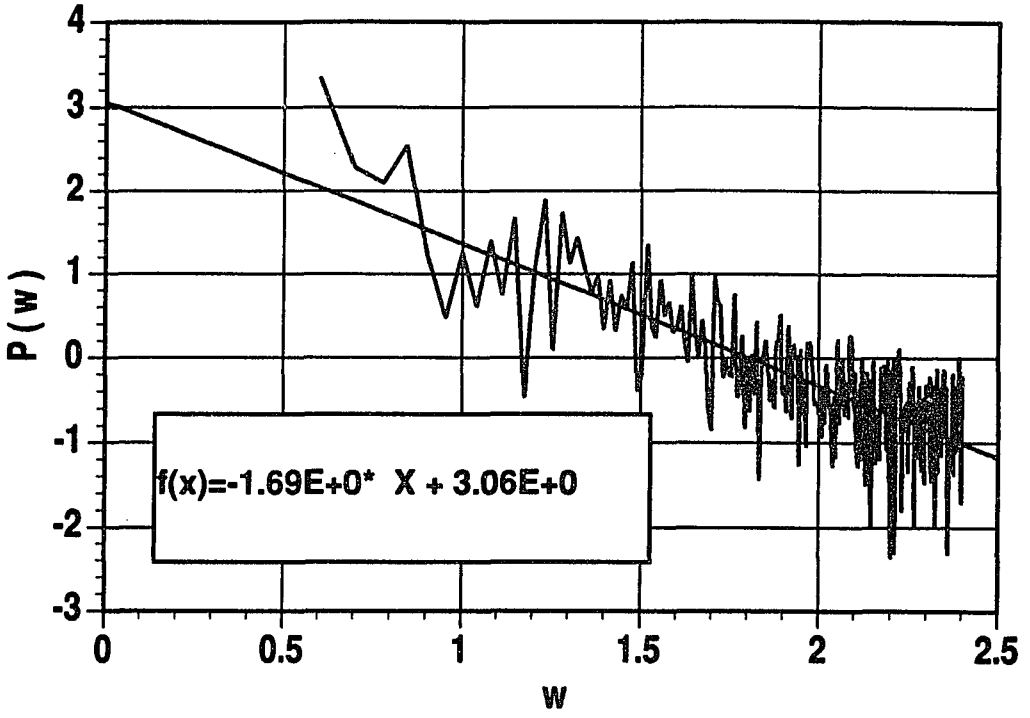

(a) before the shocklet

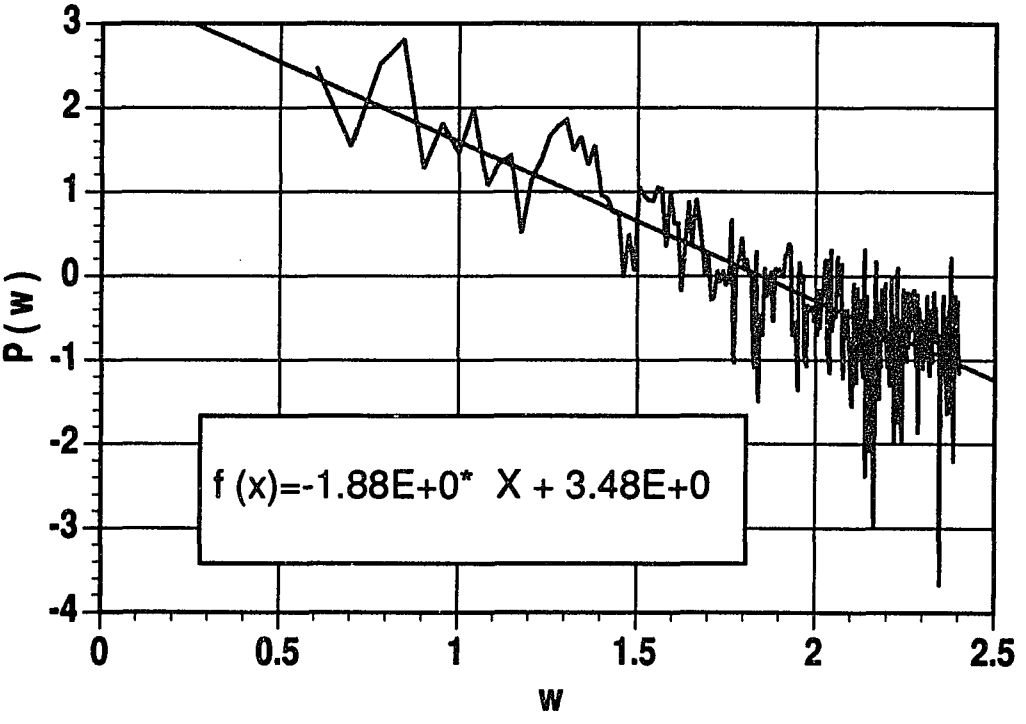

(b) after the shocklet

Fig. 4.4.1 The power spectrums of density fluctuations before and after the shocklet at y = 3.0 mm, x = 25 mm.

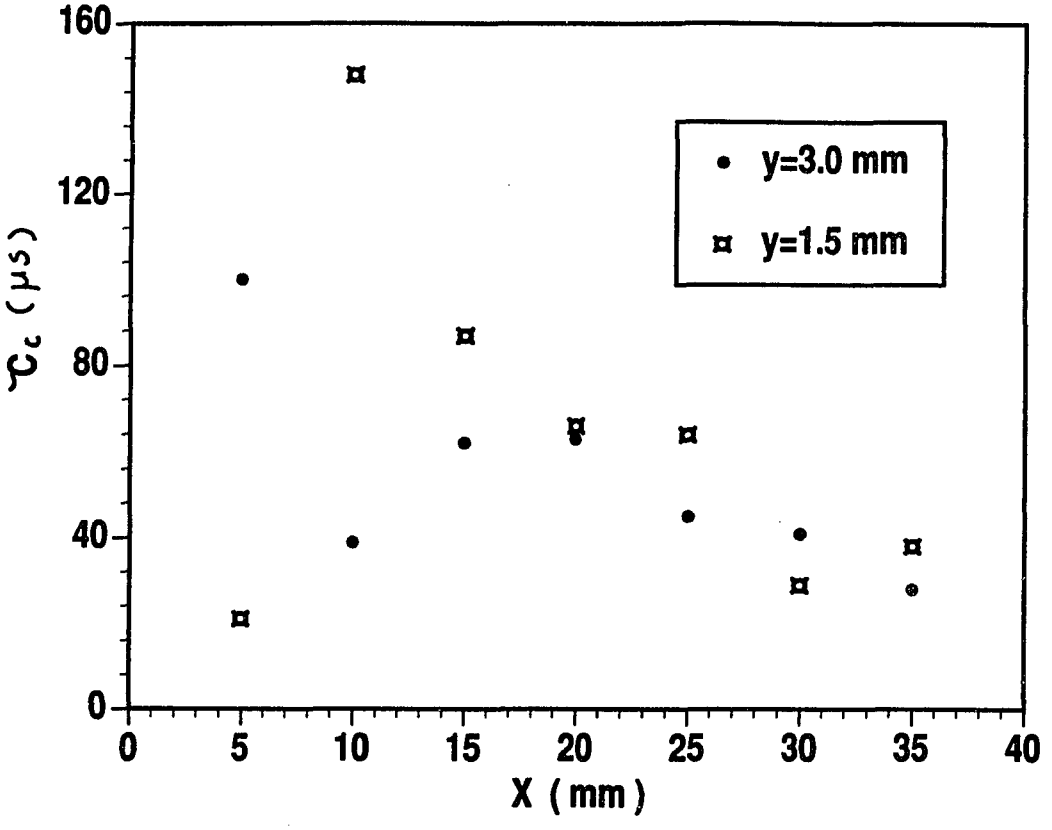

Fig. 4.4.2 The variation of large correlation times at different y along the streamwise direction.

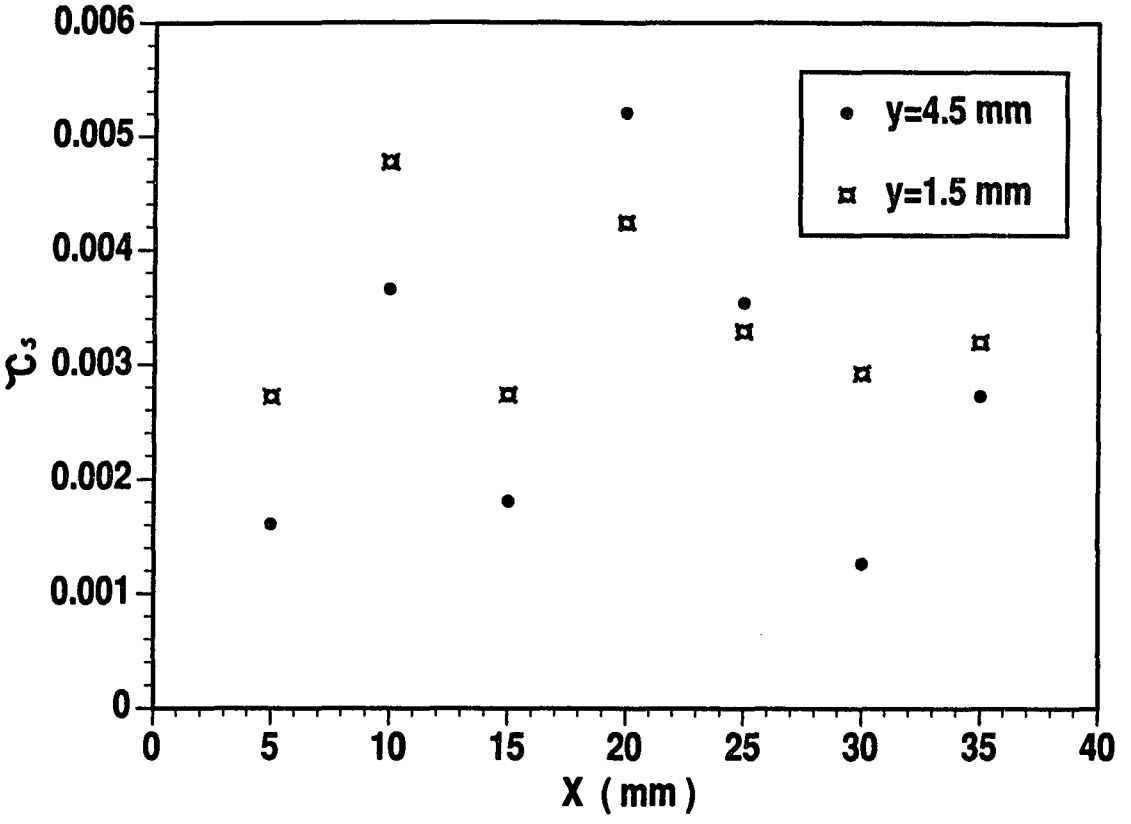

Fig. 4.4.3 The variation of small correlation times at different y along streamwise locations.

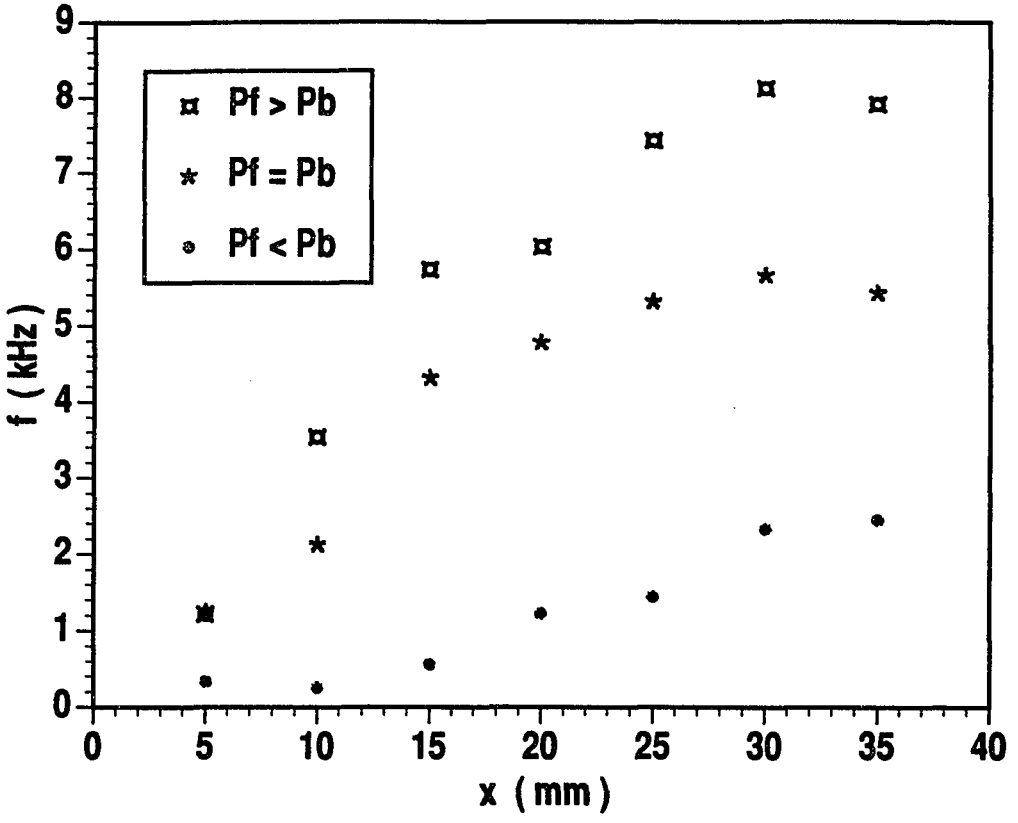

Fig. 4.5.1 The distribution of shocklet for different flow pressure, P_f, and the pressure at the outlet of the nozzle, P_b.

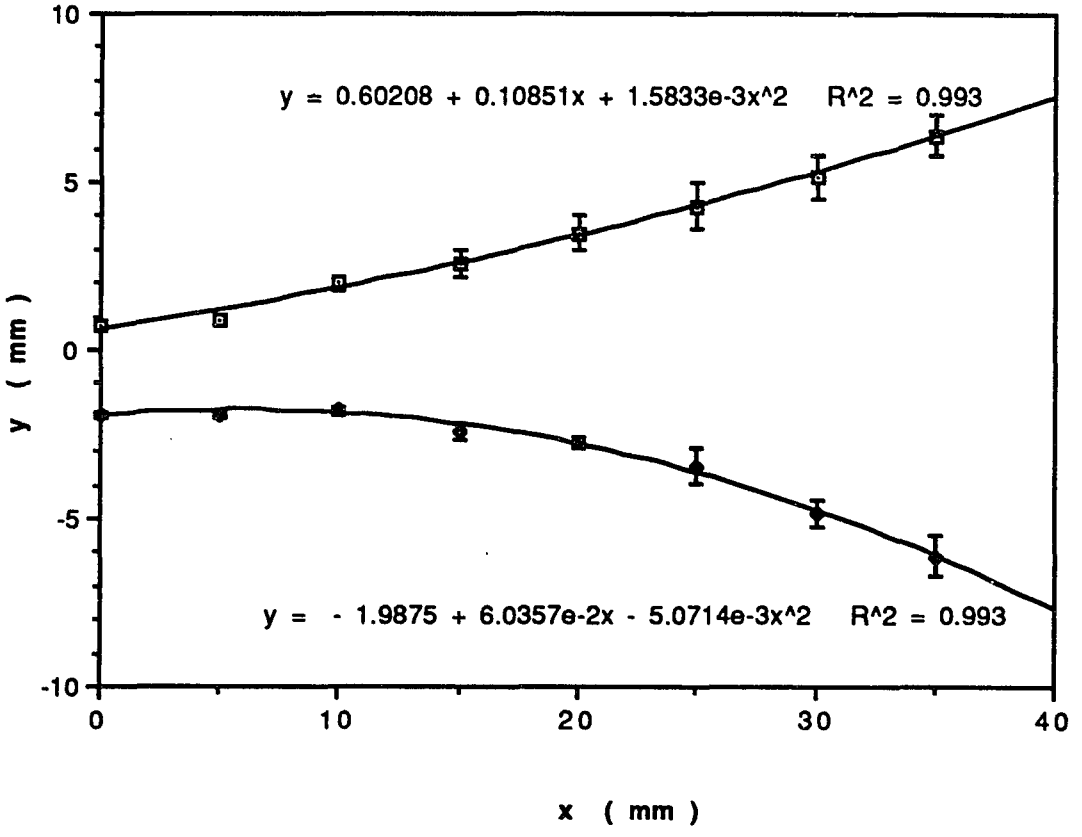

Fig. 4.5.2 The extent of the free shear layer at various streamwise locations for Pf > Pb.

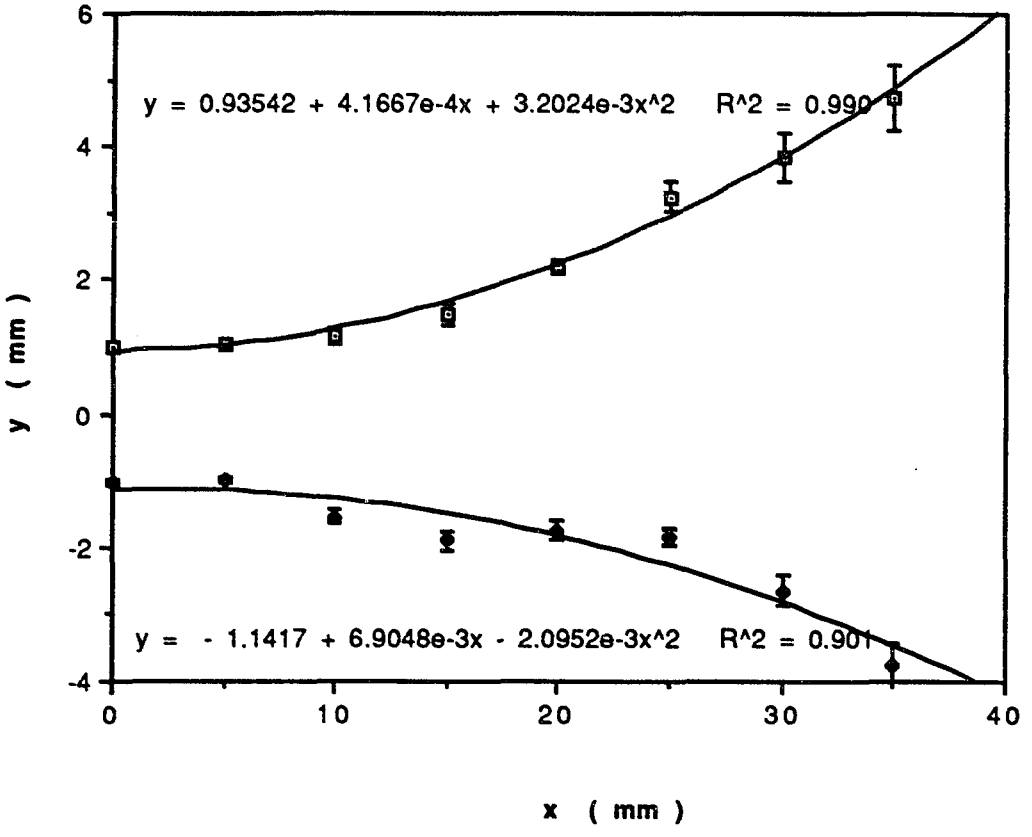

Fig. 4.5.3 The extent of the free shear layer at various streamwise locations for Pf < Pb.

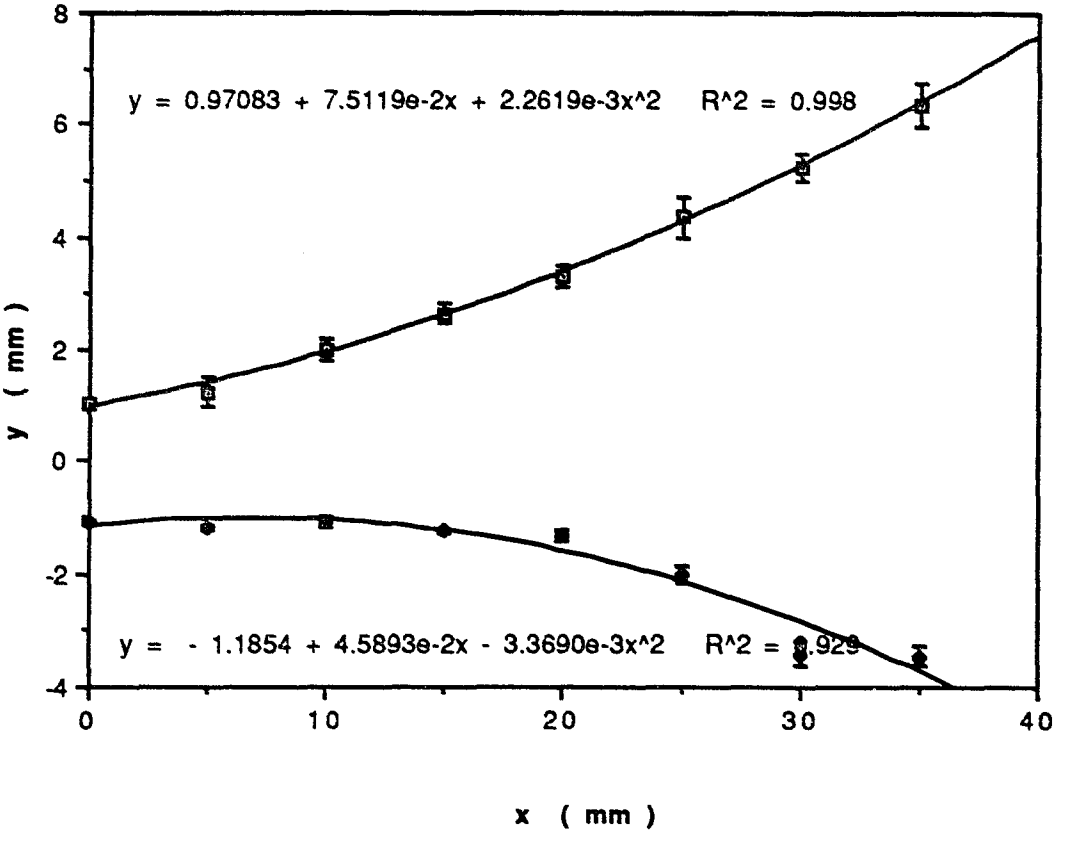

Fig. 4.5.4 The extent of the free shear layer at various streamwise locations for Pf = Pb.

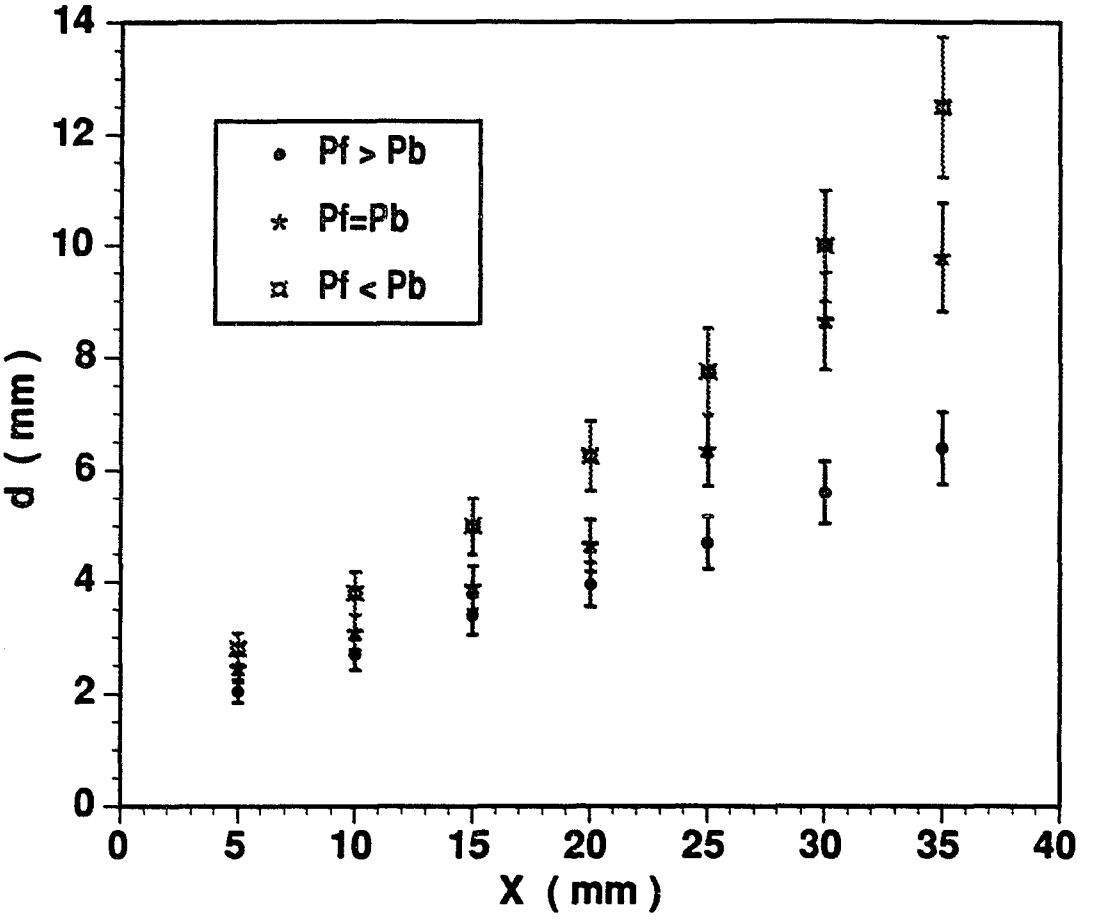

Fig. 4.5.5 Spatial evolutions of the shear layer width for different flow pressure P_f and back pressure P_b.

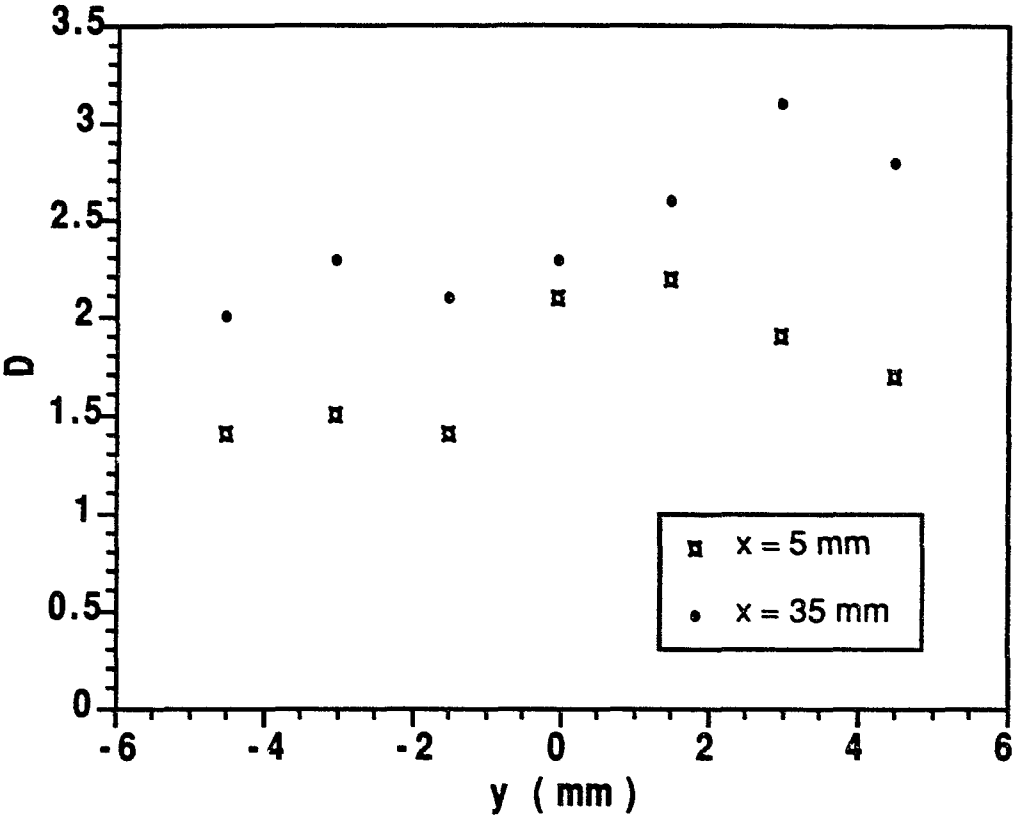

Fig. 4.6.1 The fractal dimension variation along the transverse direction at different streamwise locations.

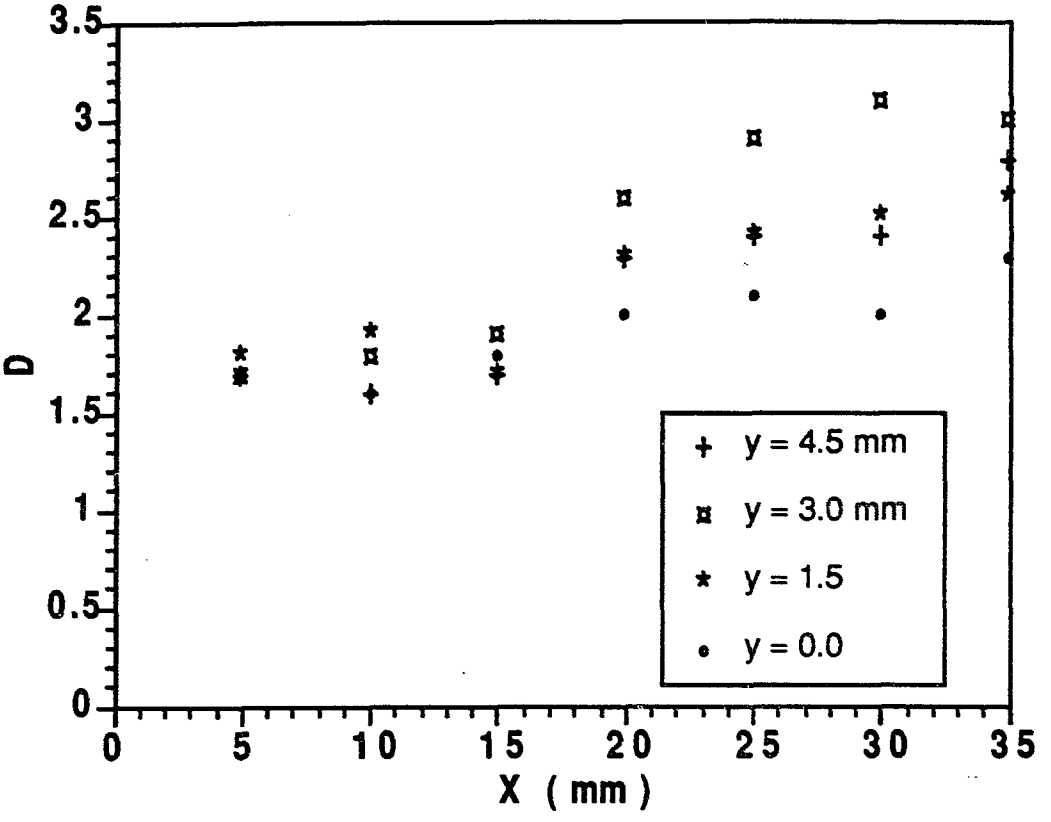

Fig. 4.6.2 The fractal dimension variation at differenty along the streamwise direction.

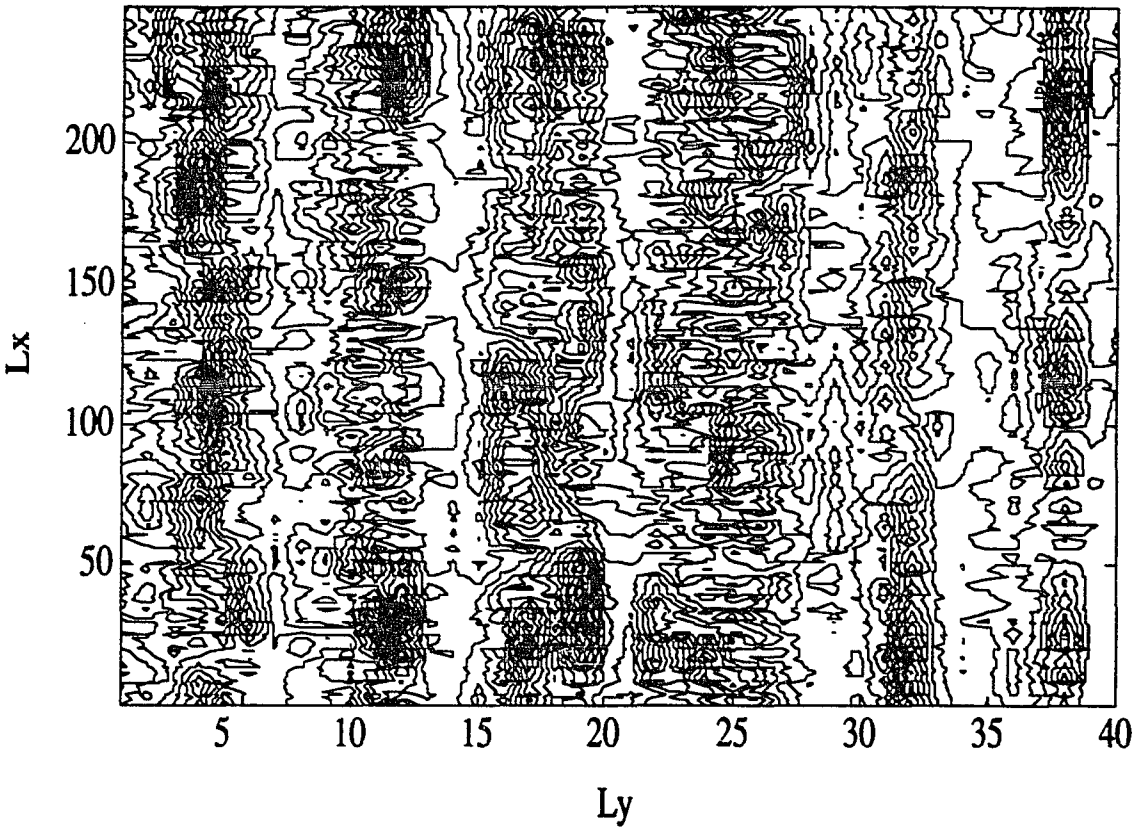

Fig. 4.7.1 Contour plot of streaky structures at different transverse locations along the streamwise direction.

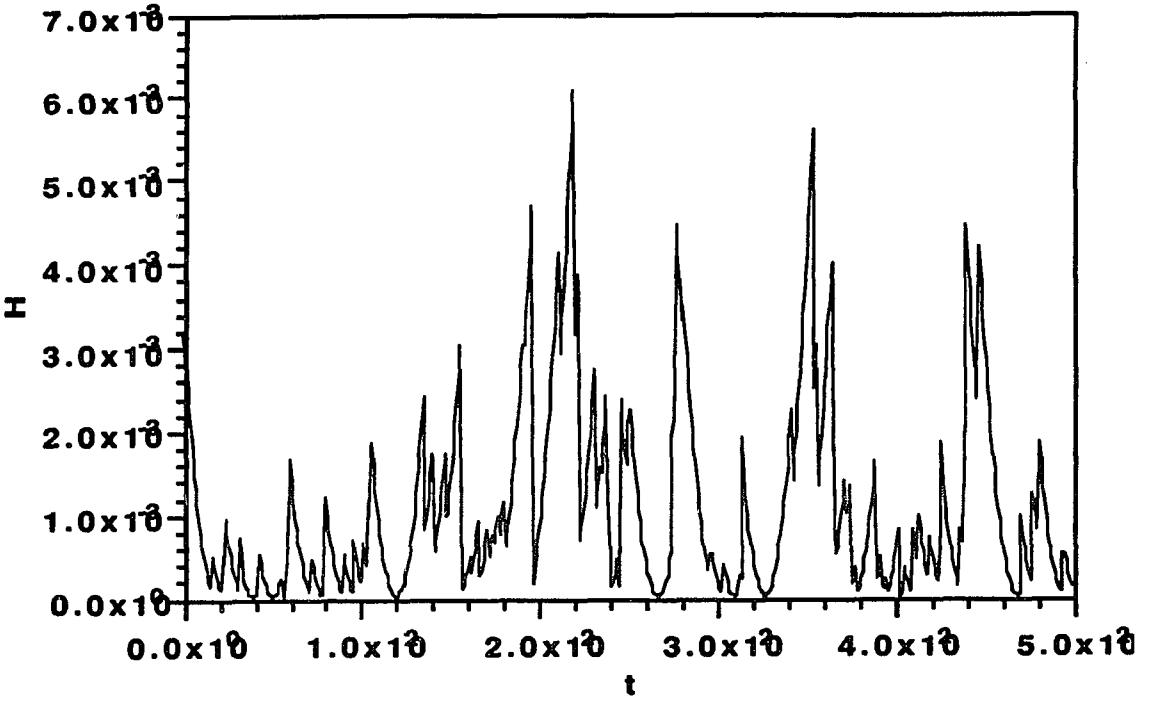

Fig. 4.8.1 Evolution of bursts at y = 1.5 mm and 1.0 cm downstream from the nozzle's lip.

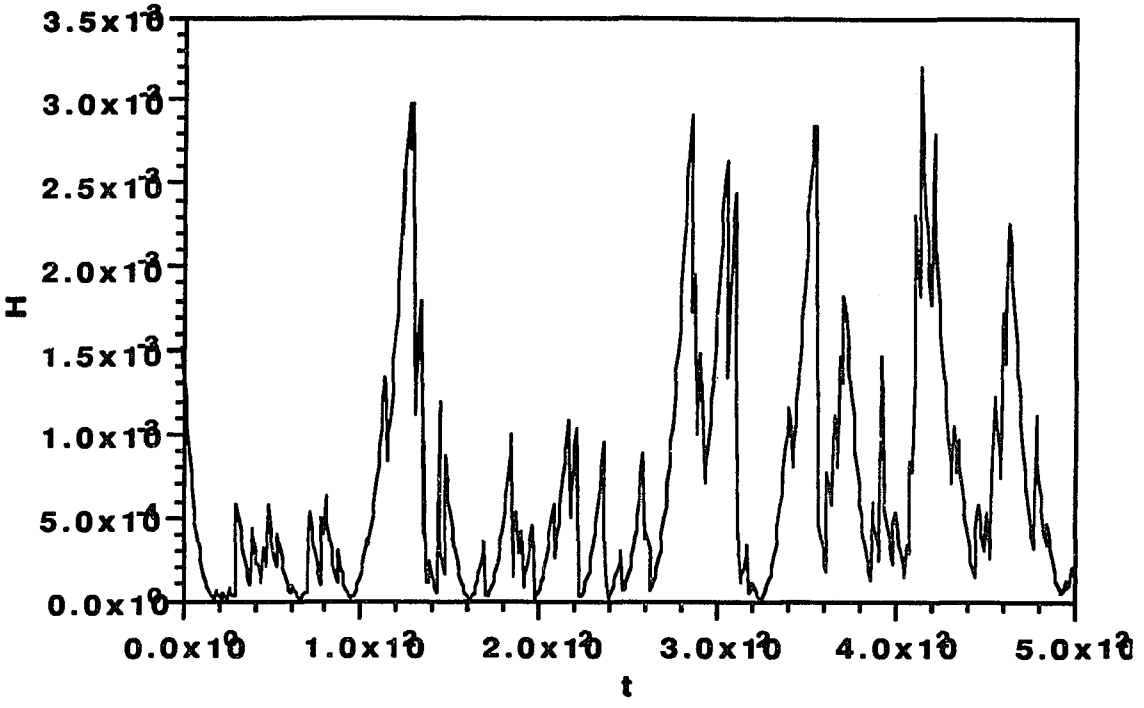

Fig. 4.8.2 Evolution of bursts at y = 1.5 mm and 1.5 cm downstream from the nozzle's lip.

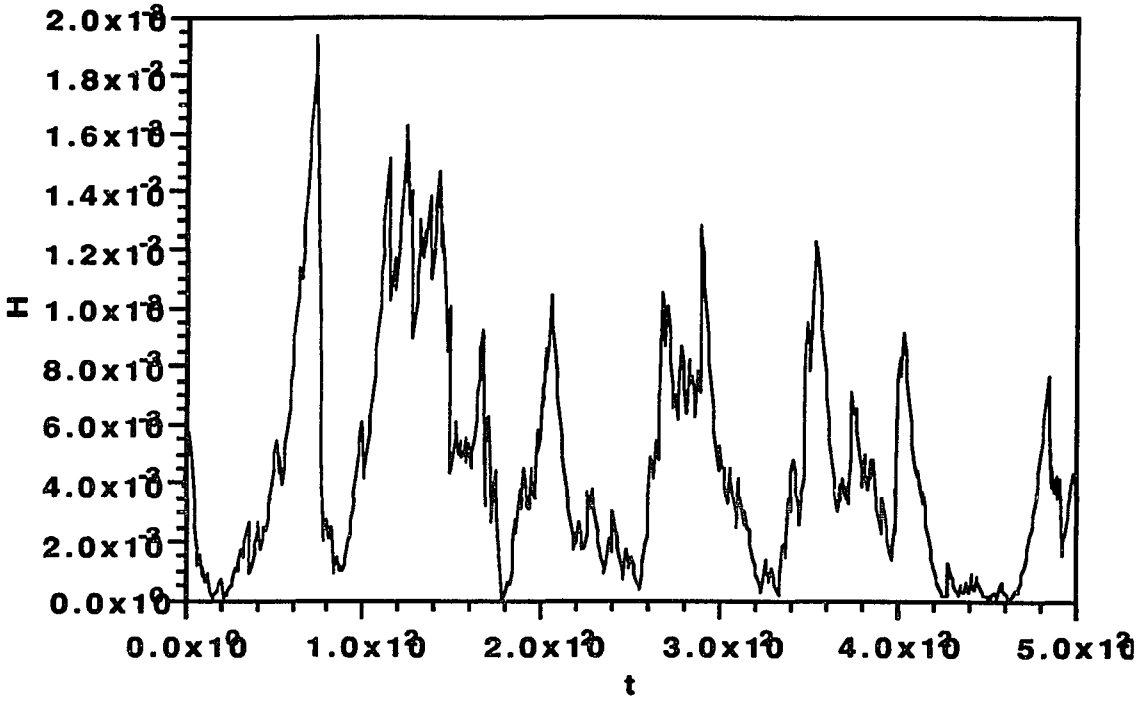

Fig. 4.8.3 Evolution of bursts at y = 1.5 mm and 2.0 cm downstream from the nozzle's lip.

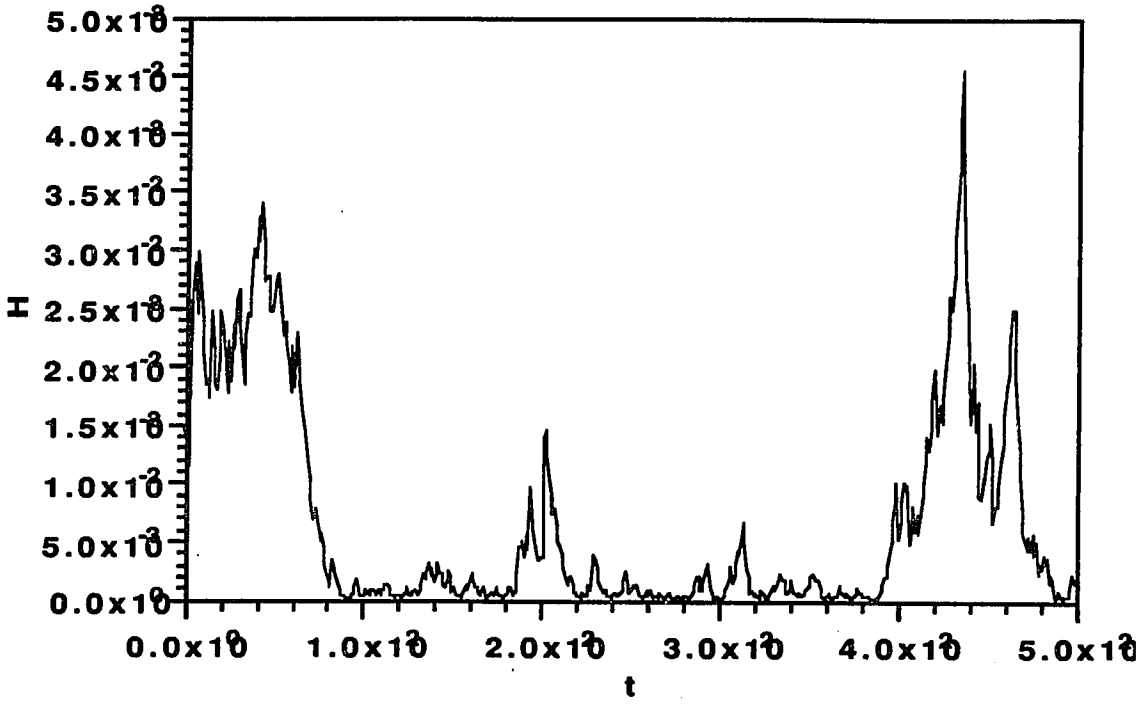

Fig. 4.8.4 Evolution of bursts at y = 1.5 mm and 2.5 cm downstream from the nozzle's lip.

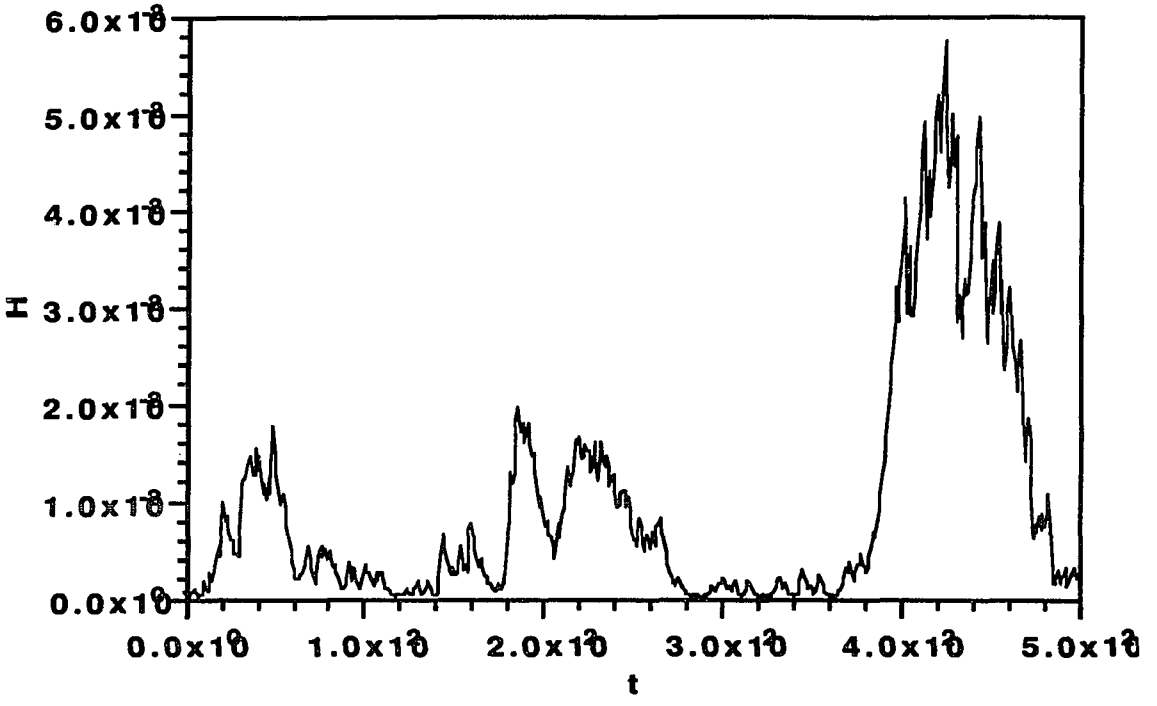

Fig. 4.8.5 Evolution of bursts at y = 1.5 mm and 3.0 cm downstream from the nozzle's lip.

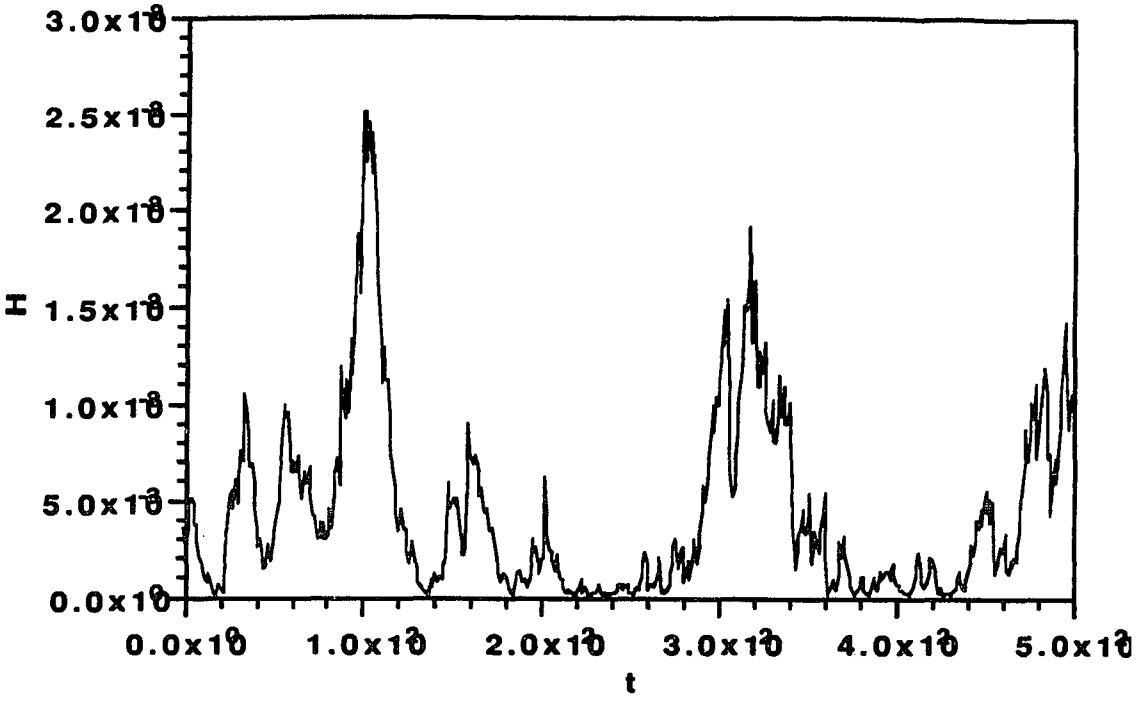

Fig. 4.8.6 Evolution of bursts at y = 1.5 mm and 3.5 cm downstream from the nozzle's lip.

V. Analytical Modeling of the Eddy Shocklet

5.1 The transient shock waves generation

To model the shocklet process, we can consider that the vortex structures or eddies are rigid. Their shapes or boundaries will not change during the interaction between the eddies and environmental field. The interaction is generally not strong. The transient shocks produced from the interactions are relatively weak shock waves. Therefore, it will be assumed that the effects of gas dissociation and relaxation phenomena can be neglected. We also consider that the Reynolds number is high; the flow is ideal gas flow. If the stagnation temperature does not exceed about 2000° K, the equation of state for ideal gas and the equation of continuity in a fixed Cartesian reference frame are

$$p = R \rho T \tag{5.1.1}$$

$$\frac{1}{\rho}\frac{D\rho}{Dt} + \frac{\partial u_i}{\partial x_i} = 0 \tag{5.1.2}$$

where R is the gas constant and p, ρ, T represent the pressure, density and temperature of the gas. Since the density can be considered a function of pressure and entropy S, this equation can be expressed as

$$\frac{1}{\rho}\left(\frac{\partial \rho}{\partial p}\right)_S \frac{Dp}{Dt} + \frac{1}{\rho}\left(\frac{\partial \rho}{\partial S}\right)_p \frac{DS}{Dt} + \frac{\partial u_i}{\partial x_i} = 0 \tag{5.1.3}$$

From the second law of thermodynamics

$$dS = C_v \frac{dT}{T} + \left(\frac{\partial p}{\partial T}\right)_p d\left(\frac{1}{\rho}\right) \tag{5.1.4}$$

where Cv is the specific heat at constant volume. Therefore

$$\left(\frac{\partial S}{\partial \rho}\right)_p = \frac{C_v}{T}\left(\frac{\partial T}{\partial \rho}\right)_\rho - \frac{1}{\rho^2}\left(\frac{\partial p}{\partial T}\right)_\rho$$

$$= -\rho^{-1}(C_v + R)$$

$$= -\frac{C_v}{\rho} \tag{5.1.5}$$

from the equation of state for ideal gas and the equation Cp - Cv = R, where Cp is the specific heat at constant pressure. Then

$$\left(\frac{\partial p}{\partial \rho}\right)_s = a^2 = \frac{\gamma p}{\rho} \tag{5.1.6}$$

where a is the local speed of sound and γ the ratio of specific heats, so that the equation of continuity can be expressed as

$$\frac{\partial u_i}{\partial x_i} = -\frac{1}{\gamma p}\frac{Dp}{Dt} + \frac{1}{C_p}\frac{DS}{Dt} \tag{5.1.7}$$

The momentum equation for the fluid flow is

$$\frac{Du_i}{Dt} = \frac{1}{\rho}\frac{\partial p_{ij}}{\partial x_j} \tag{5.1.8}$$

where p_{ij} represents the stress tensor which is of the form

$$p_{ij} = -p\,\delta_{ij} + \mu\,(s_{ij} - \frac{2}{3}\theta\,\delta_{ij})$$

where δ_{ij} is the Kronecker delta, s_{ij} the rate of strain tensor and $\theta = \partial u_i / \partial x_i$ is the fluid dilatation.

Since

$$\frac{\partial}{\partial x_i}\frac{D}{Dt} \equiv \frac{D}{Dt}\frac{\partial}{\partial x_i} + \frac{\partial u_j}{\partial x_i}\frac{\partial}{\partial x_j}$$

from the equation of momentum we can get

$$\frac{D}{Dt}\frac{\partial u_i}{\partial x_i} = -\frac{\partial u_j}{\partial x_i}\frac{\partial u_i}{\partial x_j} - \frac{\partial}{\partial x_i}\left(\frac{1}{\rho}\frac{\partial p}{\partial x_i}\right) - \frac{\partial}{\partial x_i}\left\{\frac{1}{\rho}\frac{\partial}{\partial x_j}\left[\mu\left(s_{ij} - \frac{2}{3}\theta\,\delta_{ij}\right)\right]\right\} \tag{5.1.9}$$

Operating on equation (5.1.7) with D/Dt, and subtracting the result from the last expression, we have

$$\frac{D^2}{Dt^2}\log\left(\frac{p}{p_0}\right) - \frac{\partial}{\partial x_i}\left[a^2\frac{\partial}{\partial x_i}\log\left(\frac{p}{p_0}\right)\right]$$

$$= \gamma\frac{\partial u_i}{\partial x_j}\frac{\partial u_j}{\partial x_i} + \gamma\frac{D}{Dt}\left(\frac{1}{C_p}\frac{DS}{Dt}\right) - \gamma\frac{\partial}{\partial x_i}\left\{\frac{1}{\rho}\frac{\partial}{\partial x_j}\left[\mu\left(s_{ij} - \frac{2}{3}\theta\,\delta_{ij}\right)\right]\right\} \tag{5.1.10}$$

since

$$\frac{1}{\rho}\frac{Dp}{Dt} = \frac{D}{Dt}\log\left(\frac{p}{p_0}\right); \qquad \frac{1}{\rho}\frac{\partial p}{\partial x_i} = \frac{a^2}{\gamma}\frac{\partial}{\partial x_i}\log\left(\frac{p}{p_0}\right)$$

where p_0 is a convenient reference pressure. For our case, one can choose the initial pressure as p_0.

Equation (5.1.10) gives the pressure field generated by the eddy which convects with a velocity different from the flow field. The terms on the left-hand side are those of a wave equation in a moving medium with a variable speed of sound, the partial time derivatives of the ordinary wave equation being replaced by derivatives following the motion. The first term on the right-hand side represents the generation of pressure fluctuations by the velocity fluctuations in fluid. The remaining terms describe the effects of entropy fluctuations and fluid viscosity. If we were to be concerned with the structure of the shock waves developed inside a turbulent fluid at high Mach number, then the last two terms can not be neglected, since the internal structures of the shocks is determined by the balance between these diffusive and convective effects.

Let us instead only concern ourselves with the formation of the shock waves and ignore the internal structures of the shocks; we treat only the eddy interactions with the flow field. Let us also ignore the inside structure of the eddy and its changes during the interaction; this is acceptable since the important thing in free shear flows is the generation of the shock and consequent propagation of shock waves along with the vorticity production due to the shock waves. Under these circumstances, the last two

terms in equation 5.1.10 can be neglected. For a turbulent shear layer there is the possibility that we can consider separately the processes of generation of the pressure waves and the subsequent development of the shocks.

In most cases the boundary approximation can be applied to shear layer problems. We can consider that, in a turbulent shear zone, the mean velocity u_1 is a function of the x_2 position coordinate only. Suppose that the characteristic zone thickness is 2L, and that u_1 changes from -U to +U as x_2 moves from $-\infty$ to $+\infty$. The necessary condition for generation of shocklet in shear layer is that we have U greater than a_0, the speed of sound at infinity. For the sake of analytical convenience, we suppose that all mean point properties of the motion in the shear zone are independent of x_1, x_3 and time t, being a function of x_2 alone, the position coordinate normal to the zone. Therefore, from the equation (5.1.10), we obtain

$$\left\{\frac{D^2}{Dt^2}-\frac{\partial}{\partial x_i}a^2\frac{\partial}{\partial x_i}\right\}\log\left(\frac{p}{p_0}\right)=\gamma\frac{\partial u_i}{\partial x_j}\frac{\partial u_j}{\partial x_i} \qquad (5.1.11)$$

To further simplify the equation we can neglect, on the left-hand side, products of two fluctuating quantities with zero means, on the understanding that these will be small (in mean square) compared with the products of mean and fluctuating quantities. This neglects such physical processes as the convection and scattering of a shock wave by turbulence, and the variation of a^2 about its local mean value. The terms of generation, the processes of convection and

refraction of the shock wave by the mean flow, and by variation with x_2 of the local mean speed of shock wave are retained. The latter may be important if there are significant variations in the mean density of the flow. Equation (5.1.11) then reduces to

$$\left\{\left(\frac{\partial}{\partial t}+\overline{u_1}\frac{\partial}{\partial x_1}\right)^2-\frac{\partial}{\partial x_i}\overline{a^2}\frac{\partial}{\partial x_i}\right\}\log\left(\frac{p}{p_0}\right)=\gamma\frac{\partial u_i}{\partial x_j}\frac{\partial u_j}{\partial x_i}$$

or

$$\left\{\left(\frac{\partial}{\partial t}+\overline{u_1}\frac{\partial}{\partial x_1}\right)^2-\frac{\partial\overline{a^2}}{\partial x_2}\frac{\partial}{\partial x_2}-\overline{a^2}\frac{\partial^2}{\partial x_i^2}\right\}\log\left(\frac{p}{p_0}\right)=\gamma\frac{\partial u_i}{\partial x_j}\frac{\partial u_j}{\partial x_i} \qquad (5.1.12)$$

since $\overline{a^2}=\overline{a^2}(x_2)$. In many instances, the dominant term on the right-hand side is likely to result from the interactions of the large mean velocity gradient with the fluctuating velocity gradients, and the generation term can be approximated by

$$2\gamma\frac{\partial\overline{u_1}}{\partial x_2}\frac{\partial u_2}{\partial x_1} \qquad (5.1.13)$$

As usual we can express the equation (4.11) in dimensionless form. Let the instantaneous and mean velocities be given by

$$v_i=\frac{u_i}{U},\quad V=\overline{v_1} \qquad (5.1.14)$$

$$y_i=\frac{x_i}{L},\quad \tau=\frac{tU}{L}$$

$$A^2(y_2)=\frac{\overline{a^2}}{a_0^2}, \quad M=\frac{U}{a_0} \tag{5.1.15}$$

where a_0 is a reference sound speed; it can be choose at $y_2 = +\infty$ in the main flow. It is also clear that

$$A(y_2)\to 1 \ \ as \ \ y_2\to\pm\infty$$

The dimensionless form of (4.11) is thus

$$\left\{\left(\frac{\partial}{\partial\tau}+V\frac{\partial}{\partial y_1}\right)^2-\frac{1}{M^2}\frac{dA^2}{dy_2}\frac{\partial}{\partial y_2}-\frac{A^2}{M^2}\frac{\partial^2}{\partial y_i^2}\right\}\log\left(\frac{p}{p_0}\right)=\gamma\frac{\partial v_i}{\partial y_j}\frac{\partial v_j}{\partial y_i} \tag{5.1.16}$$

5.2 The Condition of Shocklet Generation

In free shear layers, the sizes of turbulent eddies are widely distributed from the dissipation range to the flow dimension. The shock waves generated by the interactions of the eddies and the flow should be the function of eddy wave number, k, and Mach number of the shear flow. To study the mechanism of shocklets and the eddy wave number, it convenient to do the Fourier transformation.

Before taking the Fourier transformation, equation (5.1.16) can be rewritten in different form by taking a new dependent variable

$$\zeta(\mathbf{y},\,t)\;=\;A(y_2)\log\left(\frac{p}{p_0}\right)$$

Then

$$\left\{\left(\frac{\partial}{\partial\tau}+V\frac{\partial}{\partial y_1}\right)^2+\frac{A}{M^2}\frac{d^2A}{dy_2^2}-\frac{A^2}{M^2}\frac{\partial^2}{\partial y_i^2}\right\}\zeta(y,\tau)=\gamma\,A(y_2)\,\frac{\partial v_i}{\partial y_j}\frac{\partial v_j}{\partial y_i}$$

$$= G(\mathbf{y}, \tau) \qquad (5.2.1)$$

The generation term G is significant only inside the turbulent shear zone, so that

$$G(\mathbf{y}, \tau) \to 0 \quad as \quad y_2 \to \pm\infty$$

By using the standard definition (Lighthill 1958) we can define the generalized Fourier transforms

$$\zeta(\mathbf{y}, \tau) = \iint \varpi(y_2, \mathbf{K}, n) \exp[i(\mathbf{K} \bullet \mathbf{y} + n\tau)]\, dK\, dn$$

$$G(\mathbf{y}, \tau) = \iint \Gamma(y_2, \mathbf{K}, n) \exp[i(\mathbf{K} \bullet \mathbf{y} + n\tau)]\, dK\, dn \qquad (5.2.2)$$

where $\mathbf{K} = (K_1, K_3)$ is a wave number vector in the plane of the shear layer and the integrations are made over all values of K and frequency n.

The equation relating the generalized Fourier transform ϖ and Γ corresponding to (5.2.1) is

$$\frac{d^2}{dy^2}\varpi(y, \mathbf{K}, n) + \left\{\frac{M^2}{A^2}(n + V k_1)^2 - k^2 - \frac{1}{A}\frac{d^2 A}{dy^2}\right\}\varpi(y, \mathbf{K}, n) = -\frac{M^2}{A^2}\Gamma(y, \mathbf{K}, n) \qquad (5.2.3)$$

where $k^2 = k_1^2 + k_3^2$, A and V are functions of y only.

From our experimental results using both shadowgraph and multi-point fluorescence measurements we know that the shocklets are generated in the upper edge of the shear flow and

propagate into main flow. Therefore, we can simplify equation (5.2.3) by considering only the upper edge region, that is, the region $y > 1$.

For $y > 1$, $G(y) \approx 0$, $A(y) \approx 1$ $V(y) \approx 1$. Thus equation (5.2.3) becomes

$$\frac{d^2 \varpi}{dy^2} + \left\{M^2 (n+k_1)^2 - k^2\right\} \varpi = 0 \qquad (5.2.4)$$

Since ϖ (y) must be bounded as $y - \infty$, the solutions to equation (5.2.4) must be either exponential decreasing or oscillatory according as the coefficient of ϖ is negative or positive. From equation (5.2.4), it is clear that the oscillatory solution corresponds to a radiated pattern of shock waves and the Mach number, M. For given Mach number the oscillatory solutions are associated with wave number **k** and frequency n such that

$$M^2 (n+k_1)^2 - k^2 > 0 \qquad (5.2.5)$$

As mentioned above, the upper edge region is the formation region for shocklets, that is, the radiated pressure field is largely contributed from the layer between $y = Y$ and $y = Y + \delta Y$ in the shear zone. The turbulent eddies in this neighbourhood are convected by the mean stream with velocity Vc which is approximately equal to the local mean velocity at Y. If the the flow is supersonic, it is sufficient to neglect (for the moment) the evolution of the eddy pattern as it is carried along; with this, the

frequency of the components of wave number k is just the frequency with which the wave component is swept past the fixed observation point at a rigid convected pattern. In this way we have

$$n = k_1 V_c$$

The layer of the shear zone near Y, where the convection velocity is Vc, will therefore generate a shock wave on the side of the layer y > 1 with wave numbers k such that

$$M^2 k_1^2 (1-V_c)^2 > k^2 \qquad (5.2.6)$$

Let α be the angle between the vector wave number k and the direction of the mean velocity. Then $\cos\theta = k_1/k$ and this condition becomes

$$\cos^2 \theta > \left[M(1-V_c) \right]^{-2} \qquad (5.2.7)$$

This prediction can be compared with experimental results on shocklet observations. From the equation we can see that the shocklets will therefore be generated by some wave numbers in those layers of the shear zone for which the difference between the mean velocity of the fluid outside the shear zone and the local eddy convection velocity is greater than the speed of sound outside the zone. From our measurements, the shocklets are mainly distributed in the angle between 20 and 70 degrees and the associated velocities are between 276 m/s to 520 m/s. The maximum value is at about 38 degrees, which is about 422 m/s. According to equation 5.2.7 the angular distribution is in the range

of 34.6 to 89.1 degrees and associated velocities are between 260.0 m/s to 457.8 m /s. Equation 5.2.7 is therefore in very good agreement with our results.

VI Conclusions and Suggestion

6.1 The LIF system

The laser induced fluorescence measurement technique provides simultaneous multi-point localized density and velocity measurements. The spatial resolution here is $(1.5 \pm 0.5 \text{ mm})^3$ and the time response is less than 100 ns. The velocity profiles measured by using this system show a logarithmic distribution which agrees with theory (L. D. Landau, E.M. Lifshitz 1987). These velocity profile distributions also agree with the experimental results from N.L. Messersmith (1988). The mean velocity in the outlet of the nozzle calculated based on the multi-point density measurements is 564 ± 16 m/s. The velocity based on the theoretical calculation of nozzle design is 534 m/s, and the velocity measured from taking a shadowgraph of a Mach angle is 547 ± 35 m/s. These results are in good agreement. The spreading rates of the shear layer measured by LIF technique are 0.31 ± 0.11, 0.24 ± 0.09, and 0.11 ± 0.04 for $P_f > P_b$, $P_f = P_b$ and $P_f < P_b$ flows. The spreading rates for the same flows from the photograph measurements are 0.37 ± 0.25, 0.30 ± 0.19, and 0.18 ± 0.14. From those results it can concluded that the LIF technique provides a useful and reliable measurement technique in turbulent supersonic flows.

6.2 Coherent Structures

Large scale structures were observed in lower regions of the shear layer. The scales of the structures are in the range from 2.6 $\pm$ 0.8 mm to 8.2 $\pm$ 2.7 mm. The minimum magnitude of mean periods is 0.12 ± 0.03 ms . The mean rate of spatial change is about

18.6 ± 0.16. It is believed that they are formed due to counter rotating vortices which sweep low velocity fluid from the outer region of the shear layer. The structures are lifted when they are convecting downstream. At higher shear rate regions, they break up into smaller structures.

6.3 Dynamics and Dimensionality of Shocklets

The shocklet observed in a supersonic free shear layer is strongly concentrated in the upper edge of the layer where the flow has a higher shear rate and the mean flow speed is supersonic. The shocklets are characterized by the typical density profiles and associated density jump. Experimental results for velocities of shocklets in the laboratory coordinate system are concentrated in the range of 276 m/s to 520 m/s. The shock angles between the main flow and shocklets are mainly distributed in the range 20 to 70 degrees as show in Figure 4.3.1. From the analytical modeling result in chapter 5, we find that, shocklets satisfy the condition

$$\cos^2\theta > \left[M(1-V_c)\right]^{-2}$$

where the M is the Mach number of shocklet and Vc is the convective velocity of shocklet in the shear layer. The Mach number and convective velocity are the values in the coordinate system moving with the flow. Specifically, the angle distribution from the analytical model is in the range 34.6 to 89.1 degrees; associated velocities are between 260.0 m/s to 457.8 m /s.

From the experimental results, it can be concluded that the formation of shocklets is understood in terms of the a vortex embeded in the flow moving at a speed different from that of the local flow. The vortex is accelerated by the flow field. During the acceleration, the energy transfers from the field to the vortex and a strong compression is formed. These strong disturbances in density propagate as a transient shock. From the correlation and dimension calculation results, it can be argued that the transient shocks reduce the turbulence scale of flow through two effects: (a) the break-up of the structures; and (b) the generation of vorticity field by the transient shock.

6.4 Effect of Shocklets on the Spreading Rate

The results in chapter 4 show that differences in the spreading rates for different type of flows are associated with differences in the distribution of shocklets in these flows. Specifically, as shocklets increase in production frequency, the shear layer's spreading rate decreases. The theory in chapter 2 states that the dynamical effect of shocklets in shear flows is that of reducing the size of turbulent structure and transferring turbulent energy from structures to the flow outside the shear layer. These effects will therefore result in a reduction of the spreading rate of the shear layer; thus the experimental results agree with expectations from theory. The average spreading rate for those three different type of flows is 0.22 ± 0.08. This value is about 10 time larger than that by N.L. Messersmith(1988) from the mixing layer, as would be expected. Our result is in good agreement with the value 0.267 for

the same kind turbulent shear layer discussed in L.D. Landau and E.M. Lifshitz (1987).

6.5 Shear Flow Parameters

By applying boundary-layer-approximation theory, the shear layer parameter, a, is calculated from equation (2.2.6), where the distribution function of $f(\eta)$ is obtained from the logarithmic fit of the velocity profile. The entrainment and eddy viscosity parameters are calculated from equations (2.2.11) and (2.2.12). The experimental result for the shear rate parameter, S*, at high shear rate region in our flow is larger than 35; the energy partition parameter, K*, is in the range of 9.2 ± 1.6 at x = 1.0 cm, and 6.7 ± 0.7 at x = 3.0 cm; the eddy elongation parameter, L*, is found to be 12.5 ± 1.8. Given that $S^* > 35$ in our system, our experimental results are quite consistent with the predictions ($K^* > 5$, $L^* > 8$) from M.J. Lee (1990).

6.6 Connection between Streaks and Shocklets

From the experimental results, a correlation between the streaks and shocklets is obtained; the streaks are formed at the lower regions of the free shear layer and break into small structures near the upper region where the flow speed is supersonic. These small structures should rotate in counter-clockwise direction (due to the high shear stress). They should then be ejected into the supersonic region, and due to the difference in velocities, the strong compression is formed. The subsequent process is indeed the process of generation of shocklets.

6.7 Suggestion

The first hint that there may be some connection between dynamical systems theory and turbulence was established by Lorenz (1963). Ruelle & Takens (1971) proposed a model in which turbulence would be a deterministic, chaotic regime reached after a small number of bifurcations. A review by Hussain (1986) concludes that while turbulent flows have infinite degree of freedom, the motion of coherent structures, being large-scale and organized, is likely to be low-dimensional. Aubry et al. (1988) and Holmes (1989) showed that low dimensional methods might be applied in concert with the proper orthogonal decomposition to the study of a class of turbulent flows possessing coherent structures. The instantaneous field in shear layer can be expanded in so-called empirical eigenfunctions. The results of such an expansion allow us to retain correct dynamical representation of the turbulence production phenomenon and keep as few modes as possible in order to obtain a low-dimensional system. A proper way to do that is find the cutoff modes from the experimental measurement.

Our results now define regions in the free shear layer where such measurements can be attempted, viz, regions with low dimensionality and with low shocklet production frequency. The Navier Stokes equation can be solved explicitly using the procedures outlined in section 4,8; however, to do the complete calculation for all derivatives and integrations at least 12 simultaneous measuring points in the free shear layer are required. Furthermore, the separation between measuring should be reduced (to roughly 0.5 mm), - a difficult requirement. Nonetheless, because of the potential importance for the

development of theoretical models, the cutoff modes should indeed be determined.

References

Arnold, V. I., 1983 *Geometrical methods in the theory of ordinary differential equations*, Springer Verlag, New York.

Aubry, N., Holmes, P., Lumley, J. L., and Stone, E., 1988 *The dynamics of coherent structures in the wall region of a turbulent boundary layer*, J. Fluid Mech., 192, 115.

Bell, J. H. and Mehta, R. D., 1990 *Interation of a streamwise vortex with a turbulent mixing layer*, Phys. Fluids A **2** (11), pp. 2011-2023.

Bernal, L. P., 1988 *The statistics of the organized vortical structure in turbulent mixing layers,* Phys. Fluids 31 (9) .

Bernard, P. S., Handler, R. A., 1990 *Reynolds stress and the physics of turbulent momentum transport*, J. Fluid Mech., vol. 220 pp. 99-124.

Blckwelder, R. F., 1988, AIAA Paper #89-1009, AIAA 2nd Shear Flow Conference, Some ideas on the control of near wall eddies.

Brown, G.L. & Roshko, A., 1974 *On density effects and large structures in turbulent mixing layers,* J. Fluid Mech., vol. 64, p. 775-816.

Browand, F. K. and Latigo, B. O., 1979 *Growth of the two-dimensional mixing layer from a turbulent and nonturbulent boundary layer*, Phys. Fluids **22** (6), pp. 1011-1019.

Cantwell, B.J., 1981 *Organized motion in turbulent flow,* Ann. Rev. Fluid Mech., vol 13, p. 457.

Chiueh, Tzihong, 1989 *Expansion of shear flow and vortex merger in a two-dimensional turbulent mixing layer*, Phys. Fluids B **1** (6), 1163.

Corino, E. R., and Brodkey, R. S., 1969, *A visual study of turbulent shear flow*, J. Fluid Mech.,37,1.

Constantin, P., Foias, C. Manley, O. and Temam, R., 1985 *Determining modes and fractal dimension of turbulent flows*, J. Fluid Mech., 150, 427.

Constantin, P., Foias, C., Temam, R. and Nicolaenko, B., 1989 *Integral magnifolds and inertial magnifolds for dissipative partial differential equations*, Springer Verlag, New York.

Davies, P. O. A. L. and Yule, A. J., 1975 *Coherent structures in turbulence,* J. Fluid Mech., vol. 69, p. 513-537 .

Elliott, G. S. and Samimy, M., 1990 *Compressibility effects in free shear layers*, Phys. Fluids A 2 (7), pp. 1231-1240.

Farmer, J. D., 1983*The Dimension of Chaotic Attractor,* Physica 7D, p. 153-180 .

Grinstein, F. F. and Oran, E. S., 1988*Three-Dimensional Numerical Simulation of a Compressible, Spatially Evolving Mixing Layer,* AIAA-88-0042 .

Henon, M., 1976 *A two dimensional mapping with a strange attractor,* Commun Math.Phys. 50:69-77 .

Holmes, P. J., Marsden, J. E. and Scheurie, J., 1989 *Hamiltonian dynamical system*, Cont. Meth., 81, 213.

Hussain, A. K. M. F., 1983 *Coherent structures-reality and myth,* Phys. Fluids 26 (10) .

Hussaini, M. Y., 1985 *Turbulent shock interaction*, Springer Verlag, New York.

Johnson III, J. A., Zhang, Y. and Johnson, L. E., 1988 *Evidence of Reynolds number sensitivity in supersonic turbulent shocklets*, AIAA J. 26, 502.

Jusinski, L. E., Sharpless, R. L. and Slanger, T. G., 1987 *Multiphoton dissociation in NO_2 at 532 nm and the generation of vibrationally excited O_2 and NO*, J. Chem. Phys. **86** (10), pp. 5509-5514.

Kim, H. T., Kline, S. J. and Reynolds, W. C., 1971 *The production of turbulence near a smooth wall in a turbulent boundary layer*, J. Fluid Mech.,50,133

Kim, S. -W., 1991 *Calculation of divergent channel flows with a multiple-time-scale turbulence model*, AIAA J. vol. 29, No.4, 547-554.

Kimura, Y., Zawadzki, I. and Aref, H., 1989 *Vortex motion, sound radiation, and complex time singularities*, Phys. Fluids A **2** (2), pp. 214-219.

Landau L. D. and Lifshitz M., 1987 *Fluid Mechanics,* second edition, Pergamon Press, New York.

Laufer, J., 1975 *New trends in experimental research*, Ann. Rev. Fl. Mech. 7, 307.

Lee, M. J. , Kim, J. & Moin, P., 1990 *Structure of turbulence at high shear rate,* J. Fluid Mech., vol. 216, p.516-583

Lele, S. K., 1989 *Direct numerical simulation of compressible free shear flows,* AIAA paper 89-0374.

Lepicovsky, L., L. Ahuja, K. K., Brown, W. H. and Burrin, R. H., 1986 *Coherent Large-Scale Structures in High Reynolds Number Supersonic Jets,* AIAA paper 86-1941.

Lighthill, M. J., 1958 Fourier Analysis and generalized equations, Cambridge University Press.

Liu, J. T. C., 1989 *Coherent structures in transitional and turbulent free shear flows*, Ann. Rev. Fluid Mech., 21, 285.

Meadows, K. R., Kumar, A. and Hussaini, M. Y., 1991 *Computational study on the interaction between a vortex and a shock wave*, AIAA J. vol. 29, No.2, pp. 174-179.

Messersmith, N. L., Goebel, S. G., Frantz, W. H., Krammer, E. A., Renie, J. P., Dutton, J. C. and Krier, H., 1988 *Experimental and Analytical Investigations of Supersonic Mixing Layers,* AIAA-88-0702, Jan. 11-14.

Mory, M., 1991 *A model of turbulent mixing across a density interface including the effect of rotation*, J. Fluid Mech., vol. 233, pp. 193-207.

Newell, A. C., Rand, D. A. and Russell, D., 1988 *Turbulent dissipation rates and the random occurrence of coherent events*, Phys. Lett., A., 132, 112.

Newell, A. C., Rand, D. A. and Russell, D., 1988 *Turbulent transport and the random occurrence of coherent events*, Physica, 33D, 281.

Offen, G. R., and Kline, S. J. 1974 *Combined dye-streak and hydrogen bubble visual observations of a turbulent boundary layer*, J. Fluid Mech., 62, 223.

Outt, B.,1976 *Mechanism of the Machwave Generation,* AIAA paper, 76-506.

Patel, V. C. and Scheuerer, G., 1982 *Calculation of two-dimensional near and far wakes*, AIAA J. vol. 20, No. 7, pp. 900-907.

Prasad, R. R. and Sreenivasan, K. R.,1990 *The Measurement and Interpretation of Fractal Dimensions of the Scalar Interface in Turbulent Flow,* Phys. Fluids A (5).

Praturi, A. K., and Brodkey, R. S., 1978 *A stereoscopic visual study of coherent structures in turbulent shear flow*, J. Fluid Mech., 89, 251.

Rohr, J. J., Itsweire, E. C., Helland, K. H. and Vanatta, C. W., 1988 *An investigation of the growth of turbulence in a uniform-mean-shear flow*, J. Fluid Mech., vol. 187 pp. 1-33.

Roshko, A. and Papamoschou, D., 1986 *Observations of supersonic free shear layers,* AIAA Paper 86-0162.

Roux, J. C., Rossi, A., Bachelart, S. and Vidal, C., 1981 *Experimental observations of complex behavious during a chemical reaction*, Physica, 2D, 395.

Ruelle, D. and Takens F., 1971 *On the nature of turbulence,* Communs Math. Phys. 82, p. 137-151.

Simpson, R. L., 1989 *Turbulent boundary-layer separation*, Ann. Rev. Fluid Mech., 21, 205-234.

Smalley, R. E., Wharton, L. & Levy, D. H., 1975 *The fluorescence excitation spectrum of rotationally cooled NO_2,* J. Chem. Phys., vol. 63, p. 4977.

Sreebuvasan, K. R. and Meneveau, C., 1986*The fractal facets of turbulence,* J. Fluid Mech., vol. 173, p. 357-386.

Sreenivasan, K. R., 1991 *Fractals and multifractals in fluid turbulence*, Ann. Rev. Fluid Mech., vol. 23, pp. 539-600.

Theodorsen, T., 1952 *Mechanism of turbulence*, Proc. 2nd Midwestern Conf. on Fluid Mech. Ohio State U., Colombus, Ohio.

Williams, R.F.1974 *Expanding attractors,* Pudl. Math. IHES 43: 169-203.